GREEN MOUNTAIN
RADIO RESEARCH COMPANY

50 Vermont Avenue, Fort Ethan Allen, Winooski, Vermont 05404 U.S.A. Tel. 802-655-9670

POLARIZED-INTERFEROMETER FEASIBILITY STUDY

(NASA-CR-170979) POLARIZED-INTERFEROMETER FEASIBILITY STUDY Final Report, Sep. 1982 - Jun. 1983 (Green Mountain Radio Research Co.) 132 p HC A07/MF A01 CSCL 14B

N84-20805

Unclas
G3/35 18369

by

Frederick H. Raab, Ph.D.

FINAL REPORT

July 1983

Prepared for

NASA George C. Marshall Space Flight Center
Marshall Space Flight Center, Alabama 35812

Prepared under

Contract NAS8-34960
September 1982 - June 1983

50272-101

REPORT DOCUMENTATION PAGE	1. REPORT NO.	2.	3. Recipient's Accession No.

4. Title and Subtitle
Polarized interferometer feasibility study

5. Report Date
July 1983

6. 30750

7. Author(s)
Frederick H. Raab, Ph.D.

8. Performing Organization Rept. No.
TR83-2

9. Performing Organization Name and Address

Green Mountain Radio Research Company
50 Vermont Avenue, Fort Ethan Allen
Winooski, Vermont 05404

10. Project/Task/Work Unit No.

11. Contract(C) or Grant(G) No.
(C) NAS8-34960
(G)

12. Sponsoring Organization Name and Address

National Aeronautics and Space Administration
George C. Marshall Space Flight Center
Marshall Space Flight Center, Alabama 35812

13. Type of Report & Period Covered
FINAL
September 1982 - June 1983

14.

15. Supplementary Notes

16. Abstract (Limit: 200 words)

This report presents the results of a study of the feasibility of using a polarized-interferometer system as a rendezvous-and-docking sensor for two cooperating spacecraft. The polarized interferometer is a radio-frequency system for long-range, real-time determination of relative position and attitude. Range is determined by round-trip signal timing. Direction is determined by radio interferometry. Relative roll is determined from signal polarization.

Each spacecraft is equipped with a transponder and an antenna array. The antenna arrays consist of four crossed dipoles that can transmit or receive either circularly or linearly polarized signals. The active spacecraft is equipped with a sophisticated transponder and makes all measurements. The transponder on the passive spacecraft is a relatively simple repeater.

An initialization algorithm is developed to estimate position and attitude without any a priori information. A tracking algorithm based upon minimum-variance linear estimators is also developed. Novel techniques to simplify the transponder on the passive spacecraft are investigated and a suitable configuration is determined. A multiple-carrier CW signal format is selected. The dependence of range accuracy and ambiguity-resolution error probability are derived and used to design a candidate system. The validity of the design and the feasibility of the polarized-interferometer concept are verified by simulation.

17. Document Analysis a. Descriptors

Rendezvous and docking sensors
Radio-frequency systems
Polarization measurement
Attitude-determination systems
Radio interferometer
Radio ranging
Ambiguity resolution
Minimum-variance linear estimator

b. Identifiers/Open-Ended Terms

c. COSATI Field/Group

18. Availability Statement
Approved for public release, distribution unlimited.

19. Security Class (This Report)
UNCLASSIFIED

20. Security Class (This Page)
UNCLASSIFIED

21. No. of Pages
124

22. Price

PREFACE

This report was prepared by Green Mountain Radio Research Company, Burlington, Vermont, under contract NAS8-34960 from the NASA George C. Marshall Space Flight Center. The work upon which it is based was done by the author between September 1982 and June 1983, inclusive. The contracting officer's representatives were James A. Dunkin, James D. Michael, and R. Sharma. The manuscript and artwork were prepared by Patricia L. Scott.

TABLE OF CONTENTS

LIST OF FIGURES

LIST OF TABLES

CHAPTER 1

INTRODUCTION

The reusable Space Transportation System (STS, "Shuttle"), the Teleoperator Maneuvering System (TMS), and Orbital Transfer Vehicle (OTV) will be required routinely to rendezvous and to dock with other spacecraft, including satellites, experiment platforms, and the Space Operations Center (SOC, space station). Rendezvous requires measurement of relative position and velocity, and suitable information can be provided by radar. In contrast, docking involves alignment (and therefore measurement) of both relative position and relative attitude (Figure 1-1).

Rendezvous and docking can be accomplished by manual guidance commands based upon radar and visual inputs. However, the required workload is relatively high and docking may require alignment of interfaces that are not readily visible. Visual sensing and manual control is obviously unsuitable for remote and automatic spacecraft guidance. Consequently, a relative-position-and-attitude sensor is needed.

Spacecraft such as the STS and TMS are "active" and can maneuver to accomplish rendezvous and docking. However, the target spacecraft is often unable to maneuver and is therefore designated as "passive." It is reasonable to assume that the active spacecraft can carry an active, sophisticated sensor. However, the passive spacecraft may have little or no power or space available for the sensor. It is therefore highly desirable to minimize the complexity and power requirements of the system for the passive spacecraft.

The polarized interferometer is a radio-frequency system for real-time, long-range measurement of the relative position and attitude of two spacecraft. Both spacecraft are equipped with a multi-element antenna array and a transponder. The transponder on the active spacecraft measures signal parameters and processes them to obtain position and attitude estimates for use by the guidance system. The transponder on the passive spacecraft is a simple repeater.

1.1 PRINCIPLES OF OPERATION

The polarized-interferometer is based upon three basic principles:

- The use of round-trip timing to determine range,
- The use of interferometry to determine direction of arrival, and
- The use of polarization to determine rotation.

The specific uses of each of these three principles are explained in this section; the relevant mathematics are presented in the subsequent chapters.

The operation of the polarized interferometer is most readily described in the "two-way" coordinate system shown in Figure 1-2. In the "one-way"

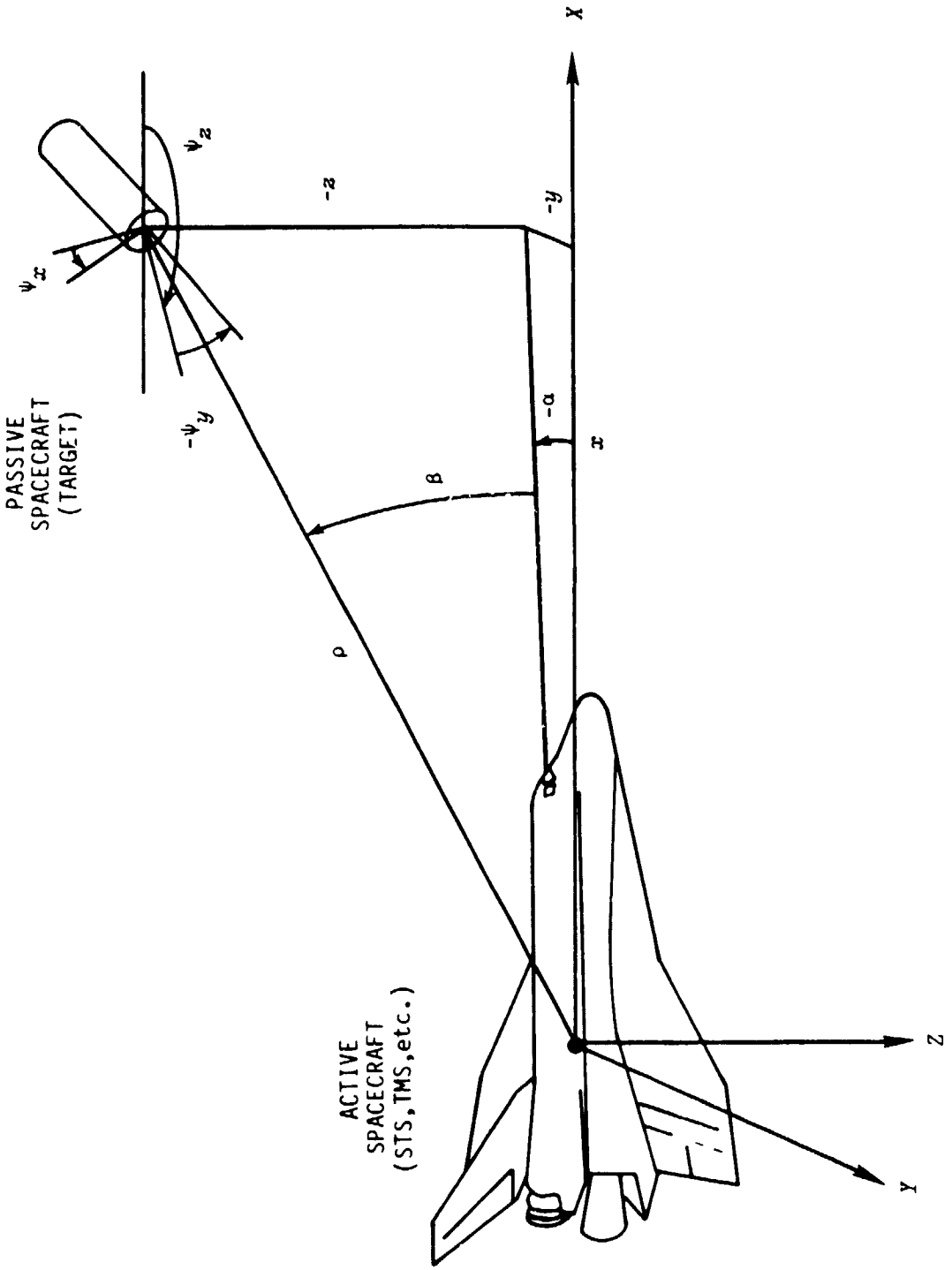

Figure 1-1. One-way coordinate system.

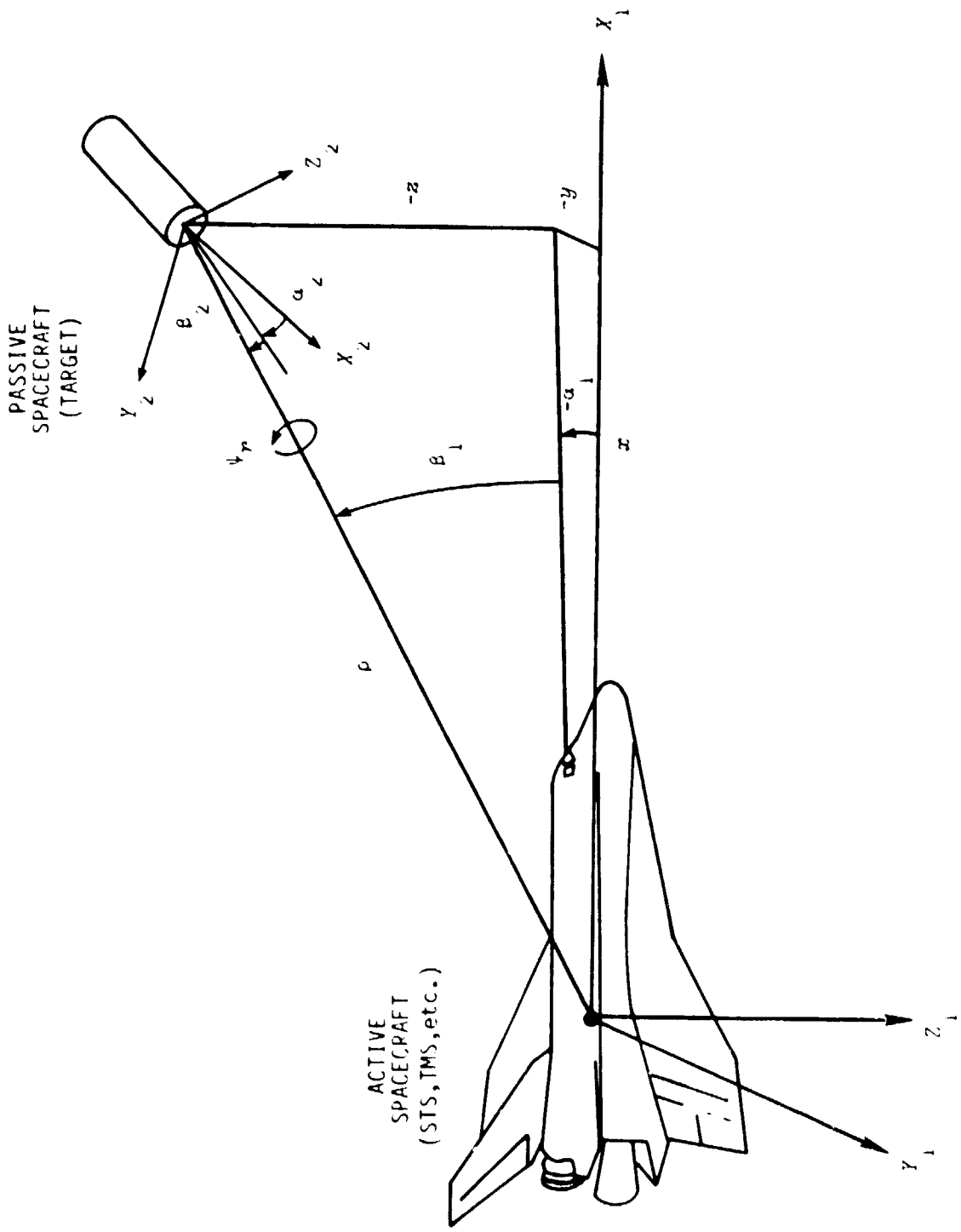

Figure 1-2. Two-way coordinate system.

coordinate frame of Figure 1-1, the position of the passive spacecraft with respect to the active spacecraft is specified by range, azimuth, and elevation (ρ, α_1, β_1); attitude is specified by a set of three Euler angles (ψ_z, ψ_y, ψ_x). In the two-way coordinate system, the position of the passive spacecraft is similarly specified. However, the two-way coordinate system specifies position (ρ, α_2, β_2) of the active spacecraft with respect to the passive spacecraft and the relative-roll angle (ψ_r) between the two spacecraft coordinate frames instead of attitude.

A typical antenna array for the active spacecraft is shown in Figure 1-3. Each of the four components consists of two crossed slots or two crossed dipoles. Component A0 is used for transmitting and is configured to produce linear polarization. Components A1, A2, and A3 are used for receiving. Component A1 is configured for linear polarization, while A2 and A3 are configured for circular polarization.

The antenna array for the passive spacecraft is similar to that for the active spacecraft, but the roles of the components are reversed. Center component P0 is used for reception, and outer components P1, P2, and P3 are used for transmitting.

Range is determined by round-trip signal timing. Accurate and unambiguous measurements can be achieved by transmitting CW signals on a number of frequencies or by employing short-pulse or spread-spectrum modulation.

The direction of the passive spacecraft with respect to the active spacecraft is determined by radio interferometry. The signal from a given component of the passive-spacecraft antenna array is received by components A1, A2, and A3 of the active-spacecraft array. The phases of the output from each antenna component are measured and compared; the differences between the phases are directly proportional to the differences in the three path lengths (Figure 1-3). Since the three paths are essentially parallel except at very short distances, the phase differences can be converted to direction angles α_1 and β_1.

Interferometric techniques are similarly used to determine the direction of arrival of the active spacecraft with respect to the passive spacecraft. Since the complexity of the transponder on the passive spacecraft must be minimized, all measurements, reverse direction finding is accomplished by comparing the phases of signals from elements P1, P2, and P3 as received by the same element (e.g., A1) of the active-spacecraft array. These phase differences are similarly converted to reverse-direction angles α_2 and β_2.

The relative-roll angle is determined from measurements of the polarization of the received signals. Component P1 transmits sequentially using both linear polarizations. Measurement of the amplitudes of each signal by the two elements of component A1 results in a set of four coupling measurements. If all four direction angles were zero, each of the four coupling measurements would be directly proportional to the sine or cosine of the rel-

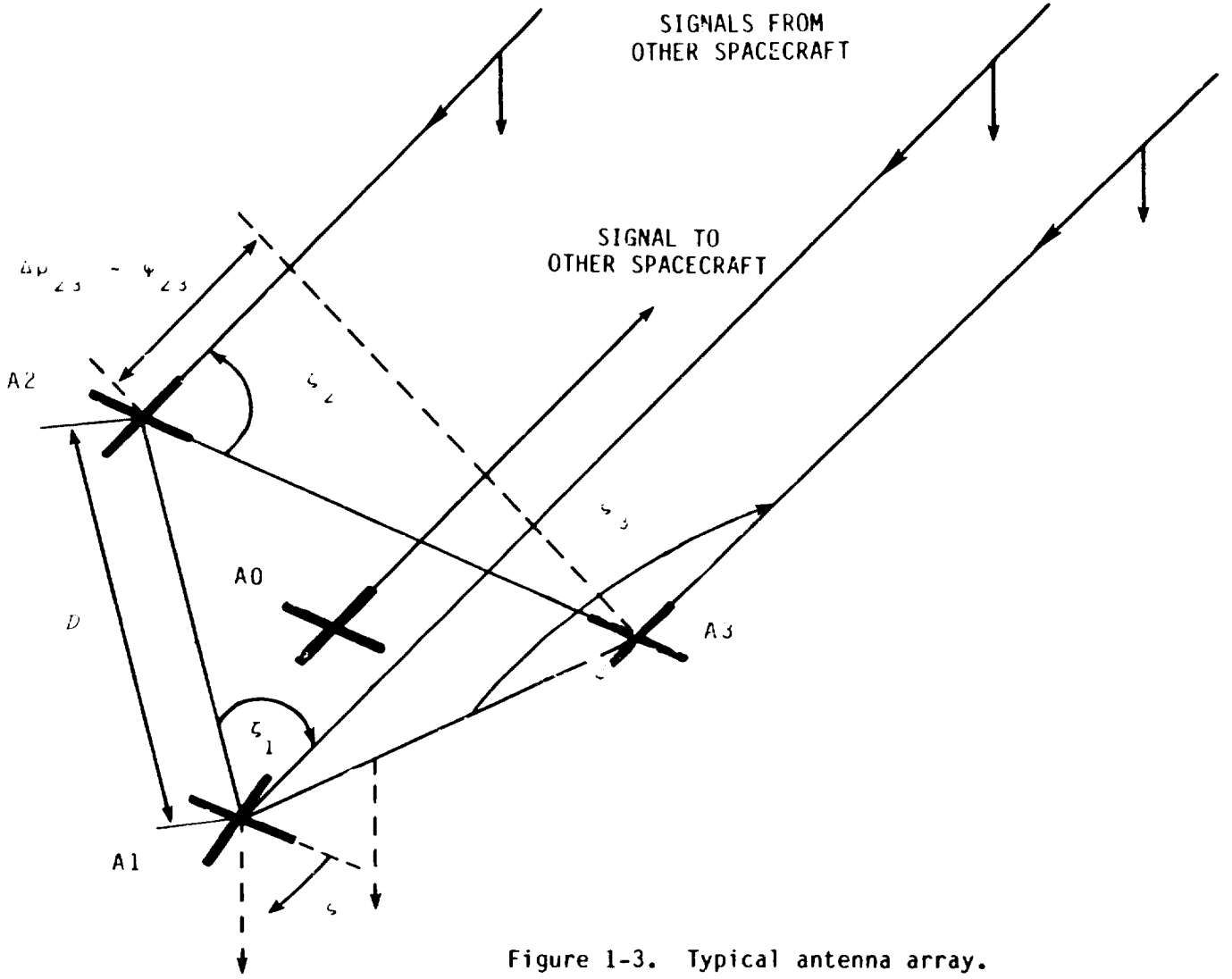

Figure 1-3. Typical antenna array.

ative-roll angle. While the mathematics are somewhat more complicated when the direction angles are nonzero, the relative-roll angle can nonetheless be extracted from the coupling measurements once the direction angles have been determined.

1.2 PERFORMANCE REQUIREMENTS

Potential applications for rendezvous and docking (R&D) sensors include the Space Shuttle (STS), the Teleoperator Maneuvering System (TMS), the Orbital Transfer Vehicle (OTV), and the Space Operations Center (SOC). Missions may be divided into rendezvous, station-keeping, and docking [Micheal, 1981]. The docking phase (range less than 30 m) has the most critical performance requirements.

Anticipated performance requirements are cited by a number of authors. The most recent and most thorough investigation is that of Laurie [1982], whose results are summarized in Table 1-1. The maximum required operating range of 50 km is the result of the availability of the STS radar and the anticipated availability of NAVSTAR/GPS navigation.

The Laurie concept uses a set of reflectors with a 1-m diameter. Similar-sized arrays on the target spacecraft are also envisioned by Tietz [1982] and Dabney [1981]. A sensor diameter of up to 1 meter therefore appears to be acceptable.

1.3 OTHER APPROACHES

Literature related to rendezvous and docking sensors was reviewed to establish typical system performance parameters and to obtain general information on alternative approaches. The results are summarized in this section.

RF Techniques

A variety of RF position and attitude sensors are discussed by Lowry [1967]. These sensors include conventional radar, rotating beacons (similar to VOR or TACAN), transponders, and passive reflectors.

Scanning Laser Radar

The scanning-laser-radar system [Flom, 1974-1975] derives position and attitude from a set of range and angle measurements to a number of reflectors on the target spacecraft. This system has a maximum range of about 50 km, a range accuracy of 10 cm or 0.01 percent of range (3σ), an angular accuracy of 0.05°, and a 30° × 30° field of view.

PARAMETER		RENDEZVOUS		DOCKING		RENDEZVOUS AND DOCKING	
		LIMITS	ACCURACY (3σ)	LIMITS	ACCURACY (3σ)	LIMITS	ACCURACY (3σ)
Range		100 m - 50 km	1% of range	2 - 100 m	1% of range	2 m - 50 km	1% of range
Range rate		±50 m/s	0.1 m/s	±1 m/s	0.01 m/s	±50 m/s	0.01 m/s ($R \leq$ 1 m/s) 0.1 m/s ($R >$ 1 m/s)
Position angles		±0.25 rad	10 mrad	±0.25 rad	10 mrad	±0.25 rad	10 mrad
Position angle rates		±20 mrad/s	0.1 mrad/s	±20 mrad/s	0.1 mrad/s	±20 mrad/s	0.1 mrad/s
Attitude Angles	Pitch, Yaw	N/A	N/A	±0.5 rad	30 mrad	±0.25 rad	30 mrad
	Roll	N/A	N/A	±π rad	30 mrad	±π rad	30 mrad
Attitude rates		N/A	N/A	±20 mrad/s	0.1 mrad/s	±20 mrad/s	0.1 mrad/s

Table 1-1. Rendezvous and docking requirements [Laurie, 1982].

Apollo Automatic Docking Sensor

An automatic-docking-sensor concept for the Apollo spacecraft is developed by Blanchard [1971]. In this concept, a number (at least four) of reflectors or light sources are affixed to the target spacecraft in a known geometry. The angles to these reflectors or sources are then measured by an optical system (probably using a vidicon). The position and attitude of the target spacecraft are then derived from the set of angle measurements.

Radar and Television

A Space-Shuttle proximity-operation senso concept was studied by Weber [1978]. The STS Ku-band radar is satisfactory for acquisition and long-range use. However, at short range (when the target occupies 10 % or more of the 3-dB beamwidth), the Ku-band radar is not accurate. Increasing the accuracy is not feasible because the monopulse antenna patterns cannot be predicted at short ranges. Weber's proposed solution slaves a television camera to the radar line of sight and mixes the angle measurements from all sensors. His simulations show that together they provide satisfactory accuracy.

Soviet Rendezvous System

An automatic rendezvous system used by the U.S.S.R. is described in general by Legostaev [1968] and Laurie [1982]. This system employs a radar on the chase spacecraft and a transponder beacon on the target spacecraft. Both spacecraft align themselves to the line of sight to the other spacecraft, thereby cancelling position-angle errors and two of the three attitude-angle errors. A supplementary sensor for roll-angle sensing is mentioned but not described. It should be noted that this system does not allow automatic rendezvous and docking with a passive or disabled spacecraft, since both spacecraft must have maneuvering capability.

Laser-Diode Radar

The R&D sensor concept developed by Laurie [1982] uses a laser-diode system to measure the ranges and angles to a set of three reflectors on the passive spacecraft. This concept is in general similar to that of Flom and Coombies [1974-1975], but uses more modern hardware.

The three reflectors are placed on a circle with a 1-m diameter. The laser-diode transmitter employs intensity modulation and electronic beam steering. Range is derived from the phase of the "tone" that modulates the transmitted signal. The receiver employs an image dissector, photomultiplier, and beam steering (for angle-of-arrival measurement).

The predicted range-measurement accuracy of this system is 15 mm (3σ) at ranges of 2 to 100 m, and 0.015 % of range thereafter. The corresponding range-rate accuracies are 0.01 and 0.1 m/s, respectively. The angle and angle-rate measurement accuracies are predicted to be 1.2 mrad (0.07°) and 0.1 mrad/s (0.006°), respectively. The system is designed to comply with the

requirements given in Table 1-1.

Ring of Lights

Dabney [1981] describes an R&D sensor based upon a ring of lights installed upon the target spacecraft. As viewed from the active spacecraft, the ring of lights forms an ellipse whose size, shape, and orientation depend upon the its position and attitude relative to the observer. A curve-fitting algorithm is used to extract position and attitude information from the observed image of the ring.

This system has a useful range of 3.2 m to 75 m; operation at shorter ranges is possible if the camera lens can be changed automatically to allow a larger field of view. Alternatively, a second, smaller ring of lights could be used. As the two spacecrafts become aligned, the symmetry of the pattern causes the roll angle to become indeterminate. However, this is not regarded as a serious problem and can easily be overcome by adding a light.

Three-Light Video System

An R&D sensor based upon a three-light array on the passive spacecraft is analyzed by Tietz and Kelly [1982]. Their analysis includes a simulation with a Kalman-filter estimator.

Individual lights must be identified; this can be accomplished by blinking upon radio command or by color. The light array weighs only 5 kg and has a volume of 0.02 m^3. The maximum linear dimension of this array appears to be about 1 m.

Updated estimates are provided at a 10-Hz rate. The accuracy is 3 % of range at 20 m and 47 percent of range at the maximum range of 300 m.

Relative position and attitude can also be measured by a technique based upon quasi-static (near-field) magnetic-dipole field patterns [Raab, 1979, 1981]. In this approach, a three-axis transmitter is placed on one spacecraft and a three-axis receiver is placed on the other spacecraft. The power requirements of this system limit its potential use to relatively short ranges (e.g., < 1 km). In addition, extensive calibration of the field patterns is required to compensate for the effects of the spacecraft.

In the late 1980s, the NAVSTAR Global Positioning System [Parkinson, 1980] will become operational. Precise position information will be available continuously, and coverage extends from the earth's surface into lower orbit altitudes. Several studies [Ellis, 1978] have shown that interferometric direction finding applied to two or more GPS satellites can provide a very accurate attitude measurement. However, considerable active circuitry is required on the passive spacecraft to enable relay of the GPS signals to the active spacecraft for processing and attitude determination. While the NAVSTAR/GPS should be a useful attitude reference for large, active spacecraft or stations, it does not appear to be an appropriate sensor for rendezvous and docking with a passive spacecraft.

1.4 OBJECTIVES OF STUDY

The polarized interferometer is not the only system capable of measuring both relative position and relative attitude. However, it has several potential advantages, including:

- Real-time operation,
- Accurate tracking at all ranges, and
- Operation unaffected by direct sunlight.

While the polarized interferometer has considerable potential, it is (to date) an untested concept. This report presents the results of a preliminary evaluation of the feasibility of the polarized-interferometer concept. The feasibility study comprises three principal areas of investigation:

- Development of position-and-attitude tracking filters and the determination of sensitivity parameters,
- Evaluation of various types of transponders suitable for the passive spacecraft, and
- Preliminary system design.

1.5 ORGANIZATION OF REPORT

This report is divided into 8 chapters.

Chapter 2 defines one-way and two-way coordinate frames, and the position and attitude variables that are used in the analyses in subsequent chapters. The locations of individual antenna elements on the host spacecraft are also specified.

An initialization algorithm for the polarized interferometer is presented in Chapter 3. This algorithm uses nonlinear estimators to determine unambiguous position and attitude estimates without the benefit of any *a priori* information.

Chapter 4 presents a minimum-variance linear tracking algorithm. This algorithm is segmented into individual minimum-variance linear estimators for range, forward direction, reverse direction, and relative roll. The sensitivities of the estimates to measurement errors are determined and plotted.

Minimization of the complexity and power consumption of the passive-spacecraft transponder is essential. Chapter 5 examines the feasibility of simple-repeater and nonlinear reflector concepts that make the transponder nearly passive. However, such techniques are shown to be suitable only for short-range operation.

Chapter 6 reviews frequency assignments, modulation techniques, and antenna elements for the passive-spacecraft transponder. Multiple-carrier CW transmissions from crossed-slot or crossed-dipole antennas are shown to

be preferable.

Multiple-carrier CW ranging is analyzed in Chapter 7. The dependence of range accuracy and the probability of ambiguity-resolution error upon SNR is determined.

Chapter 8 uses previously derived relationships and algorithms to develop and to simulate a polarized-interferometer system design. Candidate designs based upon carrier-frequency and difference-frequency tracking are developed. An RF simulation subroutine is developed and combined with the tracking algorithms to implement a system simulation. The results of simulated operation validate the system design and show the feasibility of the concept.

Chapter 9 summarizes the results and presents the conclusions of this study.

CHAPTER 2

COORDINATE DEFINITIONS

This chapter defines the position and attitude coordinate relationships used in the analysis of the polarized-interferometer system. Of the numerous possible definitions of attitude, the azimuth-elevation-roll convention is preferred here because of its direct correspondence to the angles measured by interferometric direction finding. However, no single coordinate frame is convenient for all aspects of rendezvous and docking, hence coordinate conversion is required in any case.

2.1 COORDINATE FRAMES

One-Way Coordinates

Figure 1-1 illustrates the use of standard "one-way" coordinates. Position can be defined in rectangular coordinates by the vector (x,y,z) or in polar coordinates by the three-tuple (α,β,ρ); the angles α and β are called position azimuth and position elevation. The relationships between the rectangular and polar coordinates are well known and are therefore not discussed here.

Attitude is specified by a set of three Euler angles in a particular sequence. The sequence shown in Figure 1-1 comprises attitude azimuth ψ_z, attitude elevation ψ_y, and roll ψ_x. The zero-attitude condition aligns the attitude of the target spacecraft with that of the active spacecraft. Note that in the zero-attitude condition, both spacecraft face the same direction, rather than each other.

Two-Way Coordinates

The two-way coordinate system shown in Figure 1-2 treats both spacecraft as equals. The position of the target spacecraft with respect to the active spacecraft is specified by two angles and range, as in one-way polar coordinates. However, the position of the active spacecraft with respect to the target spacecraft is similarly specified by range and two angles (α_2 and β_2) defined relative to the target spacecraft's own coordinate frame.

Position and attitude comprise six degrees of freedom. The two sets of position angles (α_1, β_1, α_2, and β_2) and range ρ account for five degrees of freedom. The relative roll angle ψ_r between the two coordinate frames in Figure 1-2 accounts for the sixth degree of freedom.

Relationship

Obviously, the one-way and two-way coordinates define the same six-degrees-of-freedom situation. The polar-coordinate form of the one-way position is identical to the two-way form of the position of the target spacecraft with respect to the active spacecraft. It is therefore apparent that the three-tuples (ψ_z, ψ_y, ψ_x) and $(\alpha_2, \beta_2, \psi_r)$ must provide equivalent attitude information. Thus the relative roll angle and the angular position of the active spacecraft with respect to the passive spacecraft are equivalent to specification of the attitude of the passive spacecraft with respect to the active spacecraft.

Two sets of attitude angles are most easily equated or converted through formation of a direction-cosine or *attitude* matrix $\boldsymbol{A}$. Individual rotations are combined by multiplying appropriate three-dimensional rotation matrices (Table 2-1) in the proper order [Raab, 1979, 1981; Thelander, 1965]. The attitude matrix in one-way coordinates is therefore

$$\boldsymbol{A} = \boldsymbol{T}_{\psi_x}\,\boldsymbol{T}_{\psi_y}\,\boldsymbol{T}_{\psi_z} =$$

$$\begin{bmatrix} \cos\psi_y \cos\psi_z & \cos\psi_y \sin\psi_z & -\sin\psi_y \\ -\cos\psi_x \sin\psi_z + \sin\psi_x \sin\psi_y \cos\psi_z & \cos\psi_x \cos\psi_z + \sin\psi_x \sin\psi_y \sin\psi_z & \sin\psi_x \cos\psi_y \\ \sin\psi_x \sin\psi_z + \cos\psi_x \sin\psi_y \cos\psi_z & -\sin\psi_x \cos\psi_z + \cos\psi_x \sin\psi_y \sin\psi_z & \cos\psi_x \cos\psi_y \end{bmatrix} \tag{2-1}$$

Note that the columns of $\boldsymbol{A}$ are the direction-cosine vectors corresponding to the axes of the target spacecraft coordinate frame.

Determining the form of the attitude matrix in two-way coordinates is somewhat more complicated. It is instructive to begin by setting the passive spacecraft at zero attitude (Figure 2-1) and noting the relationships among α_1, α_2, β_1, and β_2. When the attitudes of both spacecraft are the same, $\beta_2 = -\beta_1$ and $\alpha_2 = \pi + \alpha_1$. By starting with α_1 and working through the sequence of five rotations,

$$\boldsymbol{A} = \boldsymbol{T}_{\pi-\alpha_2}\,\boldsymbol{T}_{\beta_2}\,\boldsymbol{T}_{\psi_r}\,\boldsymbol{T}_{\beta_1}\,\boldsymbol{T}_{\alpha_1} \quad . \tag{2-2}$$

This expression can be expanded to obtain trigonometric expressions for the elements of $\boldsymbol{A}$; however, the results are too complicated to be of much use.

Conversion of two-way coordinates to one-way coordinates is achieved by calculating $\boldsymbol{A}$ from (2-2) and equating the result to (2-1). The one-way attitude angles are then obtained from

	Position	Attitude
Azimuth rotates X into Y	$T_\alpha = \begin{bmatrix} \cos\alpha & \sin\alpha & 0 \\ -\sin\alpha & \cos\alpha & 0 \\ 0 & 0 & 1 \end{bmatrix}$	$T_\psi = \begin{bmatrix} \cos\psi_z & \sin\psi_z & 0 \\ -\sin\psi_z & \cos\psi_z & 0 \\ 0 & 0 & 1 \end{bmatrix}$
Elevation rotates X into $-Z$	$T_\beta = \begin{bmatrix} \cos\beta & 0 & -\sin\beta \\ 0 & 1 & 0 \\ \sin\beta & 0 & \cos\beta \end{bmatrix}$	$T_\theta = \begin{bmatrix} \cos\psi_y & 0 & -\sin\psi_y \\ 0 & 1 & 0 \\ \sin\psi_y & 0 & \cos\psi_y \end{bmatrix}$
Roll rotates Y into $-Z$	$T_\gamma = \begin{bmatrix} 1 & 0 & 0 \\ 0 & \cos\gamma & \sin\gamma \\ 0 & -\sin\gamma & \cos\gamma \end{bmatrix}$	$T_\phi = \begin{bmatrix} 1 & 0 & 0 \\ 0 & \cos\psi_x & \sin\psi_x \\ 0 & -\sin\psi_x & \cos\psi_x \end{bmatrix}$

Notes: (1) $T_\alpha^{-1} = T_\alpha^T = T_{-\alpha}$, $T_\alpha T_\beta \neq T_\beta T_\alpha$, $T_{\beta'} T_{\beta''} = T_{\beta' + \beta''}$, etc.

(2) Position roll γ is used only as a dummy variable and does not define position or attitude.

(3) The matrices shown here rotate *coordinate frames*, not vectors. To rotate vectors, reverse the signs of the angles and the sequence of the rotations.

Table 2-1. Orthogonal rotation matrices.

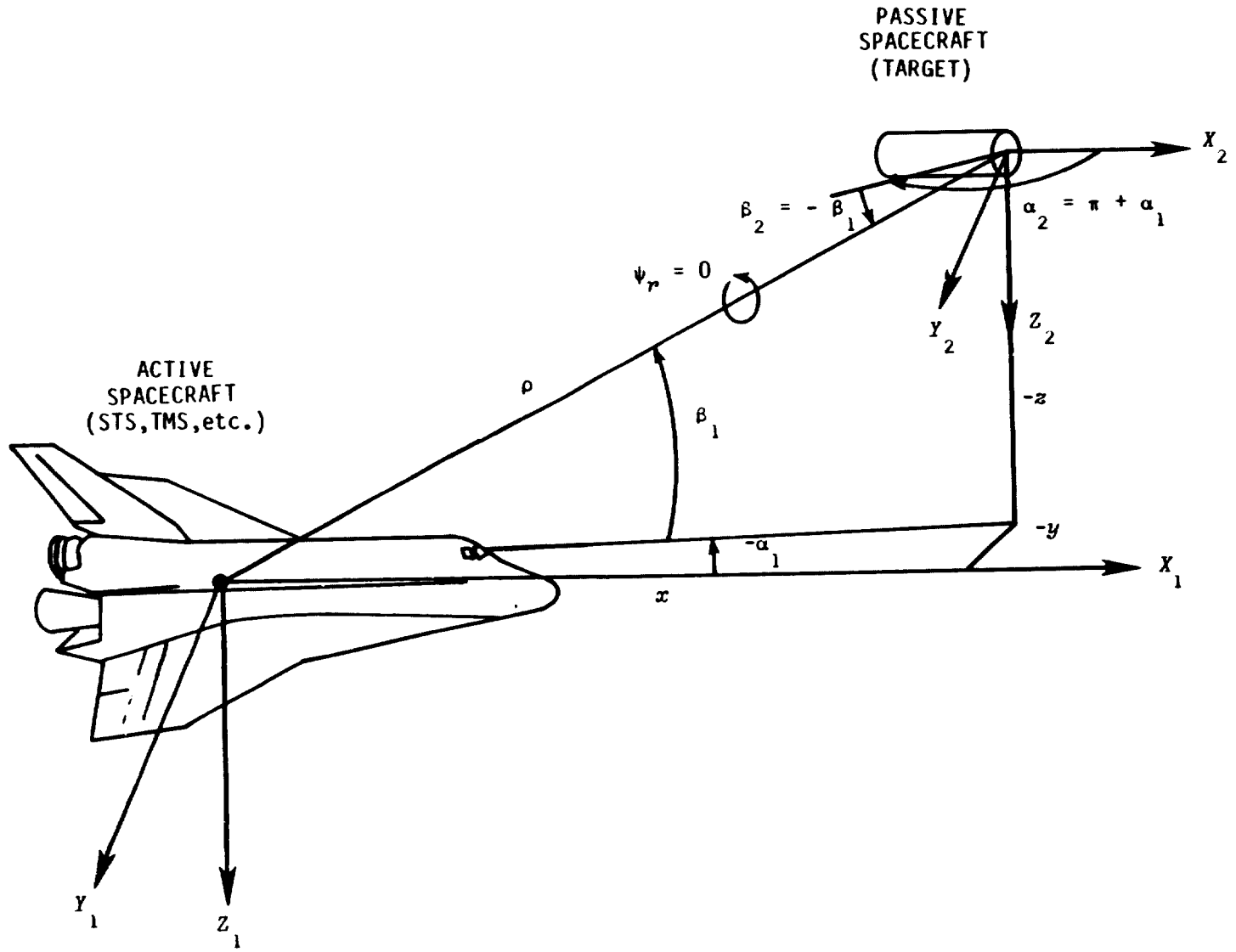

Figure 2-1. Zero attitude.

$$\psi_z = \arctan\ (A_{12}/A_{11}) \quad , \tag{2-3}$$

$$\psi_x = \arctan\ (A_{23}/A_{33}) \quad , \tag{2-4}$$

and

$$\psi_y = \arctan\ [(A_{13} \cos \psi_z)/A_{11}] \quad . \tag{2-5}$$

Using the ratio in (2-5) rather than arccos ψ_y eliminates common gain errors.

2.2 ANTENNA LOCATIONS

Antenna arrays are located in the Y-Z planes of the appropriate spacecraft, as shown in Figure 2-2. This geometry is consistant with the definition of zero attitude given in the previous section. Specific antenna-element locations and ranges are defined here for future reference.

Ranges

Each antenna array has four distinct elements; elements in the array on the active spacecraft are $\boldsymbol{a}_0$, $\boldsymbol{a}_1$, $\boldsymbol{a}_2$, and $\boldsymbol{a}_3$, while the elements in the array on the passive spacecraft are designated $\boldsymbol{p}_0$, $\boldsymbol{p}_1$, $\boldsymbol{p}_2$, and $\boldsymbol{p}_3$. A total of 16 different ranges are defined by the two sets of four elements. A particular range is designated $\rho_{m,n}$, where m is the element of the active array and n is the element of the passive array.

The principal spacecraft-to-spacecraft or array-to-array range measurement is $\rho_{0,0}$, which is the distance between the two common antenna elements. When ρ is used without subscripts or the term "range" is used without further qualification, it refers to $\rho_{0,0}$.

Coordinates of Antenna Elements

For present purposes, the three receiving elements of the active array are assumed to be spaced evenly in a circle of radius R_a. The common (transmitting) element is located at the center of the coordinate system, thus

$$\boldsymbol{a}_0(1) = [0,\ 0,\ 0]^T \quad . \tag{2-6}$$

The polarization-sensing element $\boldsymbol{a}_1$ is arbitrarily positioned on the negative Z_1 axis, thus its position vector in active-spacecraft coordinates is

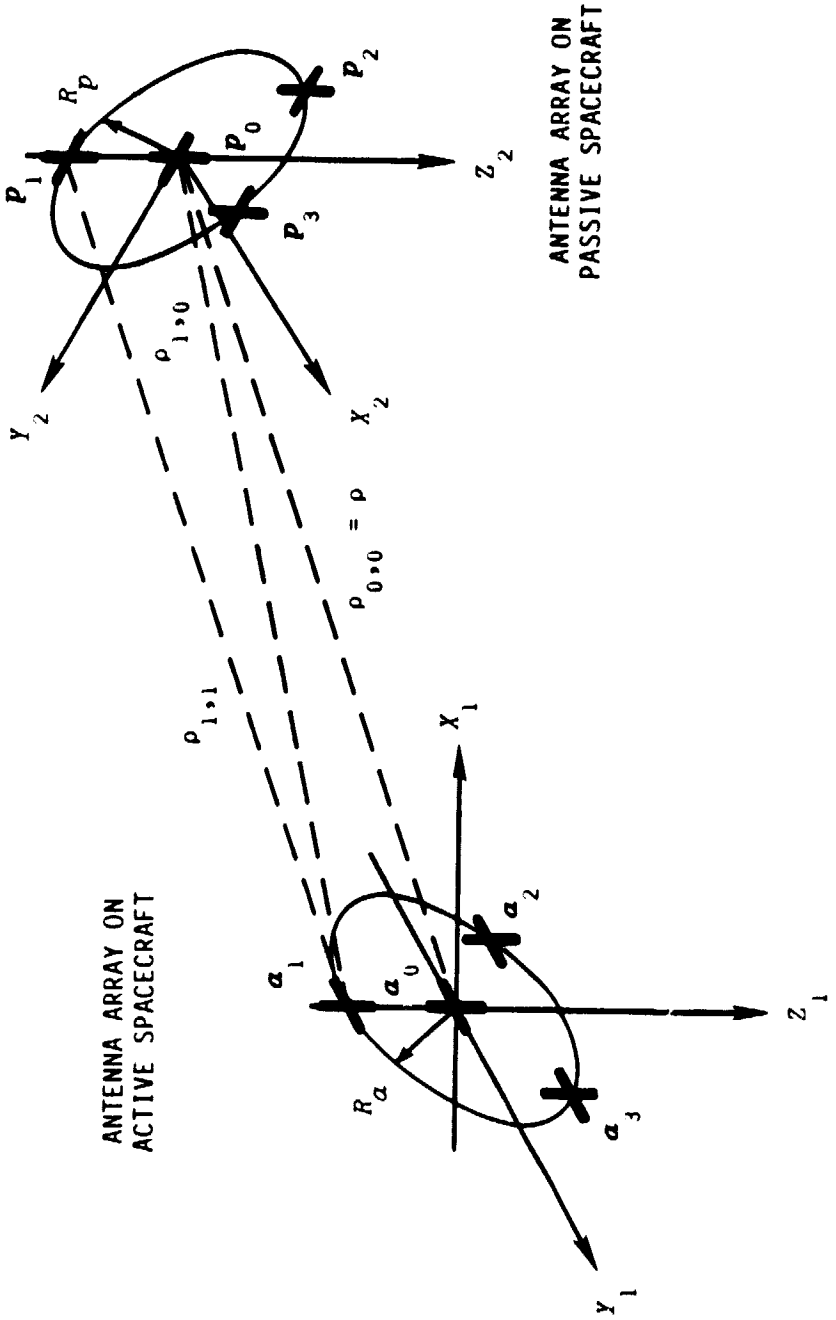

Figure 2-2. Antenna arrays.

$$a_1(1) = [0,\ 0,\ -1]^T R_a \quad . \tag{2-7}$$

The positions of circularly polarized elements A2 and A3 are then

$$\begin{aligned} a_2(1) &= [0,\ -\sin 120°,\ -\cos 120°]^T R_a \\ &= [0,\ -3^{1/2}/2,\ +1/2]^T R_a \\ &\cong [0,\ -0.866,\ +0.5]^T R_a \end{aligned} \tag{2-8}$$

and

$$a_3(1) = [0,\ +3^{1/2}/2,\ +1/2]^T R_a \quad . \tag{2-9}$$

The locations of the elements of the passive array are similarly defined. If R_p represents the radius of the passive array, then the locations of its elements in passive-spacecraft coordinates are

$$p_0(2) = [0,\ 0,\ 0]^T \tag{2-10}$$

$$p_1(2) = [0,\ 0,\ -1]^T R_p \tag{2-11}$$

$$p_2(2) = [0,\ -3^{1/2}/2,\ 1/2]^T R_p \tag{2-12}$$

and

$$p_3(2) = [0,\ +3^{1/2}/2,\ 1/2]^T R_p \quad . \tag{2-13}$$

CHAPTER 3

INITIALIZATION ALGORITHM

Systems such as the polarized interferometer may be required to acquire initial estimates of the target-spacecraft position and attitude with little or no *a priori* knowledge about the estimates. In such cases, it is often useful to use two distinct estimators. The first algorithm provides an unambiguous (but not necessarily minimum-variance) initial estimate. The second algorithm then tracks target-spacecraft position and attitude and provides minimum-variance estimates. The tracking algorithm is generally based upon Kalman-filter techniques, linearized system equations, and small changes in parameters. The initialization algorithm generally employs nonlinear and/or sorting techniques.

This chapter presents an initialization algorithm for the polarized interferometer. This algorithm is based upon four separate steps, which determine (in sequence):

- Range from round-trip timing,
- Target position angles by radio interferometry,
- Two target-attitude angles by reverse interferometry, and
- Roll angle from polarization.

The initialization algorithm is formulated under the assumption that the spacecraft-to-spacecraft distance is large in comparison to the diameters of the antenna arrays. This assumption results in parallel element-to-element paths. Consequently, differences in time of arrival are due to direction of arrival alone. This assumption is reasonable for the initialization algorithm, as the two spacecraft should be separated by a considerable distance when tracking is initiated.

3.1 RANGE

The first of the six parameters to be determined is range. In general, a measured two-way range has the form

$$R_{1,1} = \rho_{0,0} + \rho_{delay} + \rho_{1,1} \cong 2\rho_{0,0} + \rho_{delay} + \Delta\rho_{1\alpha} + \Delta\rho_{1p} \quad , \qquad (3\text{-}1)$$

where ρ_{delay} represents the delay introduced by the passive array. There are nine such measurements (Figure 2-2).

The path-length increments due to the directions of arrival at the active and passive arrays are represented by $\Delta\rho_{1\alpha}$ and $\Delta\rho_{1p}$, respectively. Let the direction of the passive array with respect to the active array be represented by unit vector $\boldsymbol{s}_{\alpha}$. The path-length increment at the active array (Figure 3-1) is obtained by projecting $\boldsymbol{s}_{\alpha}$ onto the antenna-element vector $\boldsymbol{\alpha}_1$, thus

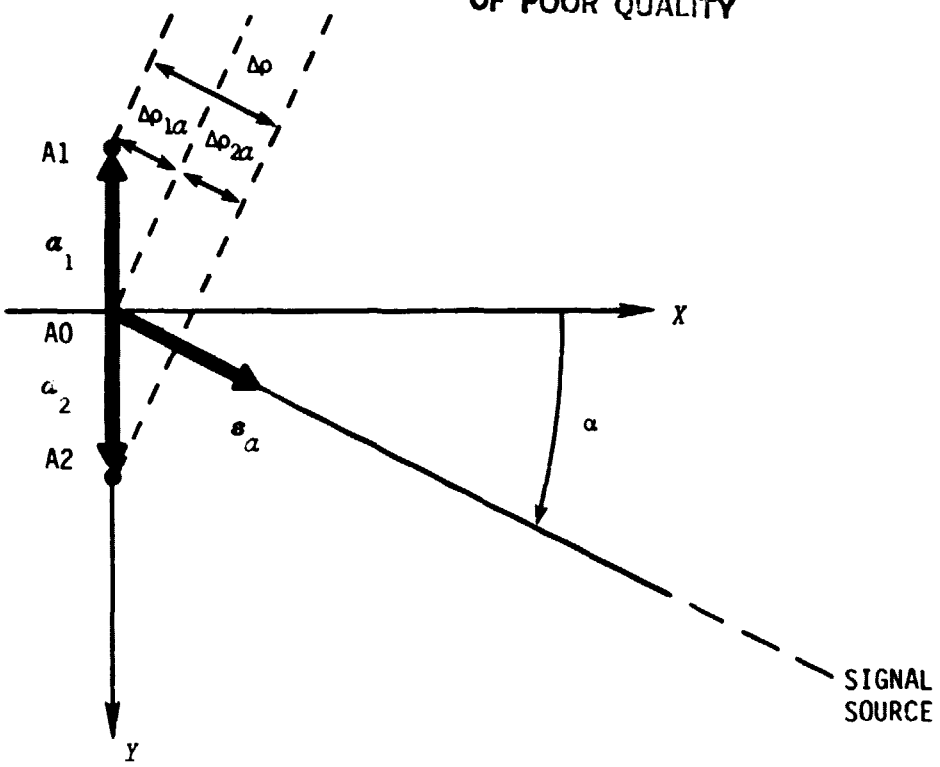

Figure 3-1. Two-element interferometer.

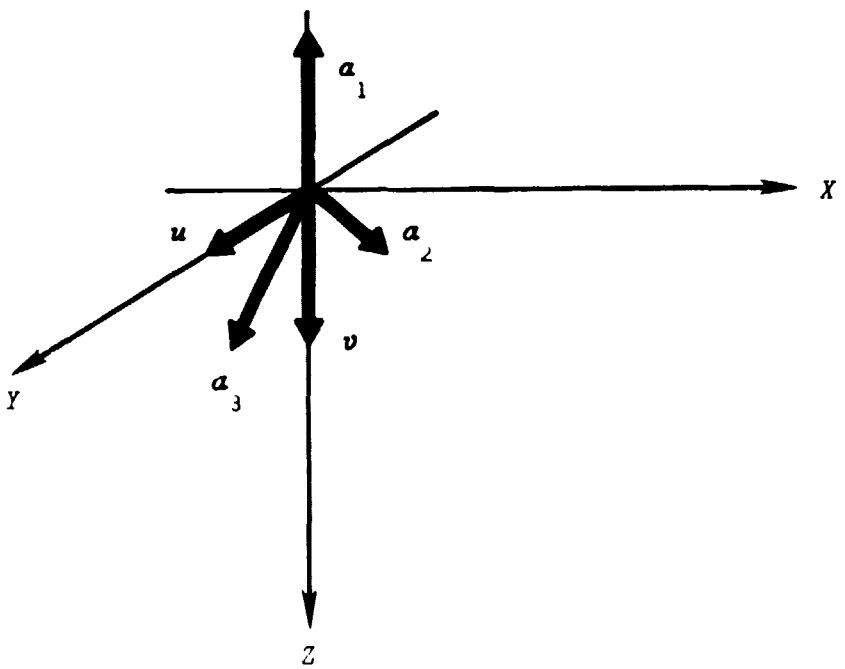

Figure 3-2. Unit vectors.

$$\Delta\rho_{1a} = \rho_{1,0} - \rho_{0,0} - \boldsymbol{a}_1^T \boldsymbol{s}_a \quad . \tag{3-2}$$

The sum of the three path-length increments at the active array is

$$\Delta\rho_{1a} + \Delta\rho_{2a} + \Delta\rho_{3a} = - \boldsymbol{a}_1^T \boldsymbol{s} - \boldsymbol{a}_2^T \boldsymbol{s} - \boldsymbol{a}_3^T \boldsymbol{s}_a$$

$$= - (\boldsymbol{a}_1 + \boldsymbol{a}_2 + \boldsymbol{a}_3)^T \boldsymbol{s}_a \quad . \tag{3-3}$$

For the symmetrical arrays envisioned for this system,

$$\boldsymbol{a}_0 = \boldsymbol{a}_1 + \boldsymbol{a}_2 + \boldsymbol{a}_3 = \boldsymbol{0} \quad , \tag{3-4}$$

hence

$$\Delta\rho_{1a} + \Delta\rho_{2a} + \Delta\rho_{3a} = 0 \quad . \tag{3-5}$$

Since the arrangement of the elements in the passive array is also symmetrical, a corresponding relationship holds for the path-length increments at the passive array.

The sum of the three distances measured from the same element of the passive array is therefore

$$R_{1,1} + R_{2,1} + R_{3,1} \cong 6\rho_{0,0} + 3\rho_{\text{delay}} \quad . \tag{3-6}$$

Rearrangement of (3-6) therefore yields the desired AO-PO distance

$$\rho = \rho_{0,0} = (R_{1,1} + R_{2,1} + R_{3,1} - 3\rho_{\text{delay}})/6 \quad . \tag{3-7}$$

Analogously, all nine range measurements should be averaged to provide greater accuracy.

3.2 DIRECTION FINDING

Interferometric direction finding is based upon the relationship between the path-length increment and the direction of arrival. Most modern radio interferometers do not actually add the signals from the various elements to produce an interference pattern. Instead, the phases of each output are measured and processed digitally to determine the angle(s) of arrival.

Two-Element Interferometer

It is instructive to begin by analyzing the two-element interferometer shown in Figure 3-1. From (3-2), the path-length increment between elements A1 and A2 is

$$\Delta\rho = \Delta\rho_{1a} - \Delta\rho_{2a} = (\boldsymbol{a}_1 - \boldsymbol{a}_2)^T \boldsymbol{s}_a \quad . \tag{3-8}$$

It is convenient to define the baseline vector as

$$\boldsymbol{b} = \boldsymbol{a}_1 - \boldsymbol{a}_2 \quad , \tag{3-9}$$

which simplifies (3-8) to

$$\Delta\rho = \boldsymbol{b}^T \boldsymbol{s} = |\boldsymbol{b}| \sin\alpha \quad . \tag{3-10}$$

The difference between the phases of the outputs from elements A1 and A2 is therefore

$$\Delta\phi = 2\pi \Delta\rho/\lambda + 2\pi k \quad , \tag{3-11}$$

where

λ is the wavelength of the signal and k is an "ambiguity constant" that maps ϕ into the range $0 \leq \phi < 2\pi$. If the phase ambiguity is properly resolved, the angle of arrival α is obtained from

$$\hat{\alpha} = \arcsin(\Delta\rho/|\boldsymbol{b}|) = \arcsin(\lambda \Delta\phi/2\pi|\boldsymbol{b}|) \quad . \tag{3-12}$$

Three-Element Interferometer

Determination of both the azimuth and elevation angles of arrival requires a minimum of three interferometer antenna elements. Consider first the direction of arrival at the active array. The applicable information is the set of three ranges from the receiving elements of the active array to the common element of the passive array. For example,

$$\rho_{1,0} \cong (\rho_{1,1} + \rho_{1,2} + \rho_{1,3})/3 \quad , \tag{3-13}$$

where

$$\rho_{1,1} = \phi_{1,1} \lambda_1/2\pi \quad . \tag{3-14}$$

The equations developed in the previous subsection can be used directly to determine the angles of arrival with respect to the three baselines of the arrays (Figure 2-2). However, since the baselines are not necessarily aligned with the coordinate axes, the baseline angles are neither readily used nor readily manipulated.

Equations (3-8) - (3-10) suggest that the path-length increment for a desired baseline (e.g., one aligned with the coordinate axes) can be synthesized from the path-length increments for the real baselines. Figure 3-2 defines the unit vectors aligned with the Y_1 and Z_1 axes as

$$\boldsymbol{u} = [0, 1, 0]^T \tag{3-15}$$

and

$$\boldsymbol{v} = [0, 0, 1]^T \quad . \tag{3-16}$$

From the array-geometry definitions given by (2-7), (2-8), and (2-9),

$$\boldsymbol{u} = (\boldsymbol{a}_3 - \boldsymbol{a}_2)/(3^{1/2} R_a) \tag{3-17}$$

and

$$\boldsymbol{v} = (\boldsymbol{a}_2 + \boldsymbol{a}_3 - 2\,\boldsymbol{a}_1)/(3 R_a) \quad . \tag{3-18}$$

The y and z components of unit vector $\boldsymbol{s}_a$ are its projections onto the Y_1 and Z_1 axes. From (3-17),

$$s_{ay} = \boldsymbol{u}^T \boldsymbol{s}_a = [\boldsymbol{a}_3^T \boldsymbol{s}_a - \boldsymbol{a}_2^T \boldsymbol{s}_a]/(3^{1/2} R_a) \tag{3-19}$$

$$= [-\Delta\rho_{3a} + \Delta\rho_{2a}]/(3^{1/2} R_a) \tag{3-20}$$

$$= [(\rho_{1,0} - \rho_{3,0}) - (\rho_{1,0} - \rho_{2,0})]/(3^{1/2} R_a) \tag{3-21}$$

$$= [\rho_{2,0} - \rho_{3,0}]/(3^{1/2} R_a) \quad . \tag{3-22}$$

Similarly, use of (3-18) yields

$$s_{az} = \boldsymbol{v}^T \boldsymbol{s}_a = (\boldsymbol{a}_2 + \boldsymbol{a}_3 - 2\boldsymbol{a}_1)^T \boldsymbol{s}/(3 R_a) \tag{3-23}$$

$$= (2\rho_{1,0} - \rho_{2,0} - \rho_{3,0})/(3 R_a) \quad . \tag{3-24}$$

Since $\boldsymbol{s}_a$ is a unit vector, the magnitude of its x component is obtained from

$$s_{ax}^2 = 1 - s_{ay}^2 - s_{az}^2 \quad . \tag{3-25}$$

Proper orientation of $\boldsymbol{s}_a$ (Figure 3-2) requires that $s_{ax} < 0$. From intuition or by analogy to the top row of the $\boldsymbol{A}$ matrix (2-1),

$$\boldsymbol{s}_a = \begin{bmatrix} \cos\beta_1 \cos\alpha_1 \\ \cos\beta_1 \sin\alpha_1 \\ -\sin\beta_1 \end{bmatrix} \quad . \tag{3-26}$$

The azimuth and elevation angles of arrival are now obtained by equating (3-26) to the components given by (3-22), (3-24), and/or (3-25).

Direction Finding at Passive Array

Techniques analogous to those developed above are used to determine the direction-of-arrival angles α_2 and β_2 at the passive array. Under the as-

sumption of a large array-to-array distance, the distances from the transmitting element A0 to the three elements of the passive array have forms such as

$$\rho_{0,1} \cong (\rho_{1,1} + \rho_{2,1} + \rho_{3,1})/3 \quad , \tag{3-27}$$

which is analogous to (3-13).

A unit vector $\boldsymbol{\varepsilon}_p$ that points from the passive array to the active array is defined by analogy to $\boldsymbol{\varepsilon}_a$. The projections of $\boldsymbol{\varepsilon}_p$ onto the passive-array Y_2 and Z_2 axes are [by analogy to (3-22), (3-24), and (3-25)]

$$\varepsilon_{py} = (\rho_{0,2} - \rho_{0,3})/(3^{1/2} R_p) \quad , \tag{3-28}$$

$$\varepsilon_{pz} = (2\rho_{0,1} - \rho_{0,2} - \rho_{0,3})/(3 R_p) \quad , \tag{3-29}$$

and

$$\varepsilon_{px}^2 = 1 - \varepsilon_{py}^2 - \varepsilon_{pz}^2 \quad . \tag{3-30}$$

In this case, $\varepsilon_{px} < 0$ causes $\boldsymbol{\varepsilon}_p$ to point toward the active array under conditions that allow signal reception. Angles α_2 and β_2 are found by analogy to (3-26).

3.3 ROLL

The remaining unknown, relative roll ψ_r, is determined from signal polarization. Relevant information is imbedded in the four amplitude measurements corresponding to the two linearly polarized transmitting elements in the passive array and the two linearly polarized receiving elements in the active array. It is necessary to determine the direction of arrival angles α_1, β_1, α_2, and β_2 *prior* to determining the roll angle.

The far-field coupling between two electrically short dipoles is determined entirely by their relative orientation and the distance separating them. Consequently, it is convenient to formulate the coupling relationships in terms of rotations by the position and attitude angles. Modified forms of these relationships can be used with longer antennas, provided their patterns are known.

Let the moment of a particular dipole in element P1 of the passive array be represented by vector $\boldsymbol{v}(2)$, which is defined in *passive-array* coordinates. The field vector observed at the active array is then the same vector $\boldsymbol{v}(1)$ converted into *active-array* coordinates. The relationship between $\boldsymbol{v}(1)$ and $\boldsymbol{v}(2)$ is obtained by applying the same rotation matrices used in (1-1) to define attitude matrix $\boldsymbol{A}$, thus

$$\boldsymbol{v}(1) = G\, \boldsymbol{T}_{-\alpha_1}\, \boldsymbol{T}_{-\beta_1}\, \boldsymbol{F}\, \boldsymbol{T}_{-\psi_r}\, \boldsymbol{T}_{-\beta_2}\, \boldsymbol{T}_{-\alpha_2}\, \boldsymbol{v}(2) \quad . \tag{3-31}$$

Above, the absence of a radial far-field component is accounted for by the matrix

$$\boldsymbol{F} = \begin{bmatrix} 0 & 0 & 0 \\ 0 & 1 & 0 \\ 0 & 0 & 1 \end{bmatrix} \quad , \tag{3-32}$$

and G represents the combined effect of receiver gain, antenna pattern, and path loss. In terms of one-way position and attitude parameters, the coupling relationship is given [Raab, 1979, 1981] by

$$\begin{aligned} \boldsymbol{v}(1) &= \boldsymbol{T}_{-\alpha_1}\, \boldsymbol{T}_{-\beta_1}\, \boldsymbol{F}\, \boldsymbol{T}_{\beta_1}\, \boldsymbol{T}_{\alpha_1}\, \boldsymbol{T}_{-\psi_z}\, \boldsymbol{T}_{-\psi_y}\, \boldsymbol{T}_{-\psi_x}\, \boldsymbol{v}(2) \\ &= \boldsymbol{T}_{-\alpha_1}\, \boldsymbol{T}_{-\beta_1}\, \boldsymbol{F}\, \boldsymbol{T}_{\beta_1}\, \boldsymbol{T}_{\alpha_1}\, \boldsymbol{A}^T\, \boldsymbol{v}(2) \quad . \end{aligned} \tag{3-33}$$

Element A1 of the active array includes two orthogonal, linearly polarized elements, and can therefore sense only the Y_1 and Z_1 components of the incident signal. Element P1 of the passive array includes two orthogonal linearly polarized elements that may be represented by

$$\boldsymbol{u}(2) = [0,\ G_u,\ 0]^T \tag{3-34}$$

and

$$\boldsymbol{v}(2) = [0,\ 0,\ G_v]^T \quad , \tag{3-35}$$

where G_u and G_v represent the processing gains of the two channels in the passive array.

The four available measurements are more than sufficient to determine the single unknown parameter ψ_r. However, the presence of matrix $\boldsymbol{F}$ in (3-31) results in a degenerate set of three-dimensional equations and precludes solution by matrix inversion.

Formulation of the coupling relationships in the tracking coordinate frame (Figure 3-3) leads to a soluble two-dimensional set of equations. First, assemble the two passive-array excitation vectors into the 3 × 2 matrix

$$\boldsymbol{W}(2) = [\boldsymbol{u}(2) \,\vdots\, \boldsymbol{v}(2)] \quad . \tag{3-36}$$

The equivalent in tracking-frame coordinates is given by

$$\boldsymbol{W}(0) = [\boldsymbol{u}(0) \,\vdots\, \boldsymbol{v}(0)] = \boldsymbol{F}\, \boldsymbol{T}_{-\psi_r}\, \boldsymbol{T}_{-\beta_2}\, \boldsymbol{T}_{-\alpha_2}\, \boldsymbol{W}(2) = \boldsymbol{Q}\, \boldsymbol{W}(2) \quad . \tag{3-37}$$

This pair of vectors can then be converted further into active-array coordi-

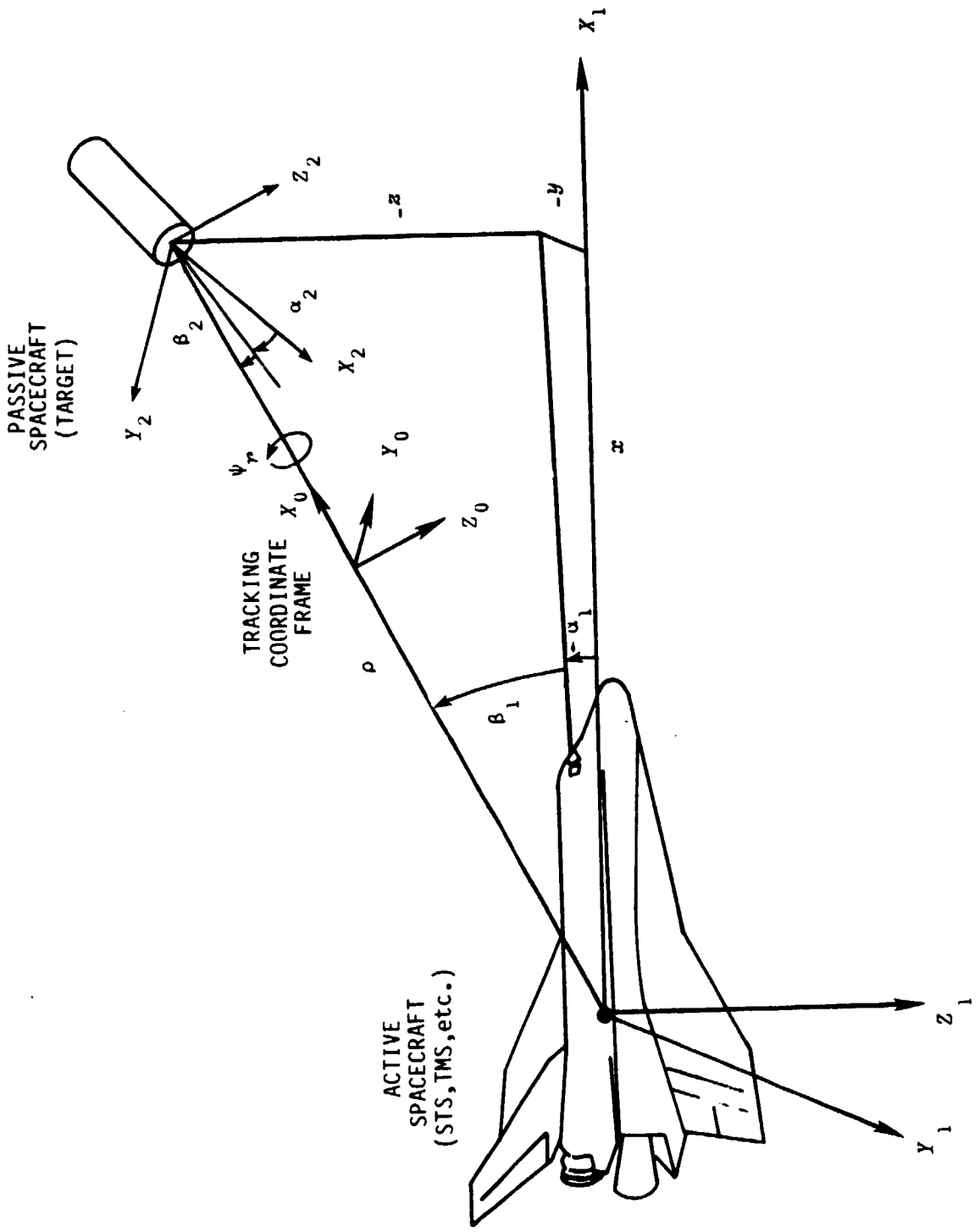

Figure 3-3. Tracking coordinate frame.

nates, thus

$$\boldsymbol{W}(1) = [\boldsymbol{u}(1) \vdots \boldsymbol{v}(1)] = G\, \boldsymbol{T}_{-\alpha_1}\, \boldsymbol{T}_{-\beta_1}\, \boldsymbol{W}(0) = G\, \boldsymbol{P}\, \boldsymbol{W}(0) \quad . \tag{3-38}$$

Equations (3-36) and (3-37) form the basis of the solution. The next step is to synthesize tracking-frame measurements from active-array measurements. This is not a simple coordinate conversion problem, since the x coordinates are either unobservable or identically zero. From Table 2-1,

$$\boldsymbol{P} = \boldsymbol{T}_{-\alpha_1}\, \boldsymbol{T}_{-\beta_1} = \begin{bmatrix} \cos\beta_1 \cos\alpha_1 & -\sin\alpha_1 & \sin\beta_1 \cos\alpha_1 \\ \cos\beta_1 \sin\alpha_1 & \cos\alpha_1 & \sin\beta_1 \sin\alpha_1 \\ -\sin\beta_1 & 0 & \cos\beta_1 \end{bmatrix} \quad . \tag{3-39}$$

The effects of the first row are unobservable, and the first column has no effect since it always acts upon the radial component of the signal, which is zero.

The lower, right four elements relate the measurements to the tracking-frame vectors. For example,

$$u_y(1) = (\cos\alpha_1)\, u_y(0) + (\sin\beta_1 \sin\alpha_1)\, u_z(0) \tag{3-40}$$

and

$$u_x(1) = (\cos\beta)\, u_z(0) \quad . \tag{3-41}$$

The y and z components of tracking-frame vector $\boldsymbol{u}(0)$ are therefore obtained from the measured components of $\boldsymbol{u}(1)$ by

$$u_z(0) = u_z(1)/\cos\beta_1 \tag{3-42}$$

and

$$u_y(0) = \frac{u_y(1) - (\sin\beta_1 \sin\alpha_1)\, u_z(0)}{\cos\alpha_1} \quad . \tag{3-43}$$

Analogous relationships apply to $\boldsymbol{v}$.

The relationship between the tracking-frame vectors and the passive-array excitation vectors is imbedded in the $\boldsymbol{Q}$ matrix, defined in (3-36). By multiplication or by inspection of (2-1),

$$\boldsymbol{Q} = \boldsymbol{F}\, \boldsymbol{T}_{-\psi_r}\, \boldsymbol{T}_{-\beta_2}\, \boldsymbol{T}_{-\alpha_2}$$

$$= \begin{bmatrix} 0 & 0 & 0 \\ * & \cos\psi_r \cos\alpha_2 & -\sin\psi_r \cos\beta_2 \\ & -\sin\psi_r \sin\beta_2 \sin\alpha_2 & \\ * & \sin\psi_r \cos\alpha_2 & \cos\psi_r \cos\beta_2 \\ & +\cos\psi_r \sin\beta_2 \sin\alpha_2 & \end{bmatrix} , \qquad (3\text{-}44)$$

where the asterisks represent unneeded elements. Premultiplying $W(2)$ by Q yields relationships among the four scalar variables:

$$u_y(0) = (\cos\psi_r \cos\alpha_2 - \sin\psi_r \sin\beta_2 \sin\alpha_2)\, G_u , \qquad (3\text{-}45)$$

$$u_z(0) = (\sin\psi_r \cos\alpha_2 + \cos\psi_r \sin\beta_2 \sin\alpha_2)\, G_u , \qquad (3\text{-}46)$$

$$v_y(0) = (-\sin\psi_r \cos\beta_2)\, G_v , \qquad (3\text{-}47)$$

and

$$v_z(0) = (\cos\psi_r \cos\beta_2)\, G_v . \qquad (3\text{-}48)$$

It is evident that the roll angle is now given by

$$\psi_r = \arctan[-v_y(0)/v_z(0)] . \qquad (3\text{-}49)$$

This is an especially desirable relationship, since it requires knowledge of neither β_2 nor G_v, and should therefore not be affected by errors in those variables. Note that the signals corresponding to vector $u(2)$ in the passive array are not necessary. However, they may prove useful in reducing the sensitivity of the tracking filter at certain attitudes.

It is interesting to note that if G_v is known, β_2 can be determined from the polarization measurements alone; i.e.,

$$\beta_2 = \begin{cases} \arccos[-v_y(0)/G_v \sin\psi_r] \\ \arccos[v_z(0)/G_v \cos\psi_r] \end{cases} . \qquad (3\text{-}50)$$

Given ψ_r and β_2, (3-44) and (3-45) can be solved for α_2. This suggests that a single linearly polarized element can suffice as the passive array. However, it is doubtfully desirable to eliminate the other elements of the passive array, since G_v may turn out to be somewhat variable, and errors in G_v lead

directly to errors in β_2, hence also α_2.

3.4 SIMULATION AND RESULTS

The validity of the algorithms developed above is verified by the simulation program listed in the Appendix. The algorithms were tested at an assortment of positions and attitudes. Proper operation was observed in all cases. Numerical errors are generally no larger than the fifth significant digit.

These tests verify the validity of the initialization algorithm. In addition, they verify the validity of the formulations used to develop the algorithm.

The initialization algorithm uses only signals from the Z-oriented linearly polarized element of the passive array. It therefore appears possible to simplify the passive array by eliminating one of the two proposed linearly polarized elements. However, sensitivity analysis (Chapter 4) shows that use of both elements is desirable.

CHAPTER 4

MINIMUM-VARIANCE TRACKING ALGORITHM

An algorithm for making initial estimates of target-spacecraft position and azimuth is described in Chapter 3. That algorithm uses nonlinear functions to produce unambiguous estimates, and requires no *a priori* information on the target-spacecraft parameters.

However, nonlinear estimators do not ensure optimum blending of all available information, and may even accentuate noise under certain conditions. Consider, for example,

$$\hat{y} = (x + \varepsilon)^{1/2} \quad , \tag{4-1}$$

and suppose $\varepsilon = 0.01$. If $x = 1$, $\Delta y = 0.005$. However, if $x = 0$, $\Delta y = 0.1$, which represents a factor-of-ten amplification of the error.

In contrast, a minimum-variance linear estimator (MVLE) blends all available information into the best possible estimate of the unknown parameters. For a Gaussian-noise environment, an MVLE is the best of all possible estimators (linear and nonlinear) with respect to both minimum-squared-error (minimum-variance) and maximum-likelihood criteria [Nahi, 1969; Monzingo, 1980]. It is therefore desirable to include such an estimator in the tracking algorithm for the polarized interferometer.

The Kalman filter [Brown, 1983] is a recursive type of MVLE based upon a state-space model of system (in this case, spacecraft) dynamics. Kalman filters make full use of known interrelationships between position, velocity, and acceleration, and are therefore widely used in navigation and tracking systems. However, a Kalman filter is effective only when the system model is accurate; a Kalman filter with an inaccurate system model may produce poorer estimates than a simple MVLE that has no provision at all for dynamics. In general, Kalman filters are used to estimate parameters such as gyro drift (that have stable statistics), rather than position and velocity (whose statistics may vary at the whim of a pilot).

The polarized interferometer may be used with a number of different chase and target spacecraft. Neither the spacecraft, their dynamics, nor their guidance/control algorithms had been specified at the time of this study. It is therefore preferable to implement an MVLE algorithm that estimates position and attitude only. At some later date, a Kalman filter can be developed to process the MVLE output to extract position, velocity, attitude, and attitude rate.

4.1 MVLE THEORY

The theory behind minimum-variance linear estimators can be found in a number of texts [Nahi, 1969; Monzingo, 1980; Brown, 1983]. For a Gaussian-noise environment, the form of the MVLE can be derived either by minimizing the squared estimation error or by maximizing the log-likelihood function.

For estimation of a scalar from several uncorrelated measurements, the MVLE simply amounts to an inverse-variance weighting of the measurements.

The polarized-interferometer system measures a set of ranges and field amplitudes that are related to target-spacecraft position and attitude through a system of nonlinear equations. The use of an MVLE in a nonlinear system requires linearization of the system equations in the vicinity of the estimate. The nonlinear position-and-attitude estimator (Chapter 3) provides initial estimates suitable for this purpose.

The MVLE for a linearized system deals with small changes in the measurements and small changes in the estimates. The general form of the MVLE for a linearized system is

$$\hat{\boldsymbol{x}}(k) = \hat{\boldsymbol{x}}(k - 1) + \Delta\hat{\boldsymbol{x}} \quad , \tag{4-2}$$

where $\hat{\boldsymbol{x}}(k)$ is the vector of estimates at sample k. The estimated change in the estimate vector from one sample to the next is

$$\Delta\hat{\boldsymbol{x}} = \boldsymbol{B}\ \Delta\boldsymbol{y} \quad , \tag{4-3}$$

where $\boldsymbol{B}$ is the *blending matrix* and

$$\Delta\boldsymbol{y} = \boldsymbol{y}(k) - \boldsymbol{y}(k - 1) \tag{4-4}$$

is the sample-to-sample change in the measurements vector $\boldsymbol{y}(k)$.

The blending matrix is obtained from the product of three matrices:

$$\boldsymbol{B} = \boldsymbol{H}\ \boldsymbol{G}^T\ \boldsymbol{L}^{-1} \quad . \tag{4-5}$$

Above, the error-covariance matrix $\boldsymbol{H}$ is given by

$$\boldsymbol{H} = (\boldsymbol{G}^T\ \boldsymbol{L}^{-1}\ \boldsymbol{G})^{-1} \quad , \tag{4-6}$$

where

$$\boldsymbol{L} = \mathrm{E}[\boldsymbol{n}\ \boldsymbol{n}^T] \tag{4-7}$$

is the covariance of additive measurement noise $\boldsymbol{n}$ and

$$\boldsymbol{G} = \begin{bmatrix} \partial y_1/\partial x_1 & \partial y_1/\partial x_2 & \cdots \\ \partial y_2/\partial x_1 & \partial y_2/\partial x_2 & \\ & \cdots & \partial y_M/\partial x_N \end{bmatrix} \tag{4-8}$$

contains the set of gradients of the measurements with respect to the parameters to be estimated at the point of linearization. Matrix $\boldsymbol{G}$ is a generalization of the gradient vector, and $M > N$. The same estimates can be obtained by formulating N scalar MVLEs that act upon the same M-element meas-

urement vector y.

4.2 MVLE IMPLEMENTATION

The parameters to be estimated include:

- Three position-coordinate changes,
- Three attitude increments, and
- Two excitation factors.

The first six parameters represent changes in the desired position and attitude information. The two excitation factors [Λ_u and Λ_v in (3-34) and (3-35)] are not useful *per se*. However, they enter into the amplitude-coupling relations and are unknown, and must therefore be estimated if the roll angle is to be estimated accurately.

A straightforward "brute-force" implementation of the MVLE would follow the form given in Section 4.1. The measurement vector y would comprise the nine range measurements and four amplitude measurements. The incremental estimate vector Δx would comprise three position increments, three attitude increments, and two excitation factors. Position would be tracked as a vector, while attitude would be tracked as either a quaternion or a direction-cosine (attitude) matrix. The estimated position vector would be updated by simple addition, while the attitude matrix or quaternion would be updated by suitable multiplications [Farrel, 1976; Tietz, 1982]. The G matrix would be determined by numerical calculations, using the previously derived range and coupling equations (Chapter 2).

The brute-force approach is theoretically sound. However, it is subject to practical computation problems due to the greatly differing magnitudes of the different parameters (position coordinates, attitude angles, and excitation factors) to be estimated. Furthermore, the radial component of position error is very small in comparison to the cross-track component of position error. Even if the brute-force approach were implemented with double- or quadruple-precision computations, the linearization problem discussed subsequently would prevent it from working properly.

The solution is to implement separate MVLEs for each group of similar quantities; i.e.,

- Range,
- DF from the active array,
- DF from the passive array,
- Roll, and
- Excitation factors.

Each individual MVLE is applied in sequence and improves the estimate available to the next individual MVLE, as shown in Figure 4-1. This approach simplifies the computations somewhat, since smaller matrices must be inverted, and offers a limited degree of redundancy. It is interesting to note that a similar approach is often taken in integrated navigation filtering when in-

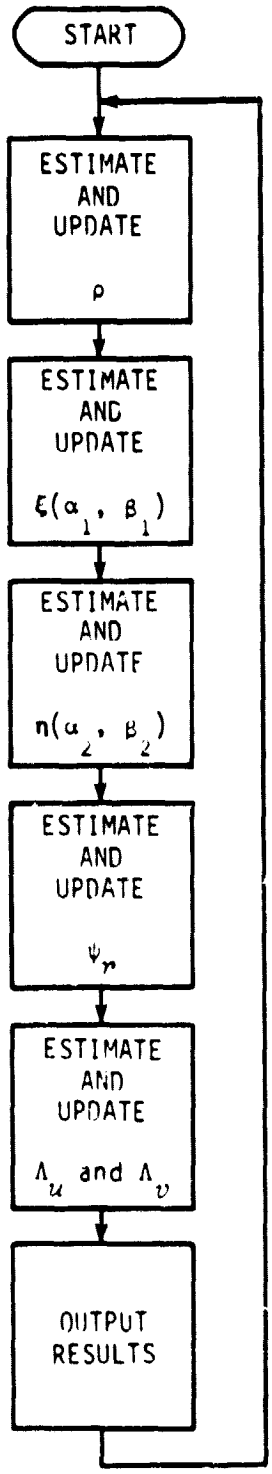

Figure 4-1. MVLE tracking filter.

puts are obtained from a variety of different sensors, some of which are not always available.

The characteristics of the individual estimators are described below. The specific implementations of the estimators can be found in the Appendix.

Range Estimator

The range MVLE estimates the scalar $\Delta\rho$ from the set of nine changes in the nine element-to-element range measurements. Its form follows Section 4.1 exactly, except that some parameters (e.g., covariance) are scalars.

For ranges of 10 km or more, this estimator can be implemented as a fixed linear average of all nine range measurements, as in the initialization algorithm (Chapter 3). However, at shorter distances, the small errors introduced by this approximation degrade DF accuracy. At very short distances (e.g., < 10 m), the use of true gradients improves the accuracy of the range estimate considerably.

Direction-of-Arrival Estimator

The direction of the passive array with respect to the active array is represented and tracked as the unit vector ξ. Tracking the direction angles α_1 and β_1 themselves is difficult and undesirable because of singularities in the coordinate-frame conversions [Raab, 1979].

It is desirable to estimate the components of position error that are orthogonal to the direction vector ξ, since range error has previously been estimated (and now is presumably very small). This is accomplished by estimating local changes $\Delta\alpha$ and $\Delta\beta$ in the direction of arrival. The MVLE output vector therefore has the form

$$\Delta\hat{\boldsymbol{x}} = [\Delta\hat{\alpha},\ \Delta\hat{\beta}]^T \quad . \tag{4-9}$$

Updating of the direction vector is then accomplished by incremental rotation:

$$\hat{\xi}(k) = \boldsymbol{T}_{-\Delta\beta}\ \boldsymbol{T}_{-\Delta\alpha}\ \xi(k-1) \quad . \tag{4-10}$$

Incremental rotation matrices can be obtained by applying small-angle assumptions to the matrices of Table 2-1, thus

$$\boldsymbol{T}_{-\Delta\beta}\ \boldsymbol{T}_{-\Delta\alpha} = \begin{bmatrix} 0 & -\Delta\alpha & \Delta\beta \\ \Delta\alpha & 0 & 0 \\ -\Delta\beta & 0 & 0 \end{bmatrix} \quad . \tag{4-11}$$

After using a rotation based upon the small-angle assumption, it is essential to normalize ξ to unit length. In general, use of the small-angle assumption followed by normalization requires less computation time than does a large-

angle rotation.

The gradient matrix is computed by dithering ξ and differencing the predicted measurements with those of the undithered ξ. Dithering of ξ is accomplished by incrementally azimuth or elevation rotations. For example, a positive incremental local-azimuth rotation is accomplished by

$$\xi' = \boldsymbol{T}_{-\Delta\alpha}\, \xi \quad . \tag{4-12}$$

The elements of $\boldsymbol{G}$ are then determined from

$$\frac{\partial y_i}{\partial \alpha} \cong \frac{y_i(\rho\xi') - y_i(\rho\xi)}{\rho\Delta\alpha} \tag{4-13}$$

or an analogous form for $\Delta\beta$.

The direction-finding MVLE was first implemented using a $\boldsymbol{y}$ vector comprised of all nine individual range measurements. Its performance was satisfactory if there was no error in the initial estimate of attitude. However, given such errors, convergence was slow, and in many cases, the combined algorithm (Figure 4-1) settled on erroneous values of direction and attitude (e.g., $\alpha_1 = 5°$ and $\psi_z = 5°$ instead of $\alpha_1 = 10°$ and $\psi_z = 0°$). This problem was found to be inherent in the linearization process and therefore unavoidable.

Obviously, it is possible to estimate both position and attitude correctly, since the initialization algorithm does so. The solution for the MVLE algorithm is to form three linear sums of the nine measurements, as is done for the initialization algorithm [e.g., (3-13)]. These sums greatly suppress the effects of attitude, thereby decoupling attitude and position effects and allowing the MVLE to operate properly. Since the estimates of angular error are based upon gradients, allowance is automatically made for operation at short ranges (in contrast to the initialization algorithm).

Reverse Direction-of-Arrival Estimator

Tracking of the direction (α_2, β_2) of the active array with respect to the passive array is completely analogous to tracking of the passive array with respect to the active array. In fact, the same software subroutine is used.

The direction of the active array with respect to the passive array is represented by unit vector η, which is analogous to ξ. Through simple geometric analogies, it can be shown that

$$\eta = -\boldsymbol{A}'\, \xi \quad , \tag{4-14}$$

where

$$A' = T_{-\psi_x} T_{-\psi_y} T_{-\psi_z} \tag{4-15}$$

is the attitude of the active array with respect to the passive array. The computation in (4-15) can be avoided by applying selective sign reversal to the elements of A.

The only required modification to the MVLE algorithm is a reordering of the nine range measurements prior to condensation into three pseudo-measurements. The reordering is accomplished by treating them as a 3 × 3 matrix and taking their transpose.

Roll Estimator

The roll MVLE estimates scalar ψ_r from the set of changes in the four amplitude measurements. The angle is tracked directly, and provision is made for mapping the updated estimate back into the range $-\pi \leq \psi_r < +\pi$. Since only one angle is tracked in this algorithm, there are no singularities due to coordinate-frame conversion.

The roll MVLE is similar to that of Section 4.1 and the previous MVLEs in most respects. To avoid cross-coupling of roll and direction effects, roll increments must be introduced in the proper sequence when predicting coupling. Thus by analogy to (3-31),

$$W(1) = C\,W(2) = G\,T_{-\hat{\alpha}_1}\,T_{-\hat{\beta}_1}\,F\,T_{\hat{\psi}_r + \Delta\psi_r}\,T_{\hat{\beta}_2}\,T_{\hat{\alpha}_2}\,W(2) \quad . \tag{4-16}$$

Excitation Constants

The excitation constants Λ_u and Λ_v are related to the total power re-radiated by the two linearly polarized elements of the passive array. Since these parameters are unknown and vary as the position and attitude change, they must be tracked along with position and attitude.

The MVLE for the excitation constants has the form described in Section 4.1. In contrast to the previous estimators, the gradient matrix for this estimator is easily computed analytically. Let the excitation in (4-16) be

$$W(2) = \begin{bmatrix} 0 & 0 \\ \Lambda_u & 0 \\ 0 & \Lambda_v \end{bmatrix} \quad . \tag{4-17}$$

The derivatives of the amplitude measurements (i.e., the amplitude gradients) with respect to Λ_u and Λ_v are then simply

$$\frac{\partial \boldsymbol{W}(1)}{\partial \Lambda_u} = \begin{bmatrix} 0 & 0 \\ C_{22} & 0 \\ C_{23} & 0 \end{bmatrix} \tag{4-18}$$

and

$$\frac{\partial \boldsymbol{W}(1)}{\partial \Lambda_v} = \begin{bmatrix} 0 & 0 \\ 0 & C_{23} \\ 0 & C_{33} \end{bmatrix} . \tag{4-19}$$

Convergence

In all cases, satisfactory convergence is obtained when the angular error does not exceed 45°. Usually, no more than 2 iterations are required to reduce the error to the level of round-off errors. In many cases, the algorithm converges (with a few more iterations) when the error is as large as 80°. The MVLE for range converges in spite of factor-of-ten errors in the range estimate.

Implementation

FORTRAN subroutines for the MVLE tracking algorithm are listed in the Appendix as part of the simulation program. An estimator for the excitation factors is not implemented as it is of little use at this stage of development. However, such an estimator will be required in any operational system.

mplementation of a MVLE tracking algorithm for the polarized interferometer is indeed a difficult problem. Operation at ranges up to 100 km necessitates the use of double-precision arithmetic in all range-related computations, since centimeter errors in range difference can produce significant DF errors. In addition, the use of true gradients is necessary for operation at short ranges where the antenna-to-antenna paths become nonparallel.

Nonetheless, considerable simplification of the algorithm for an operational implementation should be possible. Direction angles can be derived from range difference rather than range; doing so should eliminate the requirement for many of the double-precision computations. In the present implementation, all gradients are computed numerically, and are recomputed every time they are needed. Considerable time savings (perhaps half) can be achieved by eliminating redundant calculations of the same gradient. Furthermore, it may be possible to derive analytic forms for the gradients that are computationally advantageous to numerical techniques.

A crude estimate of velocity can be obtained by differencing adjacent

position vectors. Similarly, a crude estimate of attitude rates can be obtained by multiplying the current attitude matrix by the transpose (inverse) of the previous attitude matrix and extracting incremental attitude angles from the results. Given information about spacecraft dynamics, a Kalman filter can be implemented to smooth the successive velocity and attitude-rate estimates.

4.3 SENSITIVITY ANALYSIS

Designing a polarized-interferometer system requires knowledge of the sensitivity of its estimates to measurement noise. The desired sensitivity parameters are the estimate variances and covariances. These are conveniently produced by the MVLE algorithms.

Two sensitivity-analysis programs were implemented. These programs use the set of subroutines listed in the Appendix. The program determines the sensitivity parameters as functions of a roll angle ϕ and an off-boresight angle θ, as shown in Figure 4-2. The results show that the roll angle ϕ does not significantly affect the sensitivity parameters.

The range variance is independent of direction and roll, and virtually independent of range. The variance of the range error is therefore

$$V_1 = \mathrm{Var}[\tilde{\rho}] = \sigma_y^2/36 \cong 0.278\ \sigma_y^2 \quad , \tag{4-20}$$

where σ_y^2 is the variance of an individual range measurement. The factor 36 is due to averaging nine measurements that vary twice as fast as the parameter being estimated.

The total variance V_2 of the direction-finding error is three times the trace of the covariance matrix H for that estimator. A plot of V_2 as a function of the off-boresight angle is shown in Figure 4-3. This curve fits the relationship

$$V_2 \cong 0.4448\ \sigma_y^2/\cos^2\theta \quad , \tag{4-21}$$

which is the same as that for a two-element interferometer.

The DF variance is given in squared radians. For an array diameter of 1 m and $\rho > 10$ m, V_2 is nearly independent of distance and the attitude of the other array. The same relationship applies to both passive and active arrays if the baseline lengths are the same.

The roll-angle sensitivity V_4 relates the amplitude-measurement error variance to the roll-angle error variance. It is based upon a normalized maximum amplitude measurement of unity and can therefore easily be used to determine the required SNR. The variation of V_4 with α_1 is shown in Figure

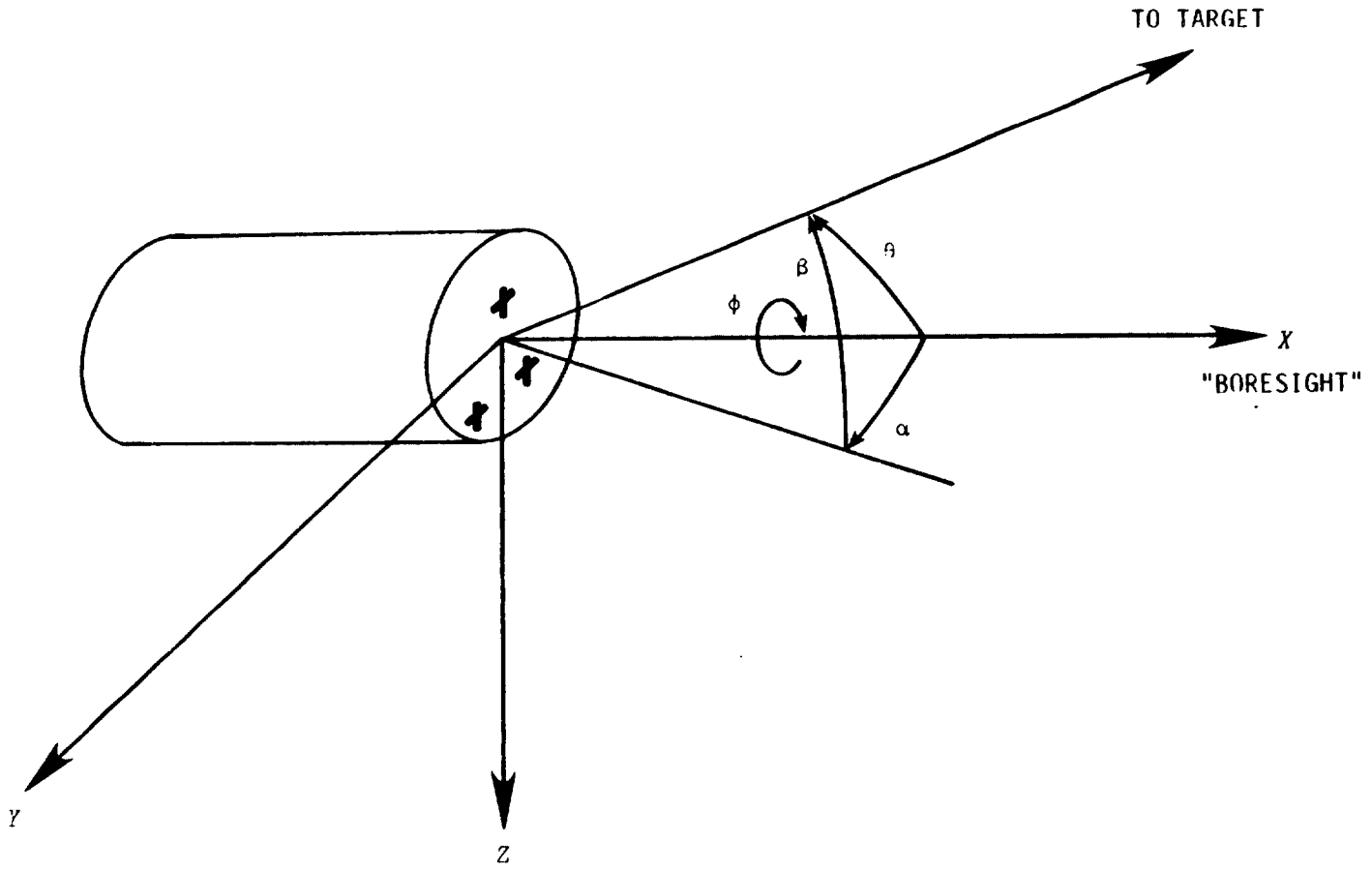

Figure 4-2. Boresight definition.

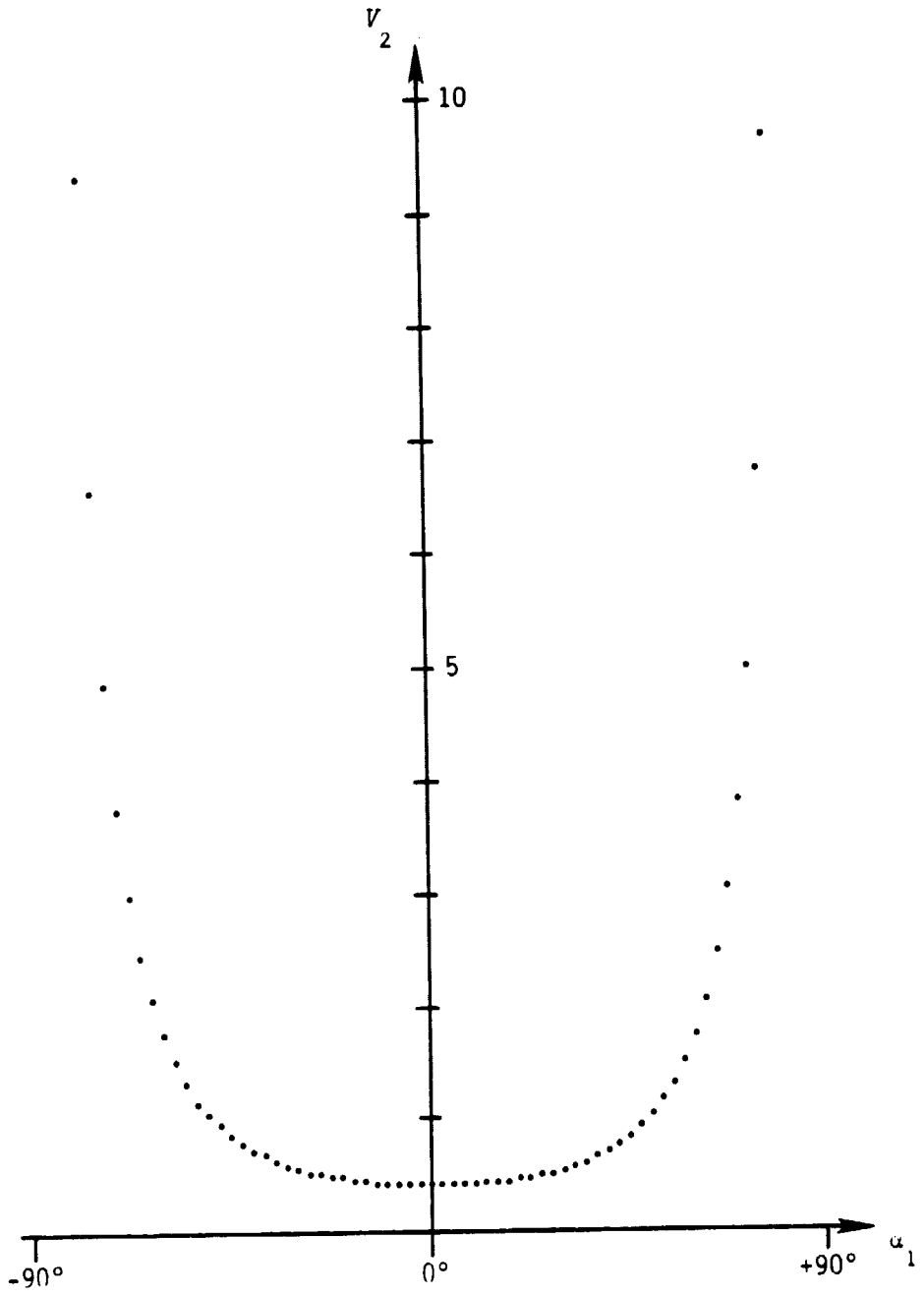

$\alpha_2 = 180°$, $\beta_1 = \beta_2 = 0°$, $\psi_n = 0°$

Figure 4-3. DF sensitivity.

4-4 for several values of α_2. The value of V_4 remains below 2.0 as long as one or the other off-boresight angle is 45° or less. As both off-boresight angles approach 90°, the two arrays face away from each other and the error sensitivity becomes infinite.

Given a good signal-to-noise ratio, relative roll can be determined from only two amplitude measurements, corresponding to the signal from only one of the elements of the passive array. However, if one element of the passive array were eliminated, situations could arise in which both of the remaining amplitude measurements have a poor SNR. Therefore both linearly polarized elements should be retained.

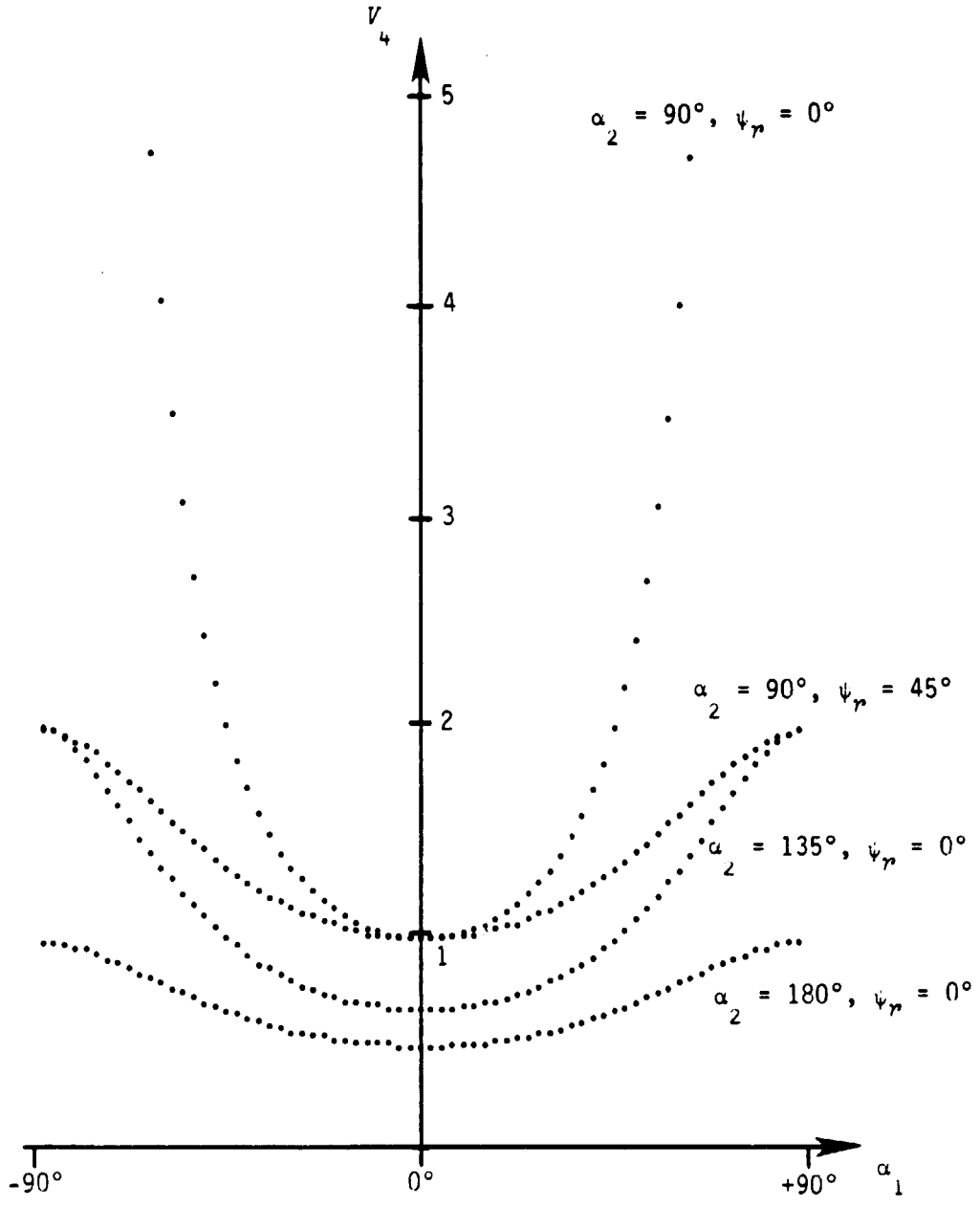

Figure 4-4. Roll sensitivity.

CHAPTER 5

TRANSPONDER CONCEPTS

The active spacecraft is powered and is assumed to be capable of supporting a relatively complex electronic system if necessary. However, the passive spacecraft may be unpowered and may offer little or no support for on-board electronic systems. The failure of systems on board the passive spacecraft may, in fact, be the reason for the rendezvous. Minimization of the complexity and power requirements of the passive-spacecraft transponder is therefore essential.

5.1 APPROACHES

A variety of conventional receiver and transmitter circuits can, of course, be used in the passive-spacecraft transponder. The objective of this chapter is to evaluate the possibility of implementing a passive or almost-passive transponder for the passive spacecraft. Two candidate approaches are:

- Simple repeater
- Nonlinear reflector.

The simple repeater (Figure 5-1) consists of a local oscillator, mixer, and suitable bandpass filters at its input and output. The filters must be wide enough to allow for anticipated Doppler shifts. Obviously, some power is required for the oscillator. Numerous options are possible, including adding gain at the input and/or output. Multiplexing of signals from the four antenna elements is accomplished by using similar circuits to drive all antennas simultaneously but on different frequencies.

The nonlinear reflector (Figure 5-2) employs bandpass filters and a nonlinear device such as a diode or FET; power may or may not be necessary. When signals are received from the active spacecraft on frequencies corresponding to the input filters, the nonlinear device generates and reradiates a signal on the difference frequency corresponding to the output filter. Multiplexing is accomplished by employing four such systems with different input-frequency pairs; the active-spacecraft transponder can thus select reradiation from a particular antenna element by transmitting on a particular pair of frequencies.

Pseudonoise modulation may be impressed on the signals to facilitate ranging and separation of the returned signal from interference. If both signals transmitted to a nonlinear reflector are biphase modulated with the same PN code, the returned signal is an unmodulated carrier. If the signals from the active-spacecraft transponder are modulated with different codes of the same length, the returned signal is itself modulated with a unique PN code. The product code [Gold, 1967] modulating the return signal has a low cross correlation product with either of the codes on the two forward signals and thereby facilitates reception in the presence of IMD products from the active-spacecraft transponder transmitter.

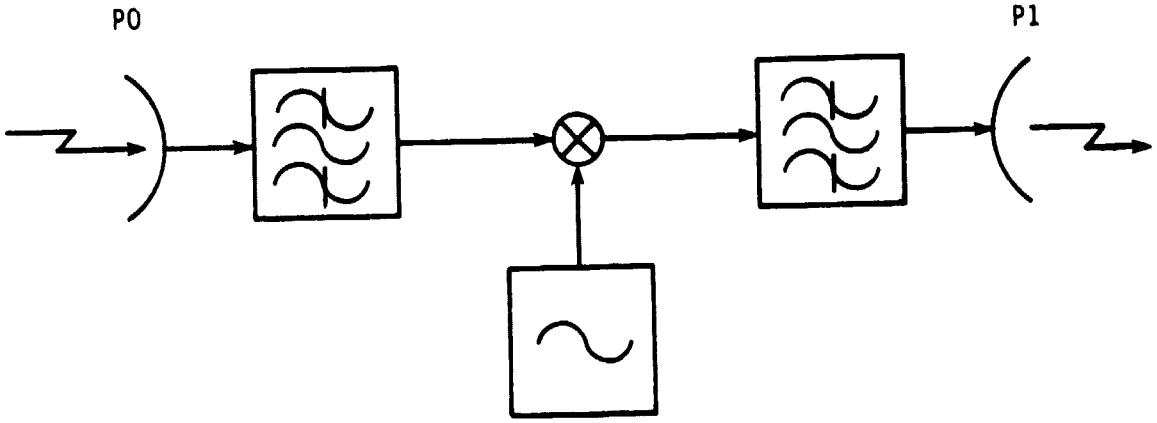

Figure 5-1. Simple repeater.

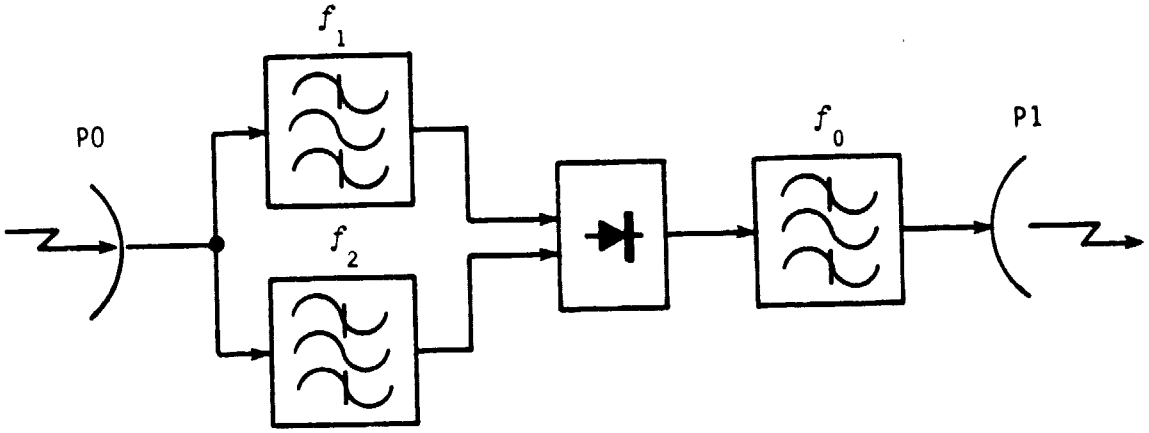

Figure 5-2. Nonlinear reflector.

5.2 MIXER CONSIDERATIONS

Both the simple-repeater and nonlinear-reflector approach mix two signals to produce a third signal that is returned to the active spacecraft. This section therefore develops a two-signal model for mixing noisy, modulated signals. This model is used to derive relationships among input and output signal-to-noise ratios (SNRs), and these relationships are then used in preliminary link calculations.

Low-power mixers suitable for use in the passive-spacecraft transponder include FETs, diodes, and BJTs. The analysis presented subsequently derives the noiseless mixing characteristics of both square-law devices (FETs) and exponential-characteristic devices (diodes and BJTs).

Signals

The input signal to the nonlinear device can (in the absence of noise) be represented by

$$v_i(t) = s_0 + s_1(t) + s_2(t) \quad , \tag{5-1}$$

where s_0 is a dc bias. The signals from the active-spacecraft transponder are

$$s_1(t) = a_1 \, m_1(t) \cos(\omega_1 t + \phi_1) \tag{5-2}$$

and

$$s_2(t) = a_2 \, m_2(t) \cos(\omega_2 t + \phi_2) \quad , \tag{5-3}$$

where a_1 and a_2 represent signal amplitudes and $m_1(t)$ and $m_2(t)$ represent the biphase PN modulation.

Range information is imbedded in code timing and the carrier phases ϕ_1 and ϕ_2. Since biphase modulation is assumed, $m_1 = \pm 1$ and $m_2 = \pm 1$, hence $m_1^2 = m_2^2 = 1$.

Square-Law Characteristic

The square-law characteristic of most FETs can be represented by

$$v_o = c \, v_i^2 \quad . \tag{5-4}$$

Note that bias is included as part of v_i.

Insertion of (5-1) and then (5-2) into (5-4) yields

$$v_o = c(s_0^2 + s_1^2 + s_2^2 + 2\,s_0 s_1 + 2\,s_0 s_2 + 2\,s_1 s_2) \tag{5-5}$$

$$\begin{aligned} = c\{&[s_0^2 + a_1^2/2 + a_2^2/2] \\ &+ [a_1 a_2\, m_3(t) \cos(\Delta\omega t + \Delta\phi)] \\ &+ [2\,s_0 a_1\, m_1(t) \cos(\omega_1 t + \phi_1) + 2\,s_0 a_2\, m_2(t) \cos(\omega_2 t + \phi_2)] \\ &+ [\,a_1^2/2 \cos(2\,\omega_1 t + 2\,\phi_1) + a_2^2/2 \cos(2\,\omega_2 t + 2\,\phi_2) \\ &\quad + a_1 a_2\, m_3(t) \cos((\omega_1 + \omega_2)t + (\phi_1 + \phi_2))]\} \quad , \end{aligned} \tag{5-6}$$

where

$$m_3 = m_1(t)\, m_2(t) \quad , \tag{5-7}$$

$$\Delta\omega = \omega_1 - \omega_2 \quad , \tag{5-8}$$

and

$$\Delta\phi = \phi_1 - \phi_2 \quad . \tag{5-9}$$

The four bracketed terms in (5-6) represent dc, the desired difference-frequency signal, input-frequency signals, and double-input-frequency signals. These products are similar to those of a true multiplier, and all unwanted products are well removed in frequency from the desired difference-frequency product. Because of their "clean" spectral characteristics, square-law devices are highly desirable for use as mixers [Krauss, 1980].

Exponential Characteristic

Mixers implemented from diodes and bipolar junction transistors are characterized [Krauss, 1980; Clarke, 1971] by an exponential relationship between their instantaneous input and output signals:

$$v_o = c \exp(q\, v_i/k\, T) \quad . \tag{5-10}$$

To analyze the use of such devices as mixers, it is convenient to factor (5-9) after insertion of (5-1), thus

$$v_o = c \exp(q\, s_0/k\, T) \exp(q\, s_1/k\, T) \exp(q\, s_2/k\, T) \quad . \tag{5-11}$$

Now let

$$x_1 = q\, a_1\, m_1(t)/k\, T = y_1\, m_1(t) \quad . \tag{5-12}$$

The third factor in (5-10) thus becomes [Krauss, 1980; Clarke, 1971]

$$\exp[x_1 \cos(\omega_1 t + \phi_1)] = I_0(x_1) + 2 \sum_{n=1}^{\infty} I_n(x_1) \cos(n\,\omega_1 t + n\,\phi_1) \quad , \tag{5-13}$$

where

$$I_n(x) = \sum_{k=0}^{\infty} \frac{x^{n+2k}}{2^{n+2k}\, k!\, \Gamma(n + k + 1)} \tag{5-14}$$

is a modified Bessel function of the first kind [Wylie, 1960, p. 418].

Since $2k$ is always even,

$$I_n(x_1) = \begin{cases} m_1(t)\, I_n(y_1), & n \text{ odd} \\ I_n(y_1), & n \text{ even} \end{cases} \quad . \tag{5-15}$$

Combination of (5-14), (5-12), and (5-10) yields

$$\begin{aligned} v_o = {} & c \exp[q\, s_0/k\, T] \\ & \cdot[I_0(y_1) + 2m_1(t)\, I_1(y_1) \cos(\omega_1 t + \phi_1) + 2I_2(y_1) \cos(2\omega_1 t + 2\phi_1) + \ldots] \\ & \cdot[I_0(y_2) + 2m_2(t)\, I_1(y_2) \cos(\omega_2 t + \phi_2) + 2I_2(y_2) \cos(2\omega_2 t + 2\phi_2) + \ldots]. \end{aligned} \tag{5-16}$$

Examination of (5-15) yields much useful information about the spectral output of an exponential-characteristic mixer:

- The desired return-signal modulation $m_3(t)$ is present only in products of two odd-order terms.
- The desired difference frequency is produced only by the product of two first-order terms.

Certain high-order products do produce signals whose frequencies (e.g., $\omega_1 - m\Delta\omega$, $\omega_2 - m\Delta_2$) are near that of the desired return signal. However, the amplitudes of the signals from the active-spacecraft transponder are relatively small, and small-signal operation of the mixer can be assumed. The amplitudes of such spurious mixer products should therefore make them negligible.

5.3 MIXING OF NOISY NARROWBAND SIGNALS

The spectral products produced by both square-law and exponential-characteristic mixers have been derived in the previous section. In either case, the signal of interest is produced primarily by the term that multiplies the two input signals. The portion of the mixing process that is of interest is therefore

$$v_0(t) = v_1(t)\, v_2(t) \quad . \tag{5-17}$$

Since the noisy input signals can be characterized as narrowband processes, they are represented here by

$$v_1(t) = a_1\, m_1(t) \cos(\omega_1 t + \phi_1) + n_{1c}(t) \cos(\omega_1 t) + n_{1s}(t) \sin(\omega_1 t) \tag{5-18}$$

and

$$v_2(t) = a_2\, m_2(t) \cos(\omega_2 t + \phi_2) + n_{2c}(t) \cos(\omega_2 t) + n_{2s}(t) \sin(\omega_2 t) \quad , \tag{5-19}$$

where a_1 and a_2 represent signal amplitudes, $m_1(t)$ and $m_2(t)$ represent modulation, and n_{1c}, n_{1s}, n_{2c}, and n_{2s} represent narrowband Gaussian noise. To simplify the analysis, the time dependences and carrier phases are dropped, thus the input signals become

$$v_1 = (a_1\, m_1 + n_{1c}) \cos \omega_1 t + n_{1s} \sin \omega_1 t \tag{5-20}$$

and

$$v_2 = (a_2\, m_2 + n_{2c}) \cos \omega_2 t + n_{2s} \sin \omega_2 t \quad . \tag{5-21}$$

Since $m_1(t)$ and $m_2(t)$ represent pseudonoise modulation, their values are either +1 or -1, and do not affect signal power. The power in signal #1 is therefore

$$P_{s_1} = a_1^2/2 \quad . \tag{5-22}$$

The in-phase and phase-quadrature noises are statistically independent and of equal power, hence the noise power accompanying signal #1 is

$$P_{n_1} = \sigma_{n_{1c}}^2/2 + \sigma_{n_{1s}}^2/2 = \sigma_{n_{1c}}^2 = \sigma_{n_{1s}}^2 = \sigma_{n_1}^2 \quad . \tag{5-23}$$

The resultant signal-to-noise ratio (SNR) for signal #1 is therefore

$$R_1 = a_1^2/(2\,\sigma_{n_1}^2) \quad . \tag{5-24}$$

By analogy, the SNR for signal #2 is

$$R_2 = a_2^2/(2\,\sigma_{n_2}^2) \quad . \tag{5-25}$$

Mixer Products

Substitution of (5-20) and (5-21) into (5-17) produces the mixer products

$$\begin{aligned} v_0 = {} & (a_1 m_1 + n_{1c})(a_2 m_2 + n_{2c}) \cos \omega_1 t \cos \omega_2 t \\ & + (a_1 m_1 + n_{1c})\, n_{2s} \cos \omega_1 t \sin \omega_2 t \\ & + n_{1s}(a_2 m_2 + n_{2c}) \sin \omega_1 t \cos \omega_2 t \\ & + n_{1s}\, n_{2s} \sin \omega_1 t \sin \omega_2 t \quad . \end{aligned} \tag{5-26}$$

Multiplication of the trigonometric functions produces

$$\begin{aligned} v_0 = {} & \frac{1}{2}(a_1 a_2 m_1 m_2 + a_2 n_{1c} m_2 + a_1 n_{2c} m_1 + n_{1c} n_{2c} + n_{1s} n_{2s}) \cos \Delta\omega t \\ & + \frac{1}{2}(-a_1 m_1 n_{2s} - n_{1c} n_{2s} + a_2 m_2 n_{1s} + n_{1s} n_{2c}) \sin \Delta\omega t \\ & + \text{h.f. terms}, \end{aligned} \tag{5-27}$$

where $\Delta\omega = \omega_1 - \omega_2$. For notational simplicity, the individual terms are denoted as nine quantities according to

$$\begin{aligned} v_0 = {} & \frac{1}{2}(q_1 + q_2 + q_3 + q_4 + q_5) \cos \Delta\omega t + \frac{1}{2}(q_6 + q_7 + q_8 + q_9) \sin \Delta\omega t \\ & + \text{h.f. terms}. \end{aligned} \tag{5-28}$$

Output Signal-to-Noise Ratio

The q_1 term in (5-28) represents the desired output signal, and its power is

$$P_{s_0} = P_{q_1} = \frac{1}{8} a_1^2 a_2^2 = \frac{1}{2} P_{s_1} P_{s_2} \quad . \tag{5-29}$$

The power in each of the four signal × noise terms in (5-28) is

$$P_{q_2} = P_{q_8} = \frac{1}{8} a_2^2 \sigma_{n_1}^2 = \frac{1}{4} P_{s_2} P_{n_1} \tag{5-30}$$

and

$$P_{q_3} = P_{q_6} = \frac{1}{8} a_1^2 \sigma_{n_2}^2 = \frac{1}{4} P_{s_1} P_{n_2} \quad . \tag{5-31}$$

Similarly, the power in each of the four noise × noise terms in (5-28) is

$$P_{q_4} = P_{q_5} = P_{q_6} = P_{q_7} = \frac{1}{2} \sigma_{n_1}^2 \sigma_{n_2}^2 = \frac{1}{2} P_{n_1} P_{n_2} \quad . \tag{5-32}$$

Since both the signal × noise terms and noise × noise terms represent noise corrupting the output signal, the total noise output power is

$$P_{n_0} = \frac{1}{4} P_{s_1} P_{n_2} + \frac{1}{4} P_{s_2} P_{n_1} + 2 P_{n_1} P_{n_2} \quad . \tag{5-33}$$

The output SNR is given by the ratio of (5-29) and (5-33), thus

$$R_0 = \frac{2 P_{s_1} P_{s_2}}{P_{s_1} P_{n_2} + P_{s_2} P_{n_1} + 2 P_{n_1} P_{n_2}} \tag{5-34}$$

$$= \frac{2 R_1 R_2}{R_1 + R_2 + 2} \quad . \tag{5-35}$$

If the two input SNRs are the same, $R_1 = R_2$, and

$$R_0 = \frac{R_1^2}{R_1 + 1} \quad . \tag{5-36}$$

This relationship between input and output SNR is graphed in Figure 5-3.

For both high and low input SNRs, (5-36) reduces to simple asymptotic relationships:

$$R_0 \cong \begin{cases} R_1 \ , & R_1 \gg 1 \\ R_1^2 \ , & R_1 \ll 1 \end{cases} \quad . \tag{5-37}$$

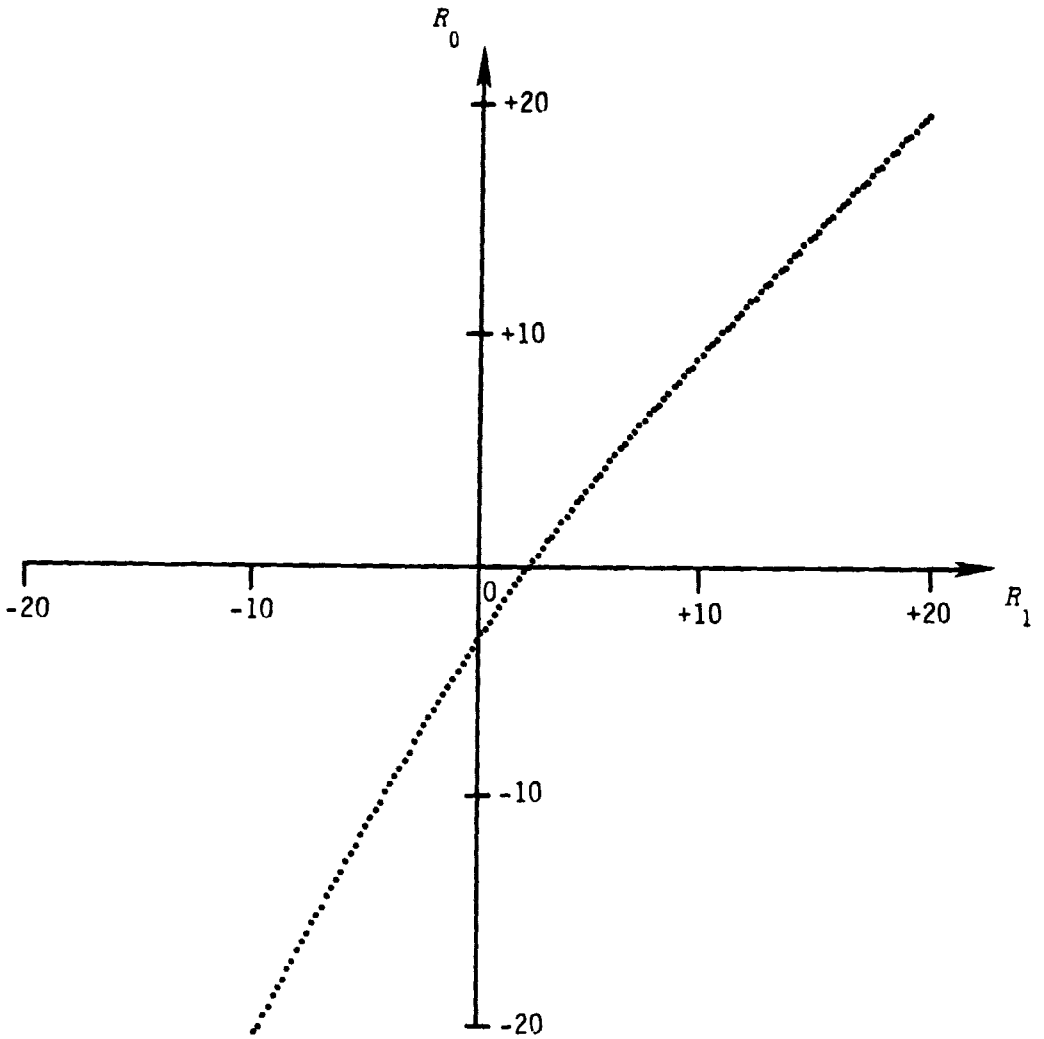

Figure 5-3. Input and output SNR

When the input SNR is high, the SNR is not degraded by the mixer. However, when the SNR is low (less than 0 dB), the SNR is degraded considerably. In such cases, the output SNR is approximately twice the input SNR in decibels. For example, a -10-dB input SNR results in a -20-dB output SNR.

5.4 LINK ANALYSIS FOR NONLINEAR REFLECTOR

The signal-and-noise power relationships derived in the previous section are now used to derive communication-link equations for the nonlinear reflector.

Analysis

A simplified system model is shown in Figure 5-4. The active-spacecraft transponder transmits two signals with power P_{st_1} and P_{st_2}. The power received at the passive-spacecraft transponder from the first signal is

$$P_{sr_1} = G_{t_1} G_{r_1} P_{st_1}/L_{p_1} \quad , \tag{5-38}$$

where the "path loss" (more correctly, the effect of capture area) is

$$L_{p_1} = (4\pi)^2 \rho^2/\lambda_1^2 \quad . \tag{5-39}$$

Since hemispherical but otherwise nondirectional antenna coverage is anticipated,

$$G_{t_1} = G_{r_1} = 2 \quad . \tag{5-40}$$

The thermal noise corrupting reception of signal #1 in the passive-spacecraft transponder is

$$P_{n_1} = k\, T\, B_1\, F_1 \quad , \tag{5-41}$$

where B_1 is the bandwidth and F_1 is the noise figure. The signal-to-noise ratio (SNR) for reception of signal #1 at the passive-spacecraft transponder is therefore

$$R_1 = P_{sr_1}/P_{n_1} \quad . \tag{5-42}$$

Analogous relationships hold for the second signal transmitted by the active-spacecraft transponder. Since the frequencies and power levels of the two signals should be similar, their SNRs should also be similar, hence the SNR at the output of the passive-spacecraft transponder is given by (5-36):

$$R_0 = \frac{R_1^2}{1 + R_1} \quad . \tag{5-43}$$

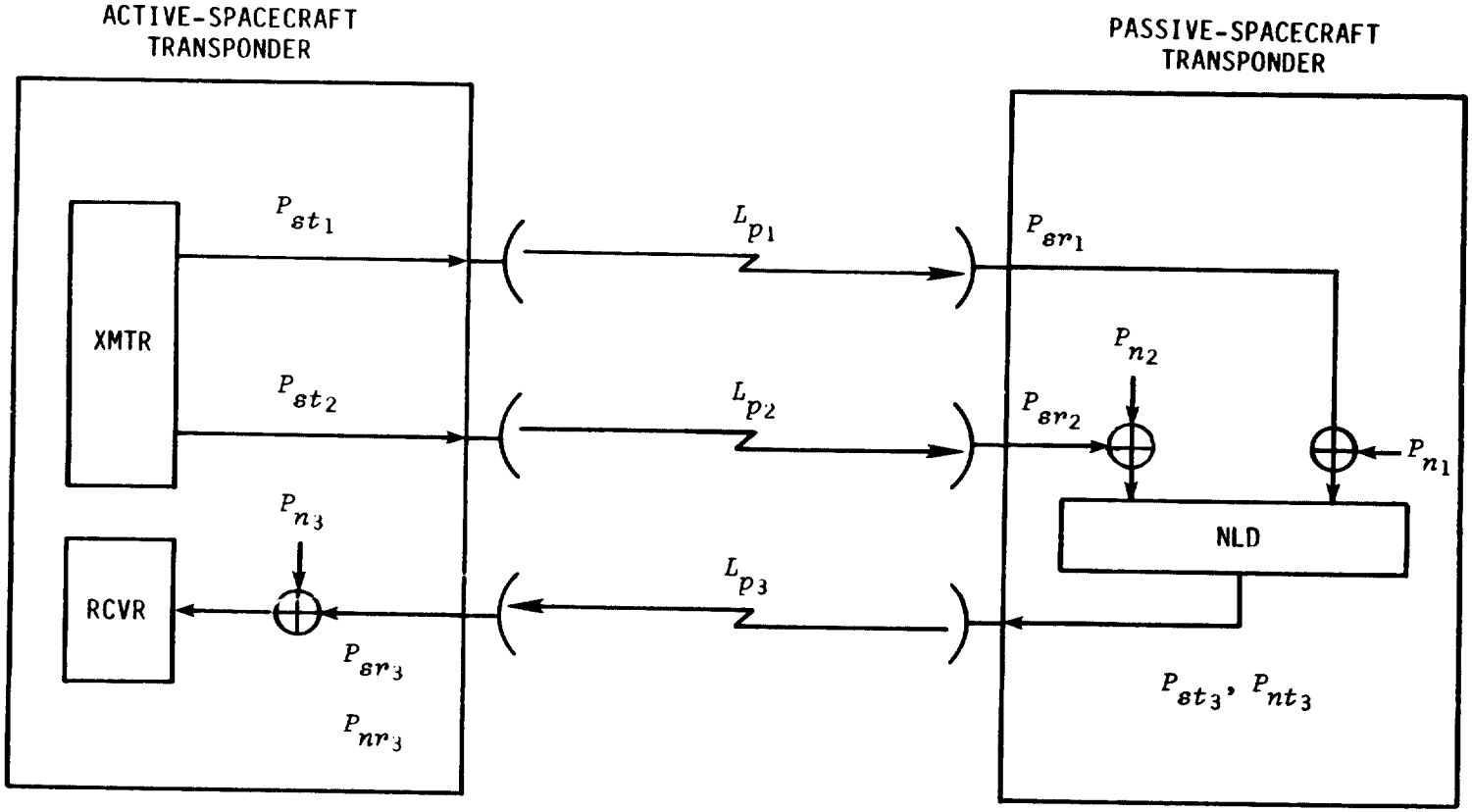

Figure 5-4. Signal and noise power in polarized interferometer.

The signal and noise powers reradiated by the passive-spacecraft transponder can be found from (5-29) and (5-35), thus

$$P_{st_3} = G_p P_{sr_1}^2/2 \tag{5-44}$$

and

$$P_{nt_3} = G_p(2 P_{n_1}^2 + P_{n_1} P_{sr_1}/2) \quad . \tag{5-45}$$

The reradiated powers captured by the active-spacecraft transponder are then

$$P_{sr_3} = G_{t_3} G_{r_3} P_{st_3}/L_{p_3} \tag{5-46}$$

and

$$P_{nr_3} = G_{t_3} G_{r_3} P_{nt_3}/L_{p_3} \quad , \tag{5-47}$$

where return path loss L_{p_3} is calculated by analogy to (5-39). The resultant SNR of the returned signal is therefore

$$R_3 = \frac{P_{sr_3}}{P_{nr_3} + P_{n_3}} \quad , \tag{5-48}$$

where P_{n_3} is the thermal noise in the active-spacecraft transponder.

Forward-Link Design

Equations (5-38) - (5-43) can be used to analyze the performance of the forward communication link. Selected plots of SNR versus distance are shown in Figure 5-5. All three curves are based upon forward-path frequencies of 20 GHz, a return-path frequency of 2 GHz, and 3-dB noise factors.

The first (lowest) curve in Figure 5-5 is for P_{st_1} = 1 W and B_1 = 10 MHz; these parameters correspond to wideband PN modulation and a practical power level for continuous transmission. Unfortunately, the SNR of the reradiated signal becomes negative at a distance of less than 10 km. Therefore, this combination of modulation and power level is suitable only for relatively short distances (e.g., < 1 km).

The second (middle) curve shows the effect of decreasing the PN chipping frequency by a factor of 10 (so B_1 = 1 MHz) and increasing transmitted power to 10 W. This combination should be suitable for distances in excess of 10 km, but is not adequate for distances of 100 km. The 10-W power level is also somewhat high for continuous transmission at 20 GHz.

To achieve a satisfactory reradiated SNR (R_0) at a distance of 100 km with only 1-W transmitted power, it is necessary to reduce bandwidth to 1

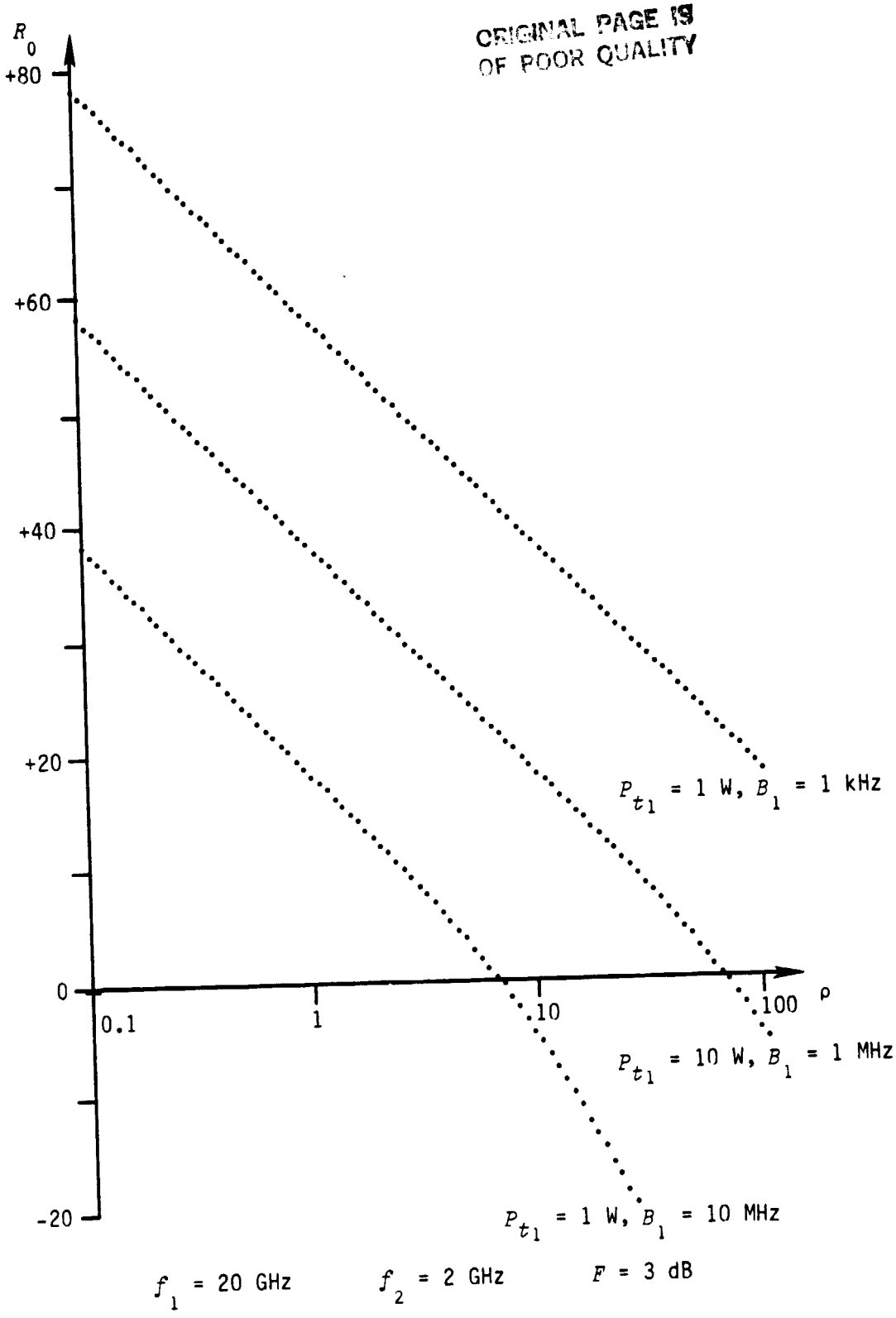

Figure 5-5. SNR at passive-spacecraft transponder output.

kHz (third curve in Figure 5-5). This can be accomplished by using multitone modulation and a 1-kHz tracking bandwidth.

Return-Link Design

For B_1 = 1 kHz and P_{st_1} = 1 W, simple mixing with G_p = 0 dB in the passive-spacecraft transponder produces returned SNRs ranging from -60 dB to -240 dB. Since these figures are based upon a 1-Hz detection bandwidth, the real-world situation may be even worse by 10 or 20 dB. Obviously, gain in the passive-spacecraft transponder is required and truely passive operation is not possible. Note that this situation is worse than that of conventional radar, since the mixing multiplies two already small power levels to get an even smaller power level.

Figure 5-6 shows the return SNR R_3 as a function of distance for several passive-spacecraft transponder gains. Note that the total gain G_p can be accomplished by adding gain $G_p^{1/2}$ to both input channels in the passive-spacecraft transponder. From the curves in Figure 5-6, it is apparent that total gains of 140 dB, 200 dB, and 260 dB are required for operation at distances of 1, 10, and 100 km, respectively.

Conclusions

The forward-link calculations show that it is possible to illuminate the passive-spacecraft transponder with signal levels high enough to produce a positive reradiated SNR. While wideband PN modulation can be used at short distances ($\leq$ 1 km), narrowband multitone modulation must be used for operation at distances of 100 km.

Considerable gain in the passive-spacecraft transponder is necessary to return adequate signal levels to the active-spacecraft transponder. The gain required (70 dB to 130 dB per channel) is not prohibitive, but is large enough to necessitate careful design.

The large reception bandwidth at the passive-spacecraft transponder and the high gain may make it possible for the system to be "captured" by a strong interfering signal. In any case, it is obvious that a simple passive or nearly passive system is not practical except for use at relatively short distances.

5.5 LINK ANALYSIS FOR SIMPLE REPEATER

The relationships developed in the previous two sections are used to derive preliminary communication-link designs for the simple repeater of Figure 5-1. Since the local oscillator has an inherently high SNR, the required gain is considerably less than that required by the nonlinear reflector.

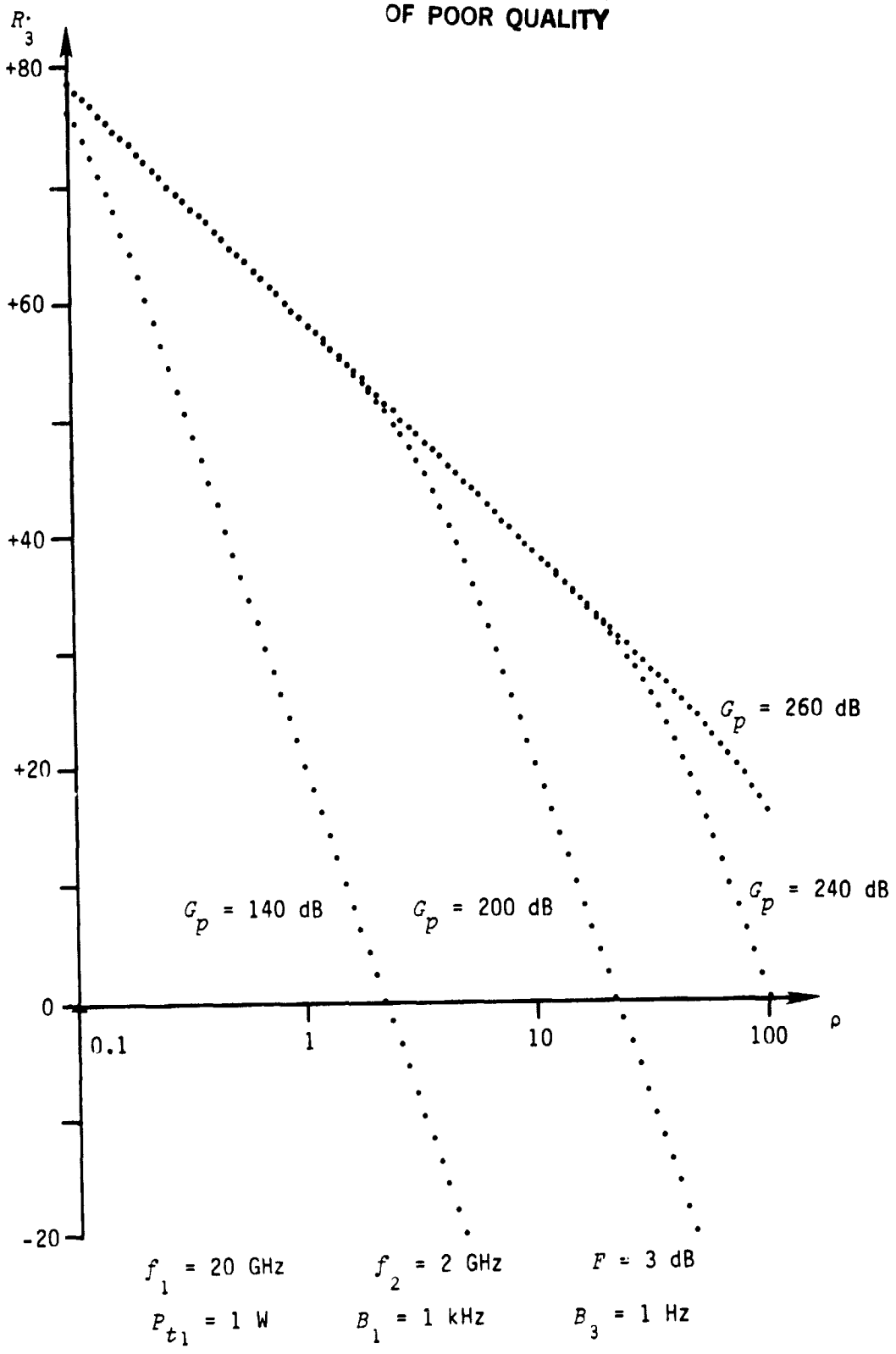

Figure 5-6. SNR at active-spacecraft transponder.

Analysis

Most of the link equations are identical to those for the nonlinear reflector (Section 5.4). However, since frequency translation is accomplished by mixing the received signal with an essentially noise-free signal from a local oscillator, the reradiated signal and noise power are

$$P_{st_3} = G_p P_{sr_1} \tag{5-49}$$

and

$$P_{nt_3} = G_p P_{n_1} \quad . \tag{5-50}$$

The input and output SNRs of the passive-spacecraft transponder are therefore identical; i.e.,

$$R_0 = R_1 \quad . \tag{5-51}$$

Link Designs

The variation of SNR with distance for a 20-GHz, 1-W forward signal and a 2-GHz return signal is shown in Figure 5-7. Operation at a distance of 100 km is possible. Since the frequencies are the same as those used in the link designs for the nonlinear reflectors, it is not suprising that the link performance is similar.

With the simple-repeater system, there is no special need to use a forward-signal frequency in the 20-GHz range. If the frequency is lowered to 3 GHz, and path loss is decreased. In addition, Doppler shifts are reduced, hence the bandwidth of the input to the passive-spacecraft transponder can be decreased to 100 Hz. As a result, satisfactory performance (Figure 5-8) at distances of up to 100 km can be achieved with a radiated power of only 100 mW.

It is desirable to apply wideband PN modulation to the forward signal to facilitate ranging. Since the active-spacecraft transponder acquires nd tracks the PN modulation, the 100-Hz tracking bandwidth applies. However, unless the passive-spacecraft transponder is equipped with a correlator or matched filter, a larger bandwidth must be used at its input. Figure 5-9 presents the SNR for a system employing a 1-MHz forward bandwidth and a 1-W radiated power. It is apparent that operation beyond 10-km is not possible unless the radiated power is increased substantially.

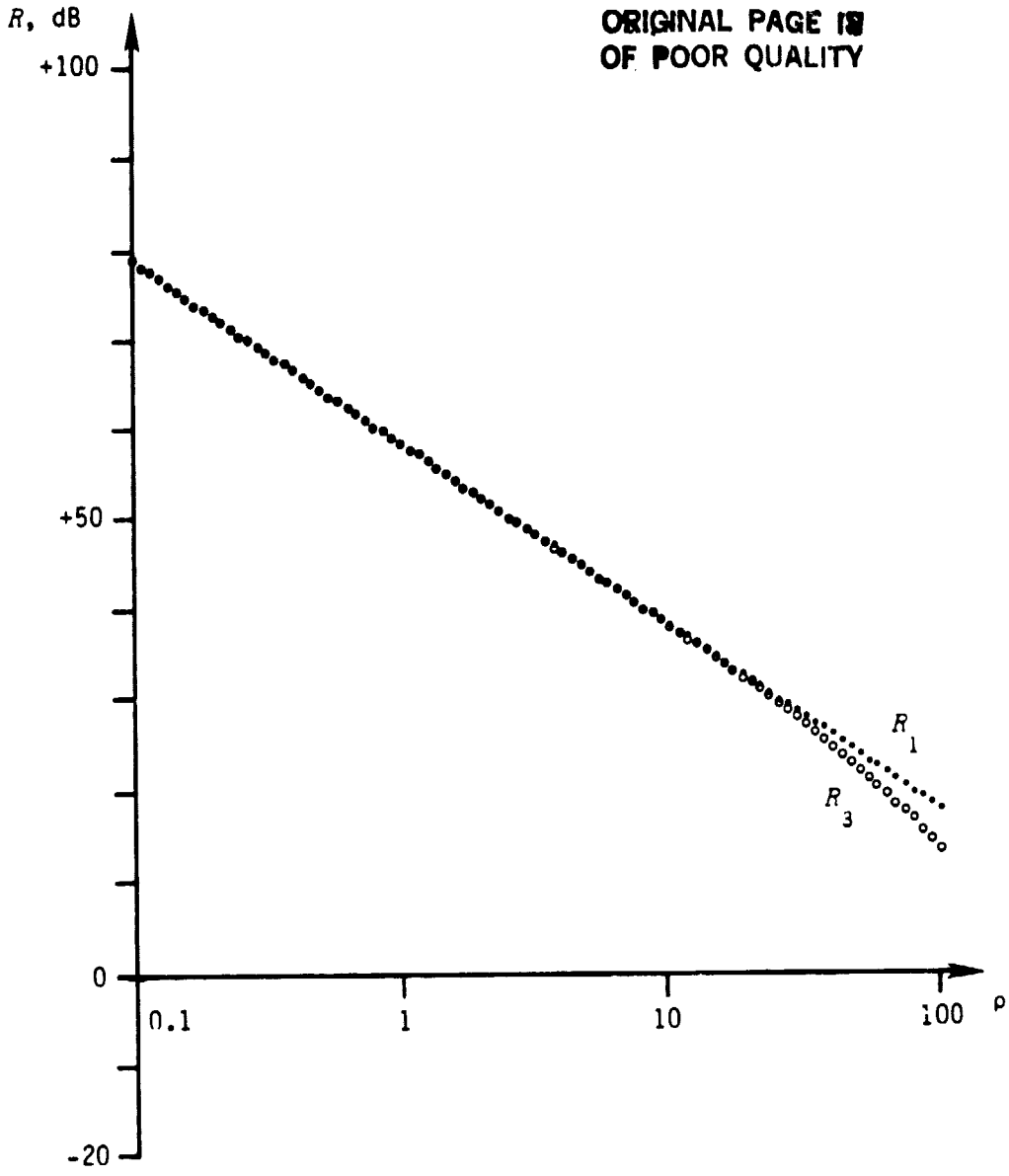

f_1 = 20 GHz $\quad$ f_3 = 2 GHz

B_1 = 1 kHz $\quad$ B_3 = 1 Hz

P_1 = 1 W $\quad$ G_p = 100 dB

Figure 5-7. Link SNR for narrowband 20-GHz/2-GHz system.

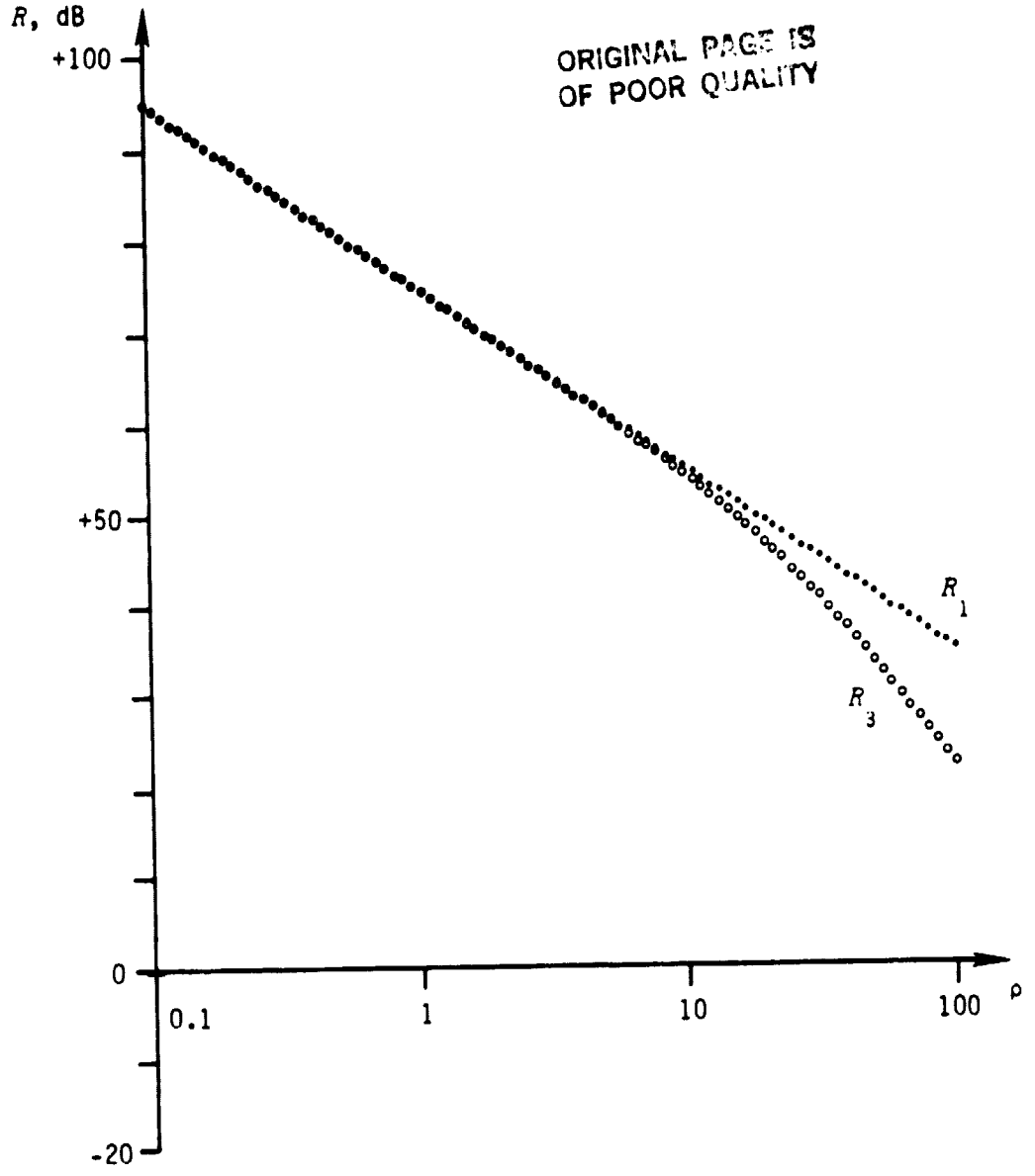

f_1 = 3 GHz $\quad$ f_3 = 2 GHz

B_1 = 100 kHz $\quad$ B_3 = 100 Hz

P_1 = 100 mW $\quad$ G_p = 120 dB

Figure 5-8. Link SNR for narrowband 3-GHz/2-GHz system.

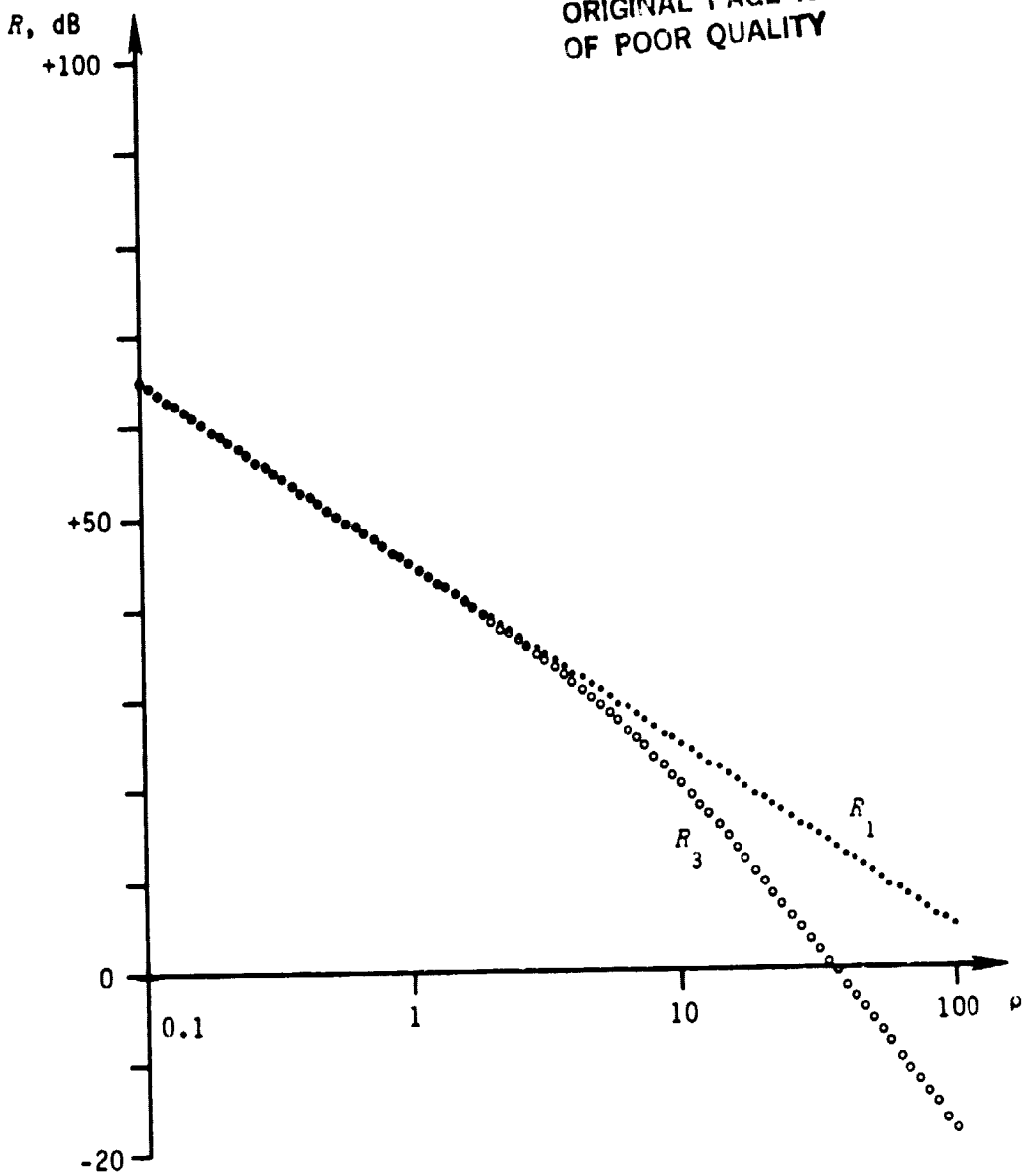

f_1 = 3 GHz $\quad$ f_3 = 2 GHz

B_1 = 100 Hz $\quad$ B_3 = 100 Hz

P_1 = 1 W $\quad$ G_p = 70 dB

Figure 5-9. Link SNR for wideband 3-GHz/2-GHz system.

CHAPTER 6

TRANSPONDER CONFIGURATION

The analysis presented in the previous chapter shows that the simple-repeater and nonlinear-reflector concepts are unsuitable for the passive-spacecraft transponder unless operation is restricted to relatively short distances. A more conventional transponder is therefore required. However, it need not be as sophisticated or as complex as the transponder on the active spacecraft, since measurements are not required by the passive spacecraft.

The three key issues in establishing the transponder configuration are:

- Frequency assignments,
- Modulation and format, and
- Type of antenna.

This chapter addresses these issues and derives a suitable transponder configuration.

6.1 FREQUENCY SELECTION

The principal issues in selecting frequencies for the forward and reverse links are:

- Avoidance of frequencies used by STS and other spacecraft,
- Adequate separation of the forward and return signals,
- Adequate bandwidth for the desired modulation, and
- Minimization of passive-spacecraft radiated power.

The fourth requirement results from the use of omnidirectional, fixed antennas, and implies the use of as low a frequency as is consistant with the other requirements.

The STS (shuttle) uses S-band (1.7 - 2.3 GHz) for a variety of purposes, including direct ground links, TDRSS links, and payload links [Carrier, 1978; Bacinski, 1978; Cager, 1978]. It also uses Ku-band (13.775 - 14.0 and 14.85 - 15.15 GHz) for radar and two-way links to the TDRSS.

The NAVSTAR/Global Positioning System (GPS) is a satellite-based radionavigation system that may be used to determine the absolute position and attitude of the active spacecraft. The GPS employs PN-modulated signals (10-MHz bandwidth) at 1.2276 and 1.57542 GHz [Milliken, 1980].

The frequencies used by the STS, TDRSS, and GPS must be avoided. However, these frequencies occupy only a small fraction of the spectrum, hence avoiding them should present no problems. Transmission just above the 2-GHz band used by the STS should provide adequate bandwidth and require relatively little radiated power.

6.2 MODULATION

The modulation technique used in the polarized-interferometer system must allow accurate and unambiguous measurement of range. Suitable modulation techniques are:

- Pulse,
- Multiple-carrier CW, and
- Pseudonoise (PN).

Multicarrier CW and PN modulation allow continuous or nearly continuous transmission. This keeps the peak power relatively close to the average power, thereby minimizing the requirements for the passive-spacecraft transmitter circuitry. In contrast, pulse modulation requires quite high peak transmitter power and is therefore undesirable.

Pseudonoise modulation [Dixon, 1976] is desirable because it rejects interference and allows precise and unambiguous tracking. However, it requires more signal-processing circuitry than is required for multicarrier CW.

In light of the above-mentioned constraints upon the modulation, four candidate transponder configurations were developed, namely:

- Multiple-carrier CW repeater,
- Coherent PN transponder,
- SAW/clipper PN transponder, and
- SAW/CCD PN transponder.

The subsequent discussion in this section compares these four approaches.

Multicarrier-CW Repeater

The multiple-carrier CW repeater is a relatively simple system that is not unlike the systems commonly used for VHF/UHF FM land-mobile communication. As shown in Figure 6-1, it comprises amplifiers, filters, and mixers, as well as an FM detector, squelch circuit, and microprocessor. Link analysis (Chapter 5) shows such systems to be practical for distances up to 100 km.

Transmissions from the active spacecraft are made sequentially on a number of different frequencies to provide both range accuracy and range-ambiguity resolution. For operation at relatively short distances, a wideband repeater (Figure 5-1) can be used. However, a relatively large bandwidth degrades the SNR and allows the repeater to be captured by an interfering signal. For long-range operation, it is therefore desirable that the repeater use narrowband filtering (e.g., 100-Hz bandwidth) and establish synchronization with the signals from the active-spacecraft transponder.

The microprocessor scans through the pre-determined set of frequencies until a signal is detected (by a quiet output of the FM detector). Upon detecting a signal, the microprocessor attempts to establish synchronization by

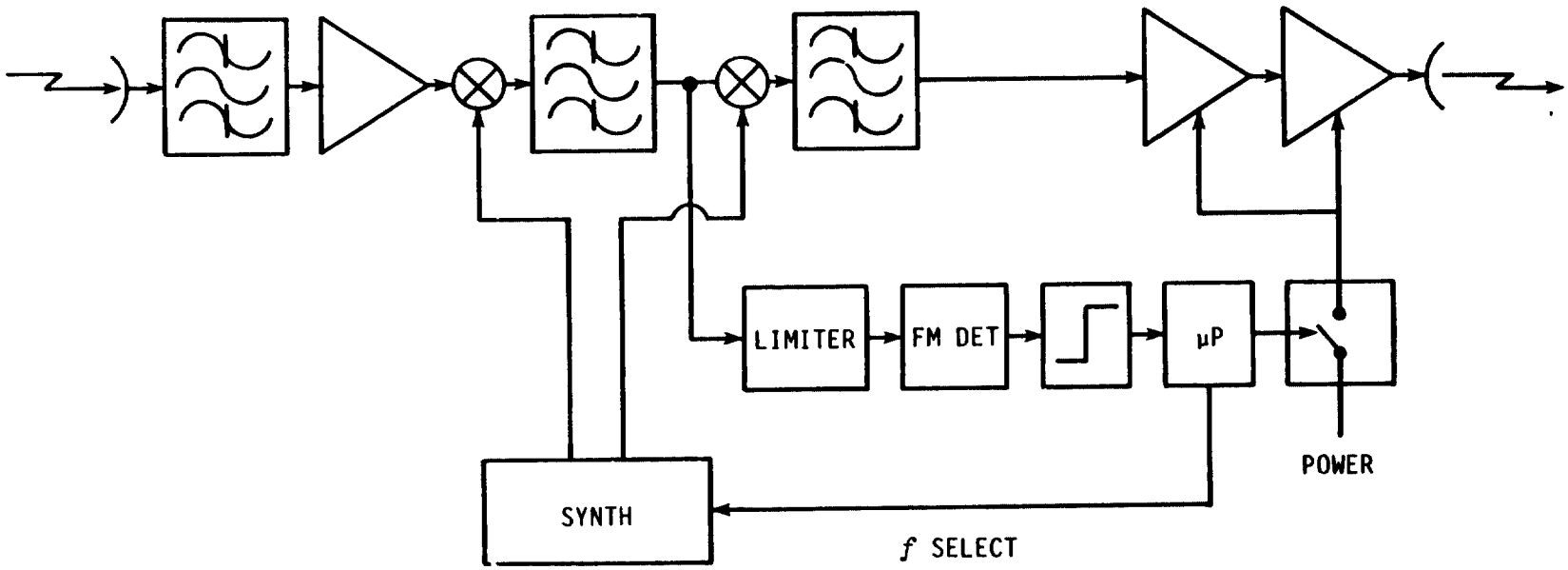

Figure 6-1. Multiple-carrier CW transponder.

selecting the next transmission frequency at the appropriate time. Once synchronization is established, dithering is used to establish precise synchronization and the transmitter is activated. If synchronization is not established, scanning is resumed. Time or frequency division can be used to multiplex transmissions from the four elements of the passive-spacecraft transponder.

The local oscillator in the passive-spacecraft transponder introduces an unknown frequency offset in the returned signals. However, all signals returned to the active-spacecraft transponder are offset by the same amount. Differencing the frequencies of the signals received at the active-spacecraft transponder therefore provides the Doppler shift without corruption by the local oscillator in the passive-spacecraft transponder.

Coherent Pseudonoise Transponder

Pseudonoise (PN) modulation is desirable because it allows both precise and unambiguous range measurement. However, the large bandwidth required by a PN-modulated signal precludes the use of a simple repeater except at short distances.

The "conventional" PN transponder shown in Figure 6-2 is based upon correlation techniques. Coherent detection produces I and Q baseband signals, which are used by the microprocessor to establish frequency, code, and phase lock to the received signal.

Upon completion of signal acquisition, the transmitter is activated and returns a signal that is modulated by its own unique PN code. The carrier frequency, carrier phase, and code phase of the returned signal are locked to those of the received signal. Different PN codes are used to allow simultaneous transmissions from all four elements of the passive-spacecraft transponder.

This system is well suited to this application, as it provides a good return SNR and good rejection of interfering signals. While it is more complex than a CW/multitone repeater, it is not as complicated as a navigation receiver, since estimates of time of arrival and position are not required. The increasing use of the NAVSTAR/GPS radio-navigation system may make such technology commonplace a few years hence.

SAW Pseudonoise Transponder

Surface-acoustic-wave (SAW) devices can be used to implement matched filters for PN-modulated signals. A PN transponder based upon SAW technology may be somewhat simpler than the coherent transponder described above.

Figure 6-3 presents a block diagram of a PN transponder based upon SAW matched filters. The received signal is downconverted to VHF for processing by the SAW filter. The first SAW filter converts the PN signal (1) into a rectangular CW pulse (2).

A pulse detector with AGC (3) gates the output (4) of the SAW filter to

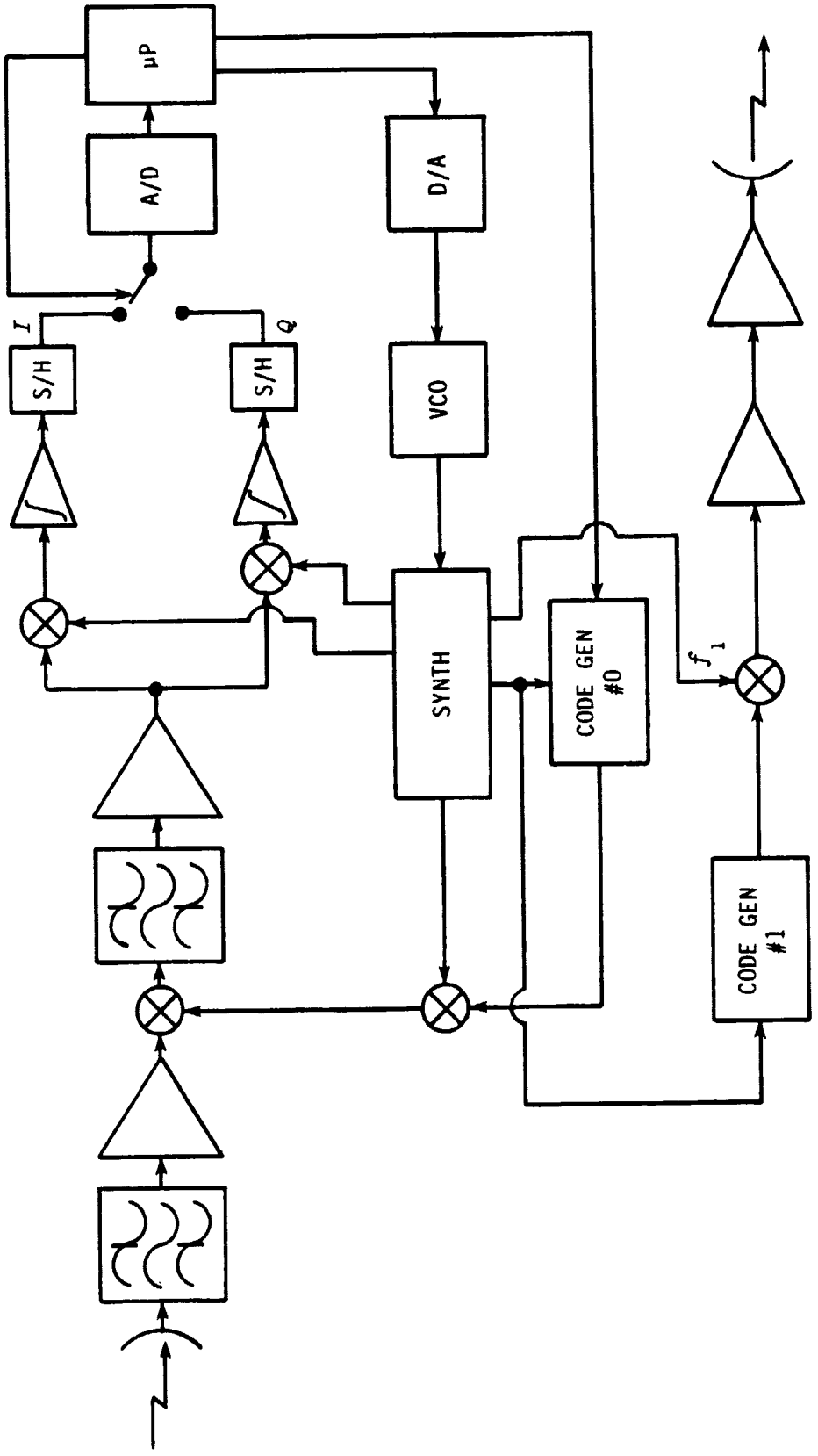

Figure 6-2. Coherent PN transponder.

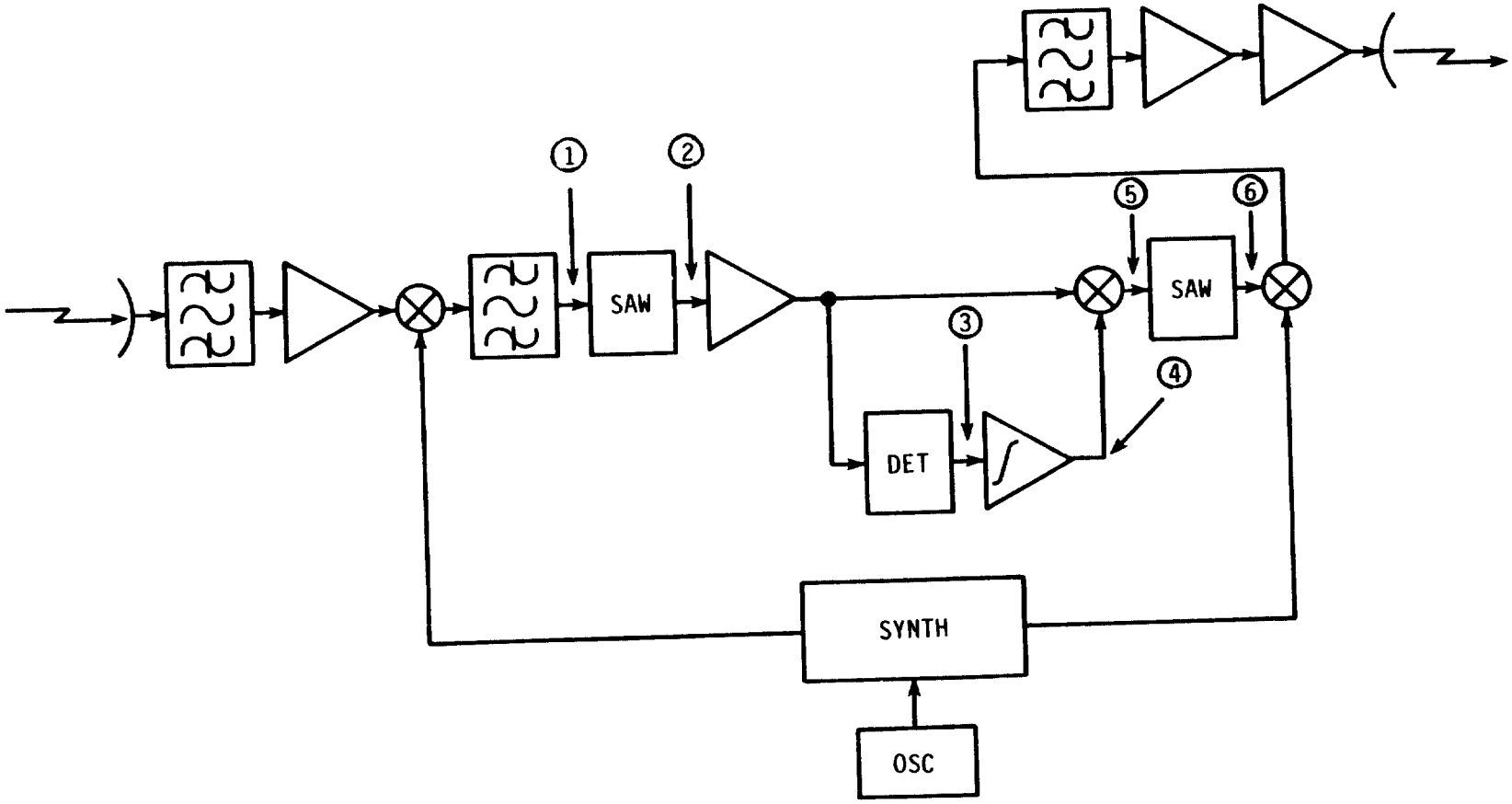

Figure 6-3. SAW-PN transponder.

the subsequent circuitry only when a CW pulse is detected. The gating effectively eliminates the noise power when the CW pulse is absent, and therefore increases the SNR as does a narrowband filter. The gated CW pulse (5) is applied to a second SAW filter to generate a return signal (6) with unique PN modulation. Optionally, the pulsed CW signal can be retransmitted directly; however, the transmitter must then have a considerably larger peak-power capability.

As shown in Figure 6-3, the system introduces an unknown and undeterminable frequency error due to the local-oscillator offset. One solution to this problem is to transmit sequentially on two different frequencies; the offset can then be derived at the active spacecraft by measuring the frequencies of the received signals and differencing the results. Alternatively, the active-spacecraft transponder can transmit on two different frequencies and the passive-spacecraft transponder can apply exactly the same frequency change to each. The Doppler shift can then be determined by frequency difference between the two returned signals.

SAW/CCD Pseudonoise Transponder

The principal problem in the SAW transponder discussed above is jitter in the timing of the returned signal. This jitter is caused by gate-timing jitter, which is in turn caused by noise corrupting the CW pulse. The SAW/CCD system of Figure 6-4 reduces the timing jitter by averaging successive pulses.

The downconverted PN signal (1) is applied to the first SAW filter to obtain a CW pulse (2), as in the previous SAW transponder. The CW pulse is applied to a noncoherent amplitude detector to obtain a baseband pulse (3); SNR is not degraded significantly if the CW pulse has positive SNR at the input of the detector. The CCD array averages the baseband pulses to reduce the effective detection bandwidth to the 1- to 10-Hz range. The averaged pulses (4) are then clipped to remove the inter-pulse noise. The clipped pulses (5) then modulate a locally generated RF signal to produce CW pulses (6), which in turn drive the second SAW filter to produce the PN-modulated return signal (7).

Conclusions

The SAW/clipper transponder may not deliver the desired performance except at high SNRs. The SAW/CCD transponder appears promising, but exceeds or at least taxes the current states of the art for both SAW and CCD technologies. Implementation of such a transponder therefore cannot be recommended at the present time. However, such a system may become feasible in the not-to-distant future.

The multiple-carrier CW and coherent PN transponders are readily implemented using current technology. The coherent PN transponder is considerably more complex than the multiple-carrier CW transponder, and the power consumption of its code generator may exceed that of its RF power amplifiers. In the absence of interference, the performances of the two systems are essentially the same. Therefore, the less complex multiple-carrier CW technique

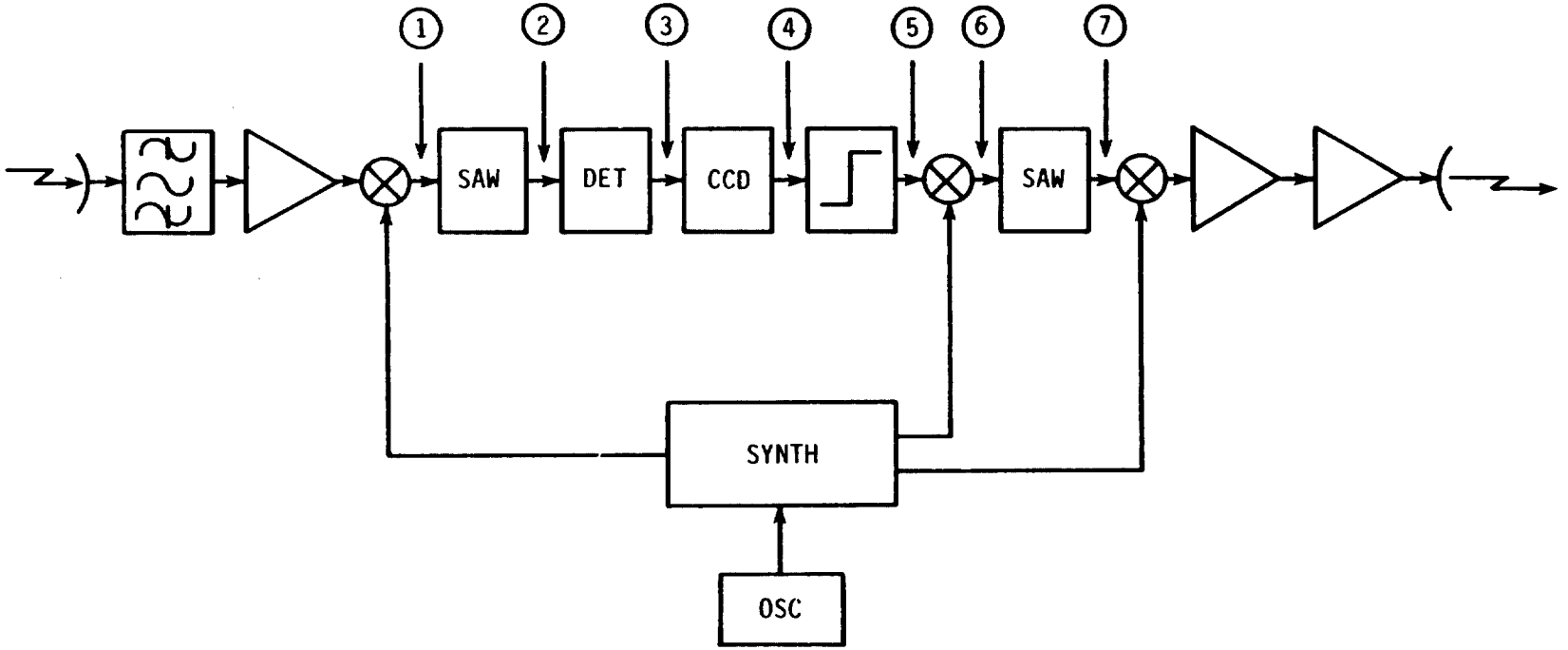

Figure 6-4. SAW/CCD PN transponder.

is preferred for applications without requirements for security or resistance.

6.3 ANTENNAS

The polarized-interferometer antenna array on the active spacecraft must

- Transmit circularly polarized signals,
- Receive circularly polarized signals, and
- Receive linearly polarized signals.

Similarly, the array on the passive spacecraft must

- Receive circularly polarized signals,
- Transmit circularly polarized signals, and
- Transmit iinearly polarized signals.

Such arrays are most easily implemented by using two linearly polarized elements in each of the four components shown in Figure 1-3. Phasing is used to obtain circular polarization when and where it is needed.

Suitable antenna components are

- Crossed dipoles,
- Crossed slots, and
- Horns.

The most stringent requirement is imposed by the necessity to measure signal amplitude with an error of 0.1 dB or less. The relevant characteristics of each type of component are discussed in this section.

Crossed dipole

The crossed dipole can be implemented in a number of forms, as shown in Figure 6-5. Normally, the elements are straight and parallel to the ground plane. However, if space is at a premium, the elements can be bent downward, effectively producing a loaded short dipole. The elements can be mounted on a strut or can be printed on low-dielectric material (PCB). The later type of construction is desirable because of its high rigidity.

The patterns of full-length and electrically short dipoles differ. In addition, the pattern of a dipole in free space differs from the pattern of a dipole above a ground plane.

Crossed Slot

The crossed-slot antenna is implemented by cutting slots in a conducting surface (Figure 6-6). Matching circuitry can be implemented on a printed-circuit board immediately behind the slots.

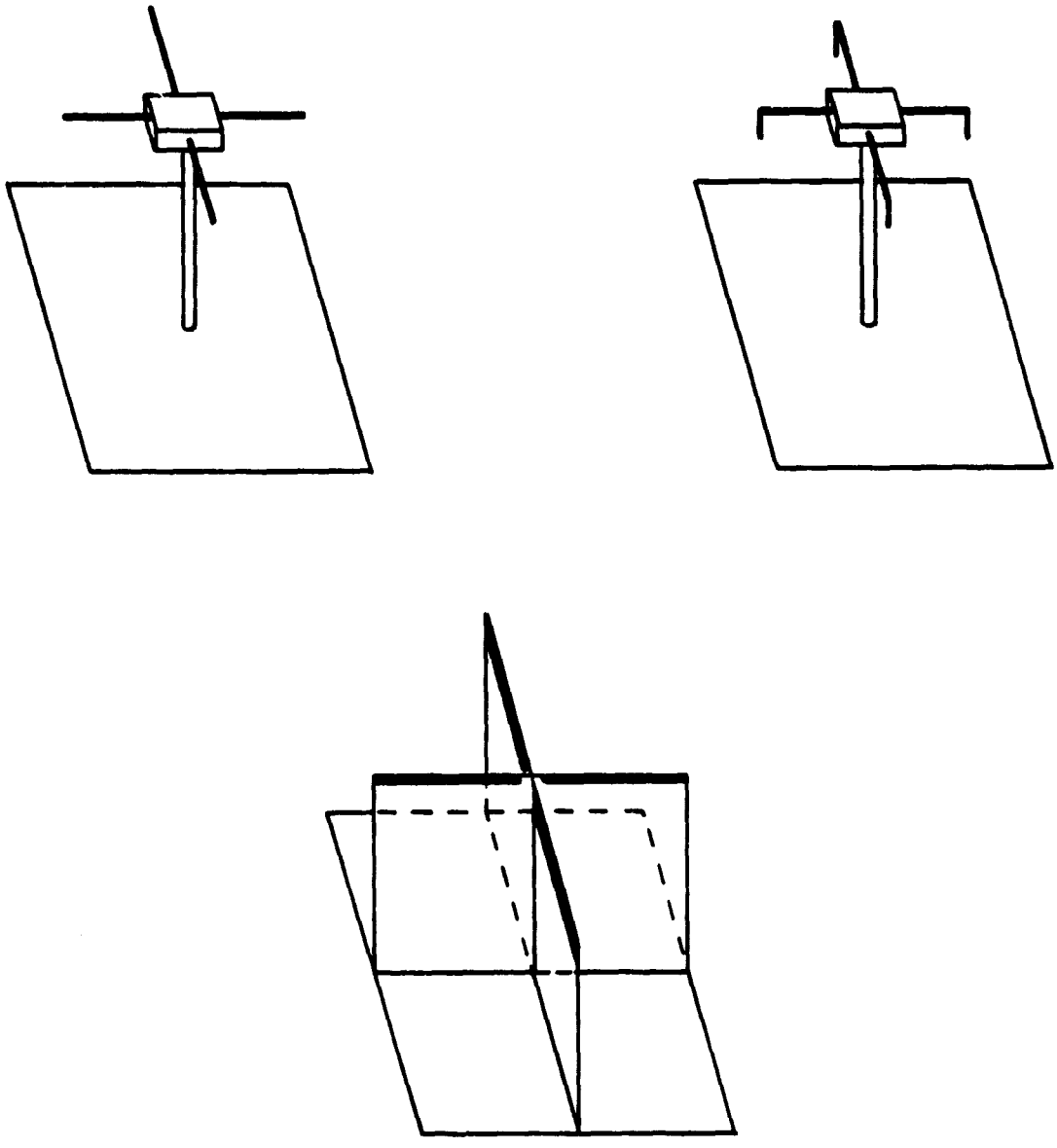

Figure 6-5. Crossed dipoles.

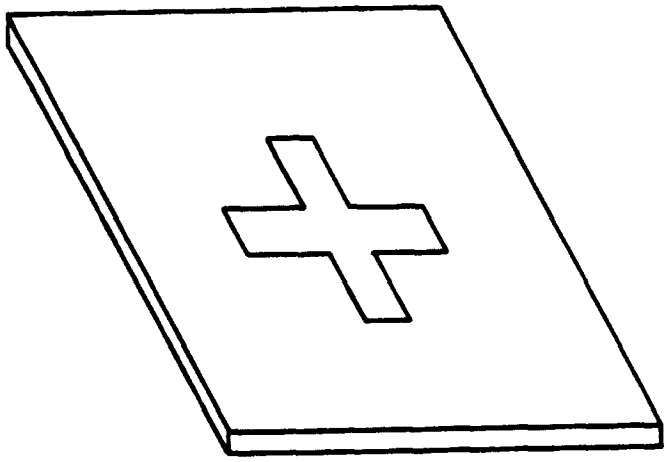

Figure 6-6. Crossed slot.

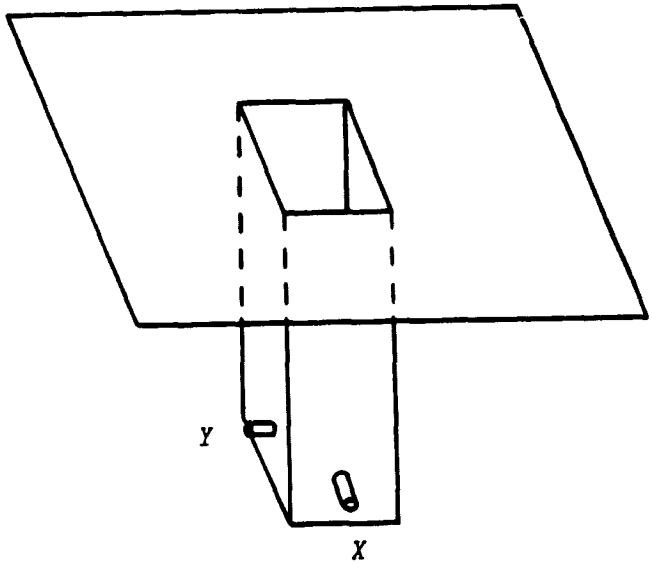

Figure 6-7. Quad-ridge horn.

The crossed slot is inherently rigid and rugged, and does not protrude from the surface. Its pattern is similar to that of a crossed dipole above a ground plane.

Horn

The rectangular ("quad-ridge") horn antenna (Figure 6-7) is also capable of producing either linear polarization when proper excitation is provided. Such antennas (e.g., Sanders CA series) are capable of operation over more than an octave in frequency. In addition, they are inherently rugged and stable.

The pattern of the horn antenna is probably affected less by its surroundings than are the patterns of crossed dipoles or crossed slots. However, the half-power beamwidth of the horn antenna is limited to a maximum of about 20° to 30°.

Comparison

If the cone of operation were limited to 20° or 30° off boresight, the horn antenna would be preferable. However, in the present application, a wide cone of operation (45° off boresight) is desired, hence the horn is not suitable.

Both the crossed dipole and the crossed slot are suitable. The choice depends primarily upon the required antenna form factor. If antenna height is not important, the crossed dipole is preferred. However, if the antenna must be stowed and deployed, antenna height may be a significant consideration. In this case, the crossed slot is preferred.

Installation and Accuracy

Repeatable pattern accuracies of 0.2 dB are readily achieved in a laboratory environment. However, installation over an irregular and/or finite ground plane can produce pattern ripple of 1 dB or more. Radomes can also introduce significant pattern distortion. Fortunately, they are not needed in this application.

The pattern ripple associated with the installation can be minimized by two techniques. First, the antennas should be mounted on a large, flat disk. This reduces the effects of finite size and curvature of the ground plane. Second, the antenna/ground-plane array should be mounted on a strut away from the spacecraft. This should be possible in an airless environment with slowly maneuvering spacecraft.

The 0.06-dB pattern-ripple requirement (Chapter 8) is fairly stringent and pushes the state of the art. However, similar requirements exist in new direction-finding systems for EW applications. The recently developed scalar-horn system ["NBS", 1982] achieves an amplitude accuracy of ±0.1 dB in its 4-to-7 GHz band of operation.

With calibration, it should be possible to meet the desired 0.06-dB error requirement, especially near the center of the field of view. In fact, the antenna design may be considerably less difficult if the cone of operation can be divided into two regions, with the minimum ripple required only in the center.

CHAPTER 7

MULTIPLE-CARRIER CW RANGING

Multiple-carrier CW ranging is of interest in the polarized-interferometer application because it requires the least complicated transponder on the passive spacecraft. In this approach, a number of CW carriers of different frequencies (Figure 7-1) are transmitted from the active spacecraft and returned (with known frequency offset) by the transponder on the passive spacecraft. This chapter analyzes multiple-carrier ranging with respect to two key aspects:

- Range accuracy
- Cycle-ambiguity resolution.

The resultant equations are used in the system design (Chapter 8).

The polarized-interferometer system uses sequential transmission on each frequency. The duration of the transmission on a given frequency is in the range of 0.1 to 0.5 s to enable a simple FM squelch circuit in the passive-spacecraft transponder to acquire the transmission pattern. The set of K different frequencies are arranged such that

$$f_2 = f_1 + \nu f_0$$

$$f_3 = f_1 + \nu^2 f_0$$

$$\cdots$$

$$f_K = f_1 + \nu^{K-1} f_0 \quad . \tag{7-1}$$

where f_0 is the minimum difference frequency and ν is the number of cycles to be resolved at each step in the ambiguity-resolution process.

7.1 RANGE ACCURACY

The polarized-interferometer system employs two-way transmissions. The total phase error in the signal returned to the active spacecraft is therefore the sum of the phase errors in both the forward and reverse paths; i.e.,

$$\Delta\phi_T = \Delta\phi_F + \Delta\phi_R \quad . \tag{7-2}$$

The phase variance caused by Gaussian noise is given by the well-known relationship

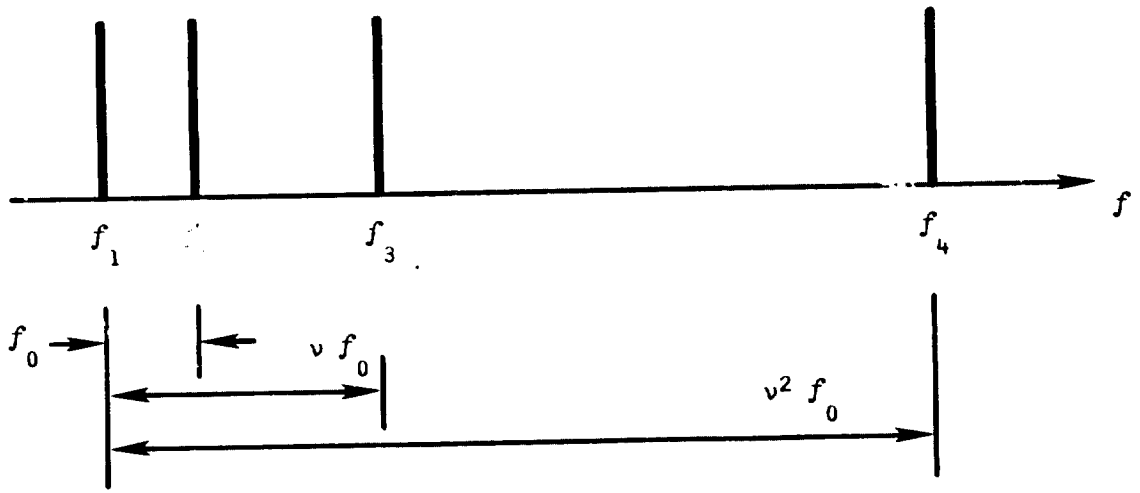

Figure 7-1. Carrier frequencies.

$$\sigma_{\phi}^2 = \frac{1}{2R} \quad , \tag{7-3}$$

where R is the signal-to-noise power ratio (SNR).

Since the noises in the forward and reverse channels are independent, the total-noise variance is

$$\sigma_{\phi_T}^2 = \frac{1}{2R_F} + \frac{1}{2R_R} \quad , \tag{7-4}$$

where R_F and R_R represent the SNRs of the forward and reverse channels, respectively. If $R_F = R_R$, then

$$\sigma_{\phi_T}^2 = \frac{1}{R_F} = \frac{1}{R_R} \quad . \tag{7-5}$$

Otherwise, the total-noise variance is determined principally by the smaller of the two SNRs.

The variation of phase with distance is determined by the wavelength (hence frequency) of the carrier, thus

$$\phi_F = \frac{2\pi\rho_F}{\lambda_F} = \frac{2\pi f_F}{c}\,\rho_F = q_F\,\rho_F \quad . \tag{7-6}$$

Since the phase of the returned signal is the sum of the phase shifts in both the forward and reverse links,

$$\phi_T = \phi_F + \phi_R = \frac{2\pi}{c}\,(f_F\,\rho_F + f_R\,\rho_R) \quad , \tag{7-7}$$

At large distances, $\rho_T \cong \rho_R$, and (7-7) simplifies to

$$\phi_T = \frac{2\pi f_T}{c}\,(\rho_F + \rho_R) = q_T\,\rho \tag{7-8}$$

where

$$f_T = (f_F + f_R)/2 \quad , \tag{7-9}$$

and

$$\rho = \rho_F + \rho_R = 2\,\rho_F = 2\,\rho_R \tag{7-10}$$

is the total *two-way* path length.

If $f_R \neq f_F$ (as in a repeater) or $\rho_F \neq \rho_R$ (at short distances), ρ cannot be recovered from the phase of a single carrier frequency. However, ρ can be recovered from the difference between the phases of two carriers, as discuss-

ed in the next section.

Given correct cycle resolution and $\rho_F \cong \rho_R$, the range estimate is derived from the phase measurement by

$$\hat{\rho} = -\frac{c}{2\pi f_T}\hat{\phi}_T = \hat{\phi}_T/q_T \quad , \tag{7-11}$$

where c represents the speed of light. The variance of the range estimate is therefore

$$\sigma_\rho^2 = \sigma_\phi^2/q_T^2 = \left(\frac{\lambda_T}{2\pi}\right)^2 \sigma_d^2 = \left(\frac{c}{2\pi f_T}\right)^2 \sigma_\phi^2 \quad . \tag{7-12}$$

All K carriers are of approximately the same frequency and same SNR and therefore can be used to derive K independent estimates of the same accuracy. Averaging of these K estimates reduces the variance shown in (7-11) by the factor 1/K. However, reducing the duration of the transmissions to allow transmissions on additional frequencies decreases the averaging done by the phase detectors. This in turn increases the variance in (7-11), causing the variance of the average of the individual estimates to remain unchanged. Assuming that ambiguities are resolved correctly, the number of carrier frequencies does not affect range accuracy.

7.2 AMBIGUITY RESOLUTION

The phase of a returned carrier goes through one cycle of 2π radians every time range ρ changes by

$$\lambda_T = c/f_T = 2c/(f_F + f_R) \tag{7-13}$$

The equivalent wavelength λ_T is the maximum unambiguous range-measurement interval. Decreasing the carrier frequencies increases the unambiguous range-measurement interval. However, lower limits on the carrier frequency are imposed by both antenna size and frequency allocations.

A greater unambiguous range interval can be obtained by using the difference between the phases of two carriers. For example,

$$\phi_{2,1} = \phi_{T_2} - \phi_{T_1} = q_{2,1}\,\rho \quad , \tag{7-14}$$

where

$$q_{2,1} = 2\pi\, f_{2,1}/c \tag{7-15}$$

and

$$f_{2,1} = [f_{F_2} + f_{R_2} - (f_{F_1} + f_{R_1})]/2 \qquad (7\text{-}16)$$

is the difference between the two carrier frequencies. By analogy to (7-11), the ambiguity interval is

$$\lambda_{2,1} = c/f_{2,1} \quad . \qquad (7\text{-}17)$$

The maximum ambiguity interval is related to the minimum difference frequency, hence from (7-1) and (7-15),

$$\lambda_{max} = \frac{c}{f_0} \quad . \qquad (7\text{-}18)$$

The derived phase measurement corresponding to the smallest frequency difference provides the least ambiguous but also the least accurate range estimate. The carrier phase measurements provide the most accurate but also the most ambiguous measurements. The estimate derived from the lowest difference frequency is therefore used only to resolve the ambiguity in the estimate derived from the second-lowest difference frequency (Figure 7-2). The estimate derived from the second-lowest difference frequency is similarly used to resolve the ambiguity in the estimate derived from the third-lowest difference frequency. This process continues until the ambiguity in the carrier phase is resolved.

Implementation

Ambiguity resolution is implemented by finding the best match between range estimate derived from two different frequencies. From inspection of (7-12), the range estimate corresponding to $f_{2,1}$ is

$$\hat{\rho}_{2,1} = \hat{\phi}_{2,1}/q_{2,1} \quad , \qquad (7\text{-}19)$$

and is assumed to be unambiguous over the interval of interest. The phase difference corresponding to carrier frequencies f_3 and f_1 is by analogy to (7-12)

$$\phi_{3,1} = \phi_{T_3} - \phi_{T_1} = q_{3,1}\,\rho \quad . \qquad (7\text{-}20)$$

The range estimate derived from this phase difference is then

$$\hat{\rho}_{3,1} = (\hat{\phi}_{3,1} + 2\pi\, l)/q_{3,1} \quad , \qquad (7\text{-}21)$$

where l represents the cycle number. (In radio-navigation systems, l is often called the *lane* number).

The cycle number is found by equating the two range estimates

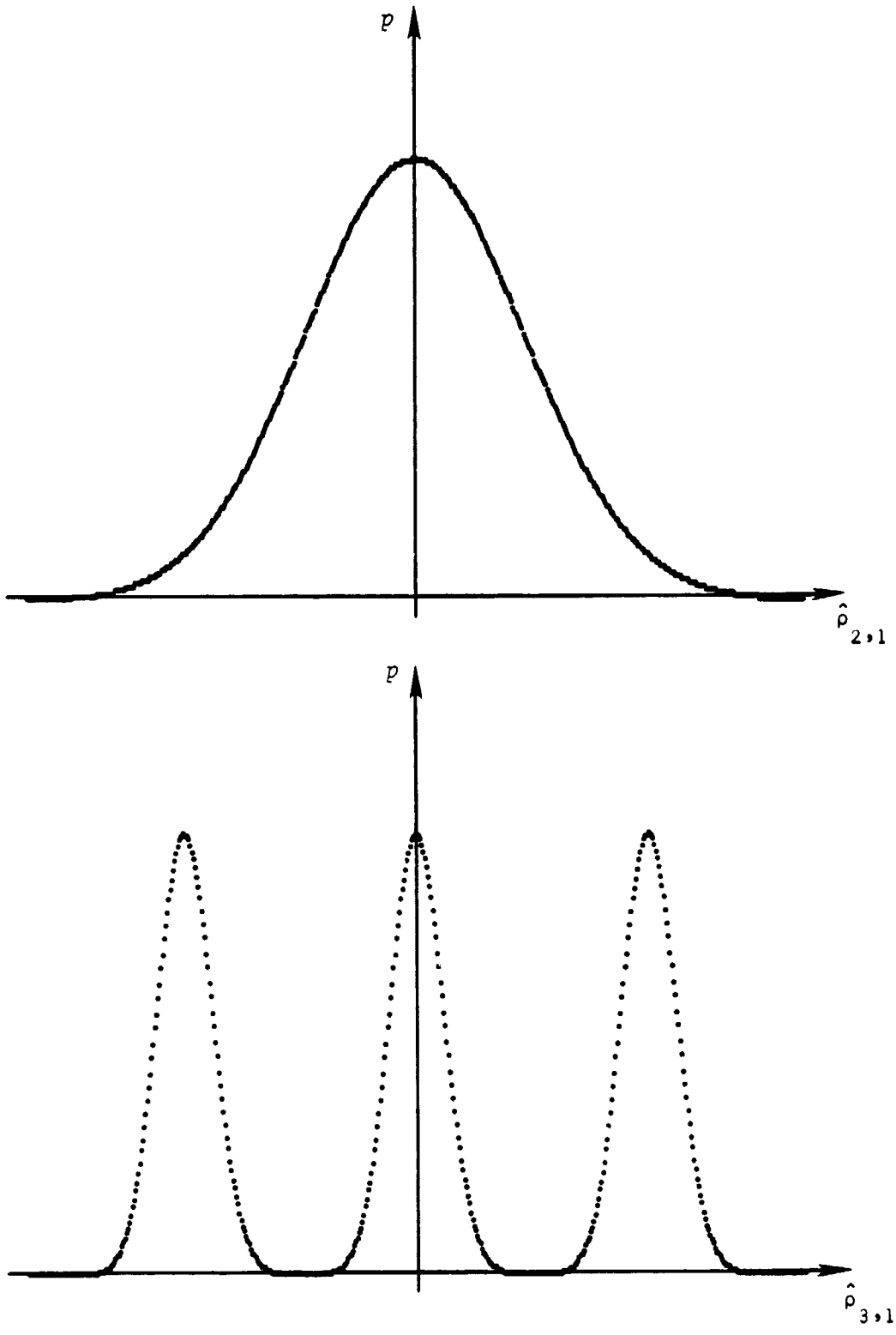

Figure 7-2. Likelihood functions for range estimates.

$$\hat{\rho}_{3,1} = \hat{\rho}_{2,1} \quad , \tag{7-22}$$

which yields

$$\hat{l} = \frac{1}{2\pi}\left(\frac{q_{3,1}}{q_{2,1}}\hat{\phi}_{2,1} - \hat{\phi}_{3,1}\right) \quad . \tag{7-23}$$

Since

$$\frac{q_{3,1}}{q_{2,1}} = \frac{f_{D_{3,1}}}{f_{D_{2,1}}} = \nu \quad , \tag{7-24}$$

the estimated lane number is simply

$$\hat{l} = \frac{1}{2\pi}\left(\nu\,\hat{\phi}_{2,1} - \hat{\phi}_{3,1}\right) \quad . \tag{7-25}$$

Note that (7-23) applies to any step in the ambiguity resolution process.

Error Analysis

Because the phase estimates used in (7-23) contain noise-induced errors, the estimated cycle number must be rounded to the nearest integer. If the total error in the two phase estimates is large enough, l is rounded to the wrong integer value and an ambiguity error occurs.

The error in determining the unrounded cycle number is related to individual phase errors by analogy to (7-23), (7-18), and (7-12), thus

$$\varepsilon_l = \frac{1}{2\pi}\left(\nu\,\varepsilon_{D_{2,1}} - \varepsilon_{D_{3,1}}\right) \tag{7-26}$$

$$= \frac{1}{2\pi}\left[\nu(\varepsilon_{T_2} - \varepsilon_{T_1}) - (\varepsilon_{T_3} - \varepsilon_{T_1})\right] \tag{7-27}$$

$$= \frac{1}{2\pi}\left[(1-\nu)\,\varepsilon_{T_1} + \nu\,\varepsilon_{T_2} - \varepsilon_{T_3}\right] \quad . \tag{7-28}$$

If the variances of all carrier phase estimates are equal, then (7-26) reduces to

$$\phi^2_{\hat{l}} = (1/2\pi)^2\left[(1-\nu)^2 + \nu^2 + 1\right]\sigma^2_{\phi_T} \quad . \tag{7-29}$$

The use of (7-5) reduces this to

$$\sigma^2_{\hat{l}} = \frac{\nu^2 - \nu + 1}{2\pi^2 R} \quad , \tag{7-30}$$

where R is the signal-to-noise ratio of each individual link.

Probability of Error

A cycle-resolution error occurs when

$$|\hat{l}| > 1/2 \quad . \tag{7-31}$$

For Gaussian noise,

$$P[|2| < L] = \text{erf}(L/2^{1/2}\ \sigma_{\hat{l}}) \quad . \tag{7-32}$$

The probability of a cycle-resolution error is therefore given by

$$p_{ei} = 1 - \text{erf}(1/2^{3/2}\ \sigma_{\hat{l}}) \quad . \tag{7-33}$$

The probability of a cycle-resolution error is shown in Table 7-1 and Figure 7-3. It is apparent that cycle ambiguity resolution is readily accomplished when the interval ratio is small.

A cycle-resolution error can occur at any step of the ambiguity-resolution process. If there are K carrier frequencies, K-1 steps are required, and

$$p_{eT} = (K - 1)\ p_{ei} \quad , \tag{7-34}$$

assuming $p_e \ll 1$ (which is required for any practical system).

Probability of error

R dB	$\nu = 2$	3	4	5	6	7	8	9	10
10.0	.0000510	.0079278	.0513752	.1252906	.2070590	.2840462	.3521332	.4109675	.4614869
11.0	.0000055	.0028910	.0288109	.0854348	.1568798	.2293676	.2964888	.3562600	.4086594
12.0	.0000003	.0008300	.0141747	.0536245	.1122007	.1774480	.2414465	.3006321	.3538883
13.0	.0000000	.0001782	.0059216	.0303620	.0747183	.1302251	.1887423	.2454884	.2982500
14.0	.0000000	.0000264	.0020158	.0151178	.0455381	.0895351	.1402990	.1925451	.2431633
15.0	.0000000	.0000024	.0005309	.0064108	.0248554	.0567769	.0980023	.1437172	.1903562
16.0	.0000000	.0000001	.0001029	.0022237	.0118222	.0325596	.0633808	.1009035	.1417481
17.0	.0000000	.0000000	.0000133	.0005996	.0047343	.0164721	.0372477	.0656715	.0992305
18.0	.0000000	.0000000	.0000010	.0001195	.0015285	.0071256	.0194284	.0388990	.0643489
19.0	.0000000	.0000000	.0000000	.0000160	.0003771	.0025340	.0087316	.0204900	.0379441
20.0	.0000000	.0000000	.0000000	.0000013	.0000674	.0007049	.0032572	.0093224	.0198748
21.0	0.0000000	.0000000	.0000000	.0000001	.0000078	.0001458	.0009621	.0035314	.0089792
22.0	0.0000000	.0000000	.0000000	.0000000	.0000005	.0000206	.0002138	.0010634	.0033716
23.0	0.0000000	.0000000	.0000000	.0000000	.0000000	.0000018	.0000331	.0002417	.0010042
24.0	0.0000000	0.0000000	.0000000	.0000000	.0000000	.0000001	.0000032	.0000386	.0002252
25.0	0.0000000	0.0000000	.0000000	.0000000	.0000000	.0000000	.0000002	.0000039	.0000354
26.0	0.0000000	0.0000000	.0000000	.0000000	.0000000	.0000000	.0000000	.0000002	.0000035
27.0	0.0000000	0.0000000	0.0000000	.0000000	.0000000	.0000000	.0000000	.0000000	.0000002
28.0	0.0000000	0.0000000	0.0000000	.0000000	.0000000	.0000000	.0000000	.0000000	.0000000
29.0	0.0000000	0.0000000	0.0000000	0.0000000	.0000000	.0000000	.0000000	.0000000	.0000000
30.0	0.0000000	0.0000000	0.0000000	0.0000000	.0000000	.0000000	.0000000	.0000000	.0000000

Table 7-1. Probability of error in cycle resolution.

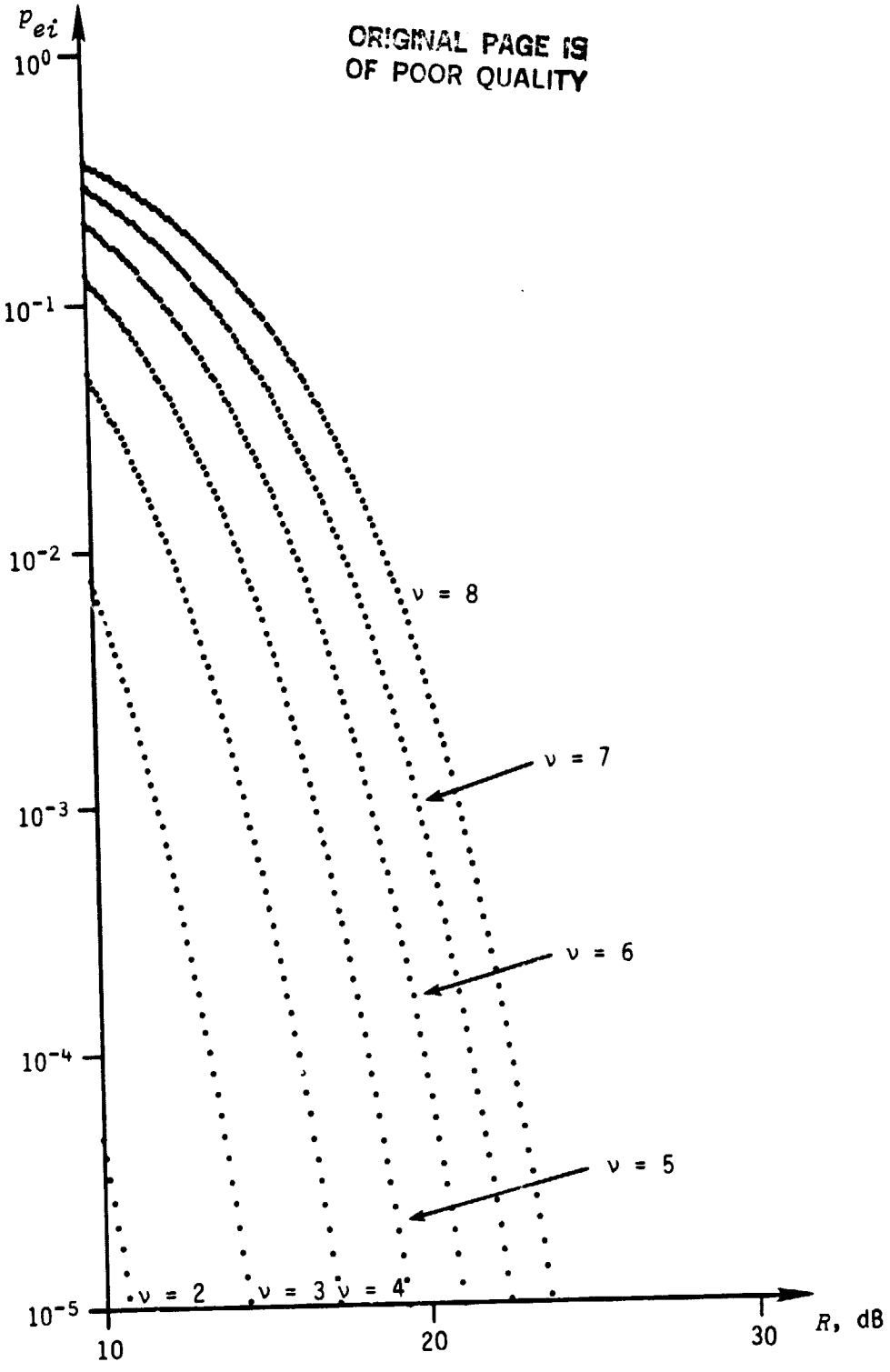

Figure 7-3. Probability of error in cycle resolution.

CHAPTER 8

SYSTEM DESIGN

Multiple-carrier CW ranging has been identified as the preferred signal format for present-day implementation of a polarized-interferometer system. The dependence of accuracy and cycle-ambiguity-error probability upon SNR is determined in the previous chapter. These relationships and the requirements from Chapter 2 are now used to develope a suitable system design. This design is then verified by simulation.

Requirements

The accuracy requirements (Table 1-1) affecting the system design are:

- Range accuracy (3σ): One percent of range,
- Direction-finding accuracy (3σ): 10 mrad $\cong$ 0.57°, and
- Roll accuracy (3σ): 30 mrad $\cong$ 1.7°.

Operation at distances up to 100 km may be required. To allow stand-alone operation, two-way range ambiguities of up to 200 km must be resolved, hence

$$f_A = \frac{c}{2 \cdot 100 \text{ km}} = 1.5 \text{ kHz} \quad . \tag{8-1}$$

To prevent noise from causing ambiguity-resolution errors at minimum and maximum range, f_0 must be smaller than f_A. To achieve approximately the same probability of ambiguity-resolution error as in the other steps, it is necessary to reduce f_0 to

$$f_0 = \frac{\nu}{\nu + 1} f_A \quad . \tag{8-2}$$

If $\nu = 6$ is assumed, then $f_0 = 1250$ Hz is satisfactory.

Since a cycle-ambiguity error produces significant range and direction-finding (DF) errors, a very low probability of error is desirable. For this design, $p_{eT} = 0.001$ is assumed.

Minimization of the power that must be radiated from the passive-spacecraft transponder is also an important consideration.

Candidate Approaches

Candidate approaches can be divided into two categories:

- Carrier-frequency tracking (CFT), and
- Difference-frequency tracking (DFT).

The CFT system derives range from carrier phase, while the DFT system derives range from the phase of a difference-frequency signal. Both systems utilize a number of CW signals to provide ambiguity resolution.

The CFT system obtains the same range accuracy with a lower SNR, since only two signals (forward and reverse) are involved, and the wavelength of the carrier is quite short. However, both SNR and hardware-induced phase biases limit the cycle-resolution ratio, hence the CFT system requires a relativly large maximum difference frequency ($f_K - f_1$). The candidate design discussed here uses f_{F_1} = 3 GHz and f_{R_1} = 2 GHz (Figure 8-1a). Assuming that the cycle-resolution ratio ν = 6, the maximum difference frequency is 420 MHz.

The DFT system requires a higher SNR. However, the smaller maximum difference frequency allows a smaller antenna bandwidth. The candidate design discussed here uses a maximum difference frequency of 100 MHz. It can therefore use somewhat lower carrier frequencies such as f_{F_1} = 2.4 GHz and f_{R_1} = 1.6 GHz (Figure 8-1b).

Excitation of the antenna elements is most readily accomplished by using individual power amplifiers dedicated to each element. Simultaneous retransmission with frequency-division multiplexing is therefore preferred. As shown in Figure 8-2, the active-spacecraft transponder transmits sequentially on each of nine different frequencies. During each of the corresponding nine time slots, all four elements of the passive-spacecraft array retransmit on slightly different frequencies. A total of thirty-six different frequencies are therefore allocated to the return transmissions. This technique adds no complexity and, in fact, minimizes the peak power in the passive-spacecraft transponder.

8.1 CARRIER-FREQUENCY TRACKING

Range-Accuracy Requirement

The minimum operating range determines the range-accuracy requirement. For operation at a distance of 1 m, the 3σ accuracy is 1 cm, hence the standard deviation (rms) of the range estimate is

$$\sigma_{\hat{\rho}} = \frac{0.01}{3} = 0.0033 \quad . \tag{8-3}$$

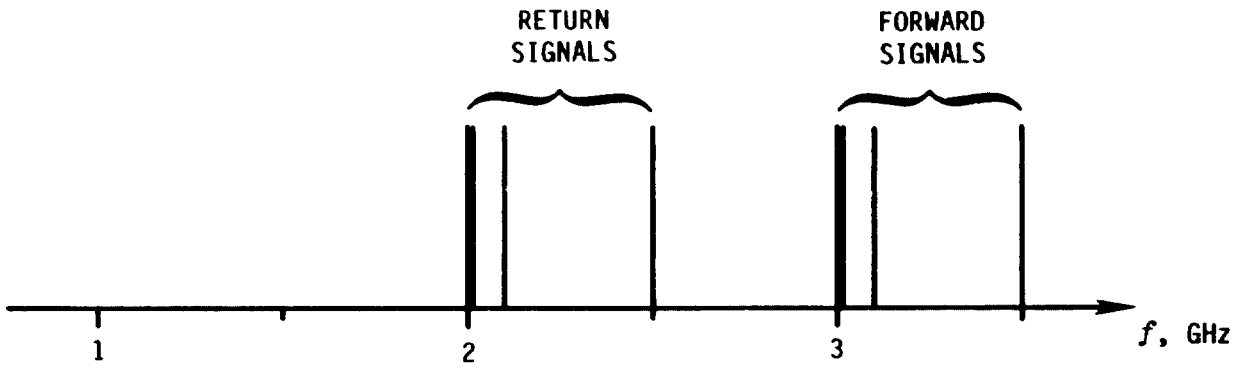

(a) CFT system.

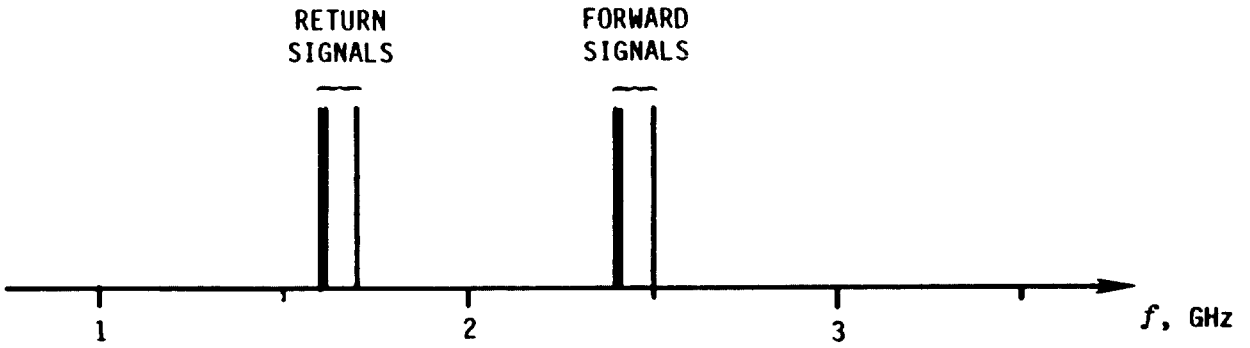

(b) DFT system.

Figure 8-1. Frequency allocations.

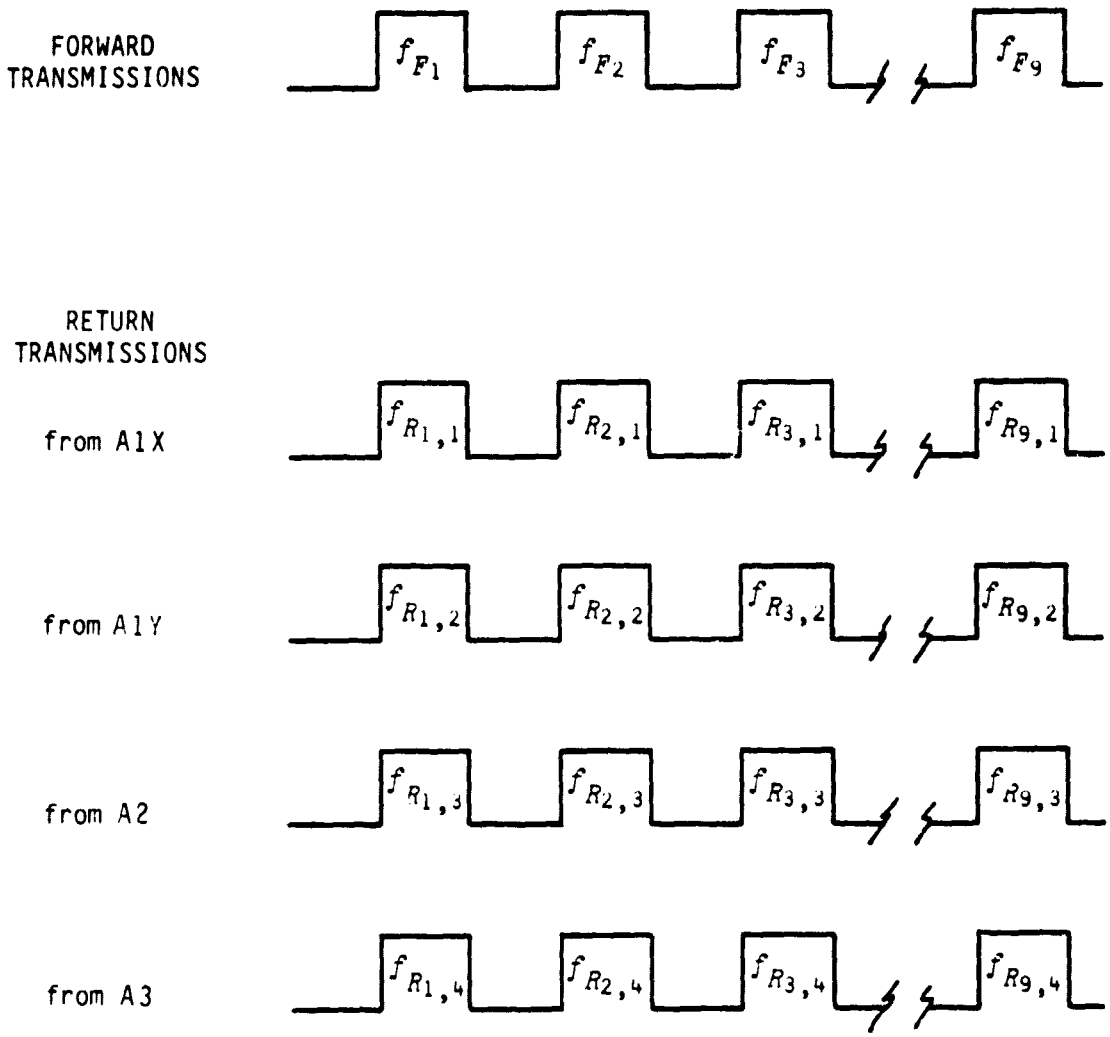

Figure 8-2. Transmission format.

The variances of the range estimate $\hat{\rho}$ and the range measurements y_i are related by (4-20), thus

$$\sigma_{\hat{\rho}} \approx 0.278\ \sigma_y^2 \tag{8-4}$$

and

$$\sigma_y = 0.1095 \text{ m} = 10.95 \text{ cm} \quad . \tag{8-5}$$

This requirement turns out not to be the most stringent and therefore does not drive the system design.

DF-Accuracy Requirement

The requirement for a 3σ direction-angle accuracy of 10 mrad implies an rms angular error of 3.33 mrad or 0.191°. From (4-21),

$$(0.0333)^2 = V_2 = \frac{0.4448\ \sigma_y^2}{\cos^2 \theta_{max}} \quad , \tag{8-6}$$

where θ_{max} is the maximum off-boresight angle. To allow operations within a 45° cone, $\theta_{max} = 45°$ and

$$\sigma_y = 0.00353 \text{ m} = 3.53 \text{ mm} \quad . \tag{8-7}$$

For the candidate CFT system,

$$f_{T_1} = (f_{F_1} + f_{R_1})/2 = 2.5 \text{ GHz} \quad , \tag{8-8}$$

hence

$$\lambda_T = 3 \cdot 10^8 / f_{T_1} = 0.120 \text{ m} = 12.0 \text{ cm} \quad . \tag{8-9}$$

Now from (7-12),

$$\sigma_\phi = (2\pi/\lambda_T)\ \sigma_y = 0.185 \text{ rad} = 10.6° \quad . \tag{8-10}$$

The required SNR is now determined by using (7-5):

$$R_F = R_R = 1/\sigma_\phi^2 = 29.22 \approx 14.7 \text{ dB} \quad . \tag{8-11}$$

Obviously, this requirement is met by any system capable of achieving phase lock.

Roll-Accuracy Requirements

Inspection of Figure 4-4 shows that $V_4 < 2$ for off-boresight angles of up to 45°. The 30-mrad 3σ roll-accuracy requirement implies an

rms roll error of 10 mrad (0.57°). Therefore, the normalized rms noise amplitude is

$$\sigma_a = \sigma_{\psi_r}/2^{1/2} = 0.00707 \quad . \tag{8-12}$$

The corresponding SNR is

$$R_R = 1/(2\,\sigma_a^2) = 10^4 \rightarrow 40 \text{ dB} \quad , \tag{8-13}$$

and the corresponding gain error is

$$\varepsilon_G = 20 \log (1.00707) = 0.061 \text{ dB} \quad . \tag{8-14}$$

Ambiguity-Resolution Requirements

The SNR required for a given probability of cycle-ambiguity-resolution error can be obtained by iterative application of (7-31). The results for the two design examples are presented in Table 8-1.

It is apparent from Table 8-1 that the transmission on nine different RF carrier frequencies requires six phase cycles to be resolved in each step of the ambiguity-resolution process. For $p_{eT} \leq 0.001$, $p_{ei} = 0.001/9 = 0.00011$, hence $R > 19.7$ dB. The nine carrier frequencies range from 2.0 GHz to approximately 2.42 GHz.

Ambiguity-resolution errors can also arise from unknown hardware phase shifts. If ϕ_{max} represents the maximum unknown hardware phase shift, then

$$\Delta\phi_{max} + \frac{1}{\nu}\,\Delta\phi_{max} = \frac{180°}{\nu} \quad . \tag{8-15}$$

For this example,

$$\Delta\phi_{max} \leq \frac{180°}{\nu + 1} = 25.7° \quad , \tag{8-16}$$

which is much less stringent than the requirement imposed by DF accuracy.

Link Design

The SNR at the receiver is given by

$$R = \frac{P_t}{P_n}\,\frac{G_t\,G_r}{L_p} \quad , \tag{8-17}$$

where P_t represents the radiated power and G_t and G_r represent the transmitting and receiving antenna gains, respectively. The receiver thermal-noise power is given by

C-2

K	p_{ei}	CARRIER-FREQUENCY TRACKING		DIFFERENCE-FREQUENCY TRACKING	
		ν	R_{min}, dB	ν	R_{min}, dB
2	.0010000	1666668.000	110.0	66666.633	102.9
3	.0005000	1290.995	66.1	258.199	55.1
4	.0003333	118.563	45.6	40.548	39.2
5	.0002500	35.930	35.3	16.069	31.2
6	.0002000	17.554	29.1	9.221	26.3
7	.0001667	10.889	24.9	6.368	23.1
8	.0001429	7.742	21.9	4.888	20.7
9	.0001250	5.994	19.7	4.009	18.9
10	.0001111	4.913	17.9	3.435	17.5
11	.0001000	4.190	16.4	3.037	16.4
12	.0000909	3.678	15.3	2.745	15.6
13	.0000833	3.300	14.3	2.523	14.8
14	.0000769	3.010	13.5	2.350	14.2
15	.0000714	2.782	12.8	2.211	13.7
16	.0000667	2.599	12.2	2.097	13.3
17	.0000625	2.448	11.7	2.002	13.0
18	.0000588	2.323	11.3	1.922	13.0
19	.0000556	2.216	10.9	1.854	13.0
20	.0000526	2.126	10.5	1.794	13.0
21	.0000500	2.047	10.2	1.743	13.0
22	.0000476	1.978	10.0	1.697	13.0
23	.0000455	1.918	10.0	1.657	13.0
24	.0000435	1.864	10.0	1.621	13.0
25	.0000417	1.817	10.0	1.589	13.0

Table 8-1. Ambiguity-resolution requirements for two example system designs.

$$P_n = k_B\ T\ B\ F \quad , \tag{8-18}$$

where k_B, T, B, and F represent, respectively, Boltzman's constant ($1.38 \cdot 10^{-23}$), temperature (°K), bandwidth (Hz), and noise figure. The path loss is given by

$$L_p = (4\pi)^2\ \rho^2/\lambda^2 \quad . \tag{8-19}$$

In the present application, hemispherical antenna coverage produces $G_t = G_r = 3$ dB. A noise figure of 10 dB or better is readily achievable at the frequencies of interest. The required SNR can then be determined by manipulation of (8-17) - (8-19).

The greatest SNR requirement is imposed by the roll-angle accuracy specification. To obtain the required 40-dB SNR at a distance of 100 km requires the active-spacecraft transponder to radiate 2.13 W and the passive-spacecraft transponder to radiate 1.07 W (Table 8-2).

However, roll-angle information is not actually needed until the two spacecraft enter the docking phase (Section 1.2). The next-most demanding SNR requirement (19.7 dB) is imposed by the ambiguity-resolution specification. To obtain a 20-dB SNR at a distance of 100 km requires forward- and reverse-link radiated powers of 21.3 mW and 10.7 mW, respectively (Table 8-2). With these power levels, SNR increases to 40 dB at a distance of 10 km, hence the roll-angle accuracy specification can be met at distances of 10 km or less.

8.2 DIFFERENCE-FREQUENCY TRACKING

The design of a DFT system is, in most respects, identical to the design of a CFT system. As in the example CFT design discussed previously, the DF accuracy specification produces a more stringent range-accuracy requirement than does the range-accuracy specification. The roll-angle accuracy specification again requires a 40-dB SNR.

DF-Accuracy Requirement

The candidate DFT system design uses a maximum frequency difference of 100 MHz to reduce antenna-bandwidth requirements. By analogy to (8-8), (8-9), and (8-10),

$$f_T = 100\ \text{MHz} \quad , \tag{8-20}$$

$$\lambda_T = 3 \cdot 10^8/f_T = 3.0\ \text{m} \quad , \tag{8-21}$$

and

SNR	POWER	
	Forward Link f_F = 3.424 GHz	Return Link f_R = 2.424 GHz
40 dB at 100 km	2.134 W	1.069 W
20 dB at 100 km 40 dB at 10 km	21.34 mW	10.69 mW

Note: B = 100 Hz, F = 10 dB, $G_t = G_r$ = 3 dB

Table 8-2. Power requirements, CFT system.

SNR	POWER	
	Forward Link f_F = 2.5 GHz	Return Link f_R = 1.7 GHz
46 dB at 100 km	4.540 W	2.099 W

Note: B = 100 Hz, F = 10 dB, $G_t = G_r$ = 3 dB

Table 8-3. Power requirements, DFT system.

$$\sigma_\phi = 0.00739 \text{ rad} = 0.423^\circ \quad . \tag{8-22}$$

The rms phase error in (8-22) is the result of differencing two phase measurements. Therefore, the required SNR is obtained by insertion of a factor of 2 into (8-11):

$$R_F = R_R = \frac{2}{\sigma_\phi^2} = 36621.9 \rightarrow 45.6 \text{ dB} \quad . \tag{8-23}$$

Ambiguity-Resolution Requirements

Inspection of Table 8-1 shows that the use of eight different carrier frequencies requires resolution of just less than five cycles per step. A SNR of 20.7 dB is required.

Link Design

A 46-dB SNR is required to meet both the DF accuracy specifications. Since the DF accuracy specification must be met at 100 km, the radiated powers of the forward and reverse links are 4.54 W and 2.10 W, respectively (Table 8-3).

8.3 SIMULATION IMPLEMENTATION

Approach

Carrier-frequency tracking requires less power than does difference-frequency tracking. Since minimization of the power required by the passive-spacecraft transponder is essential, CFT is preferable to DFT.

However, the MVLE tracking algorithm developed in Chapter 4 requires explicit determination of two-way range. In the absence of noise- and hardware-induced errors, two-way range is determined exactly by difference-frequency tracking but only approximately by carrier-frequency tracking (7-7).

The polarized-interferometer simulation is therefore implemented using difference-frequency tracking exclusively. The frequency scheme is, however, that of the CFT approach discussed in Section 8.1. The requirement for a 40-dB SNR at 100 km implies $P_F = 2.2$ W and $P_R = 1.1$ W.

Characteristics

The principal characteristics of the simulation system design are:

- $f_0 = 1250$ Hz and $\nu = 6.13$,
- Frequency-division multiplexing (Figure 8-2),

- Nine forward-link carrier frequencies (3.0 - 3.42 GHz),
- Nine return-link carrier frequencies for each of four antennas (2.0 - 2.42 GHz),
- P_F = 2.2 W and P_R = 1.1 W,
- $G_t = G_r$ = 3 dB and F = 10 dB,
- Difference-frequency tracking,
- Nine carrier-amplitude measurements are averaged to obtain each amplitude-coupling estimate,
- Range accuracy to be one percent of range or better,
- Directional accuracy to be 3.3 mrad (0.2°) rms or better,
- Roll-angle accuracy to be 10 mrad (0.6°) rms or better when $\rho < 10$ km,
- Maximum operational distance of 100 km.

Implementation

The simulation program is implemented by combining an RF-system simulation and the minimum-variance linear estimator algorithms developed in Chapter 4. The MVLE for range is replaced by the less complex estimator from the initialization algorithm (Chapter 3); this estimator simply averages the nine two-way range estimates. The complete simulation program is listed in the Appendix.

The simulation program assumes that SNR is 10 dB or better at all points of interest. The effects of noise upon carrier phase and amplitude are therefore modelled as independent, additive, Gaussian random variables. The SNR and associated random error in the forward and return paths are calculated separately.

The RF subroutine includes an ambiguity-resolution algorithm. The individual two-way range estimates are checked for ambiguity-resolution errors prior to estimating position and attitude. Ambiguity-resolution errors are tallied, and estimation of position and attitude in inhibited if an ambiguity-resolution error occurs.

Results

The results of the simulations are graphed in Figures 8-3 and 8-4. The simulation program determines rms error in range ($\hat{\rho}$), passive-spacecraft direction ($\hat{\phi}_1$), active-spacecraft direction ($\hat{\phi}_2$), and relative roll

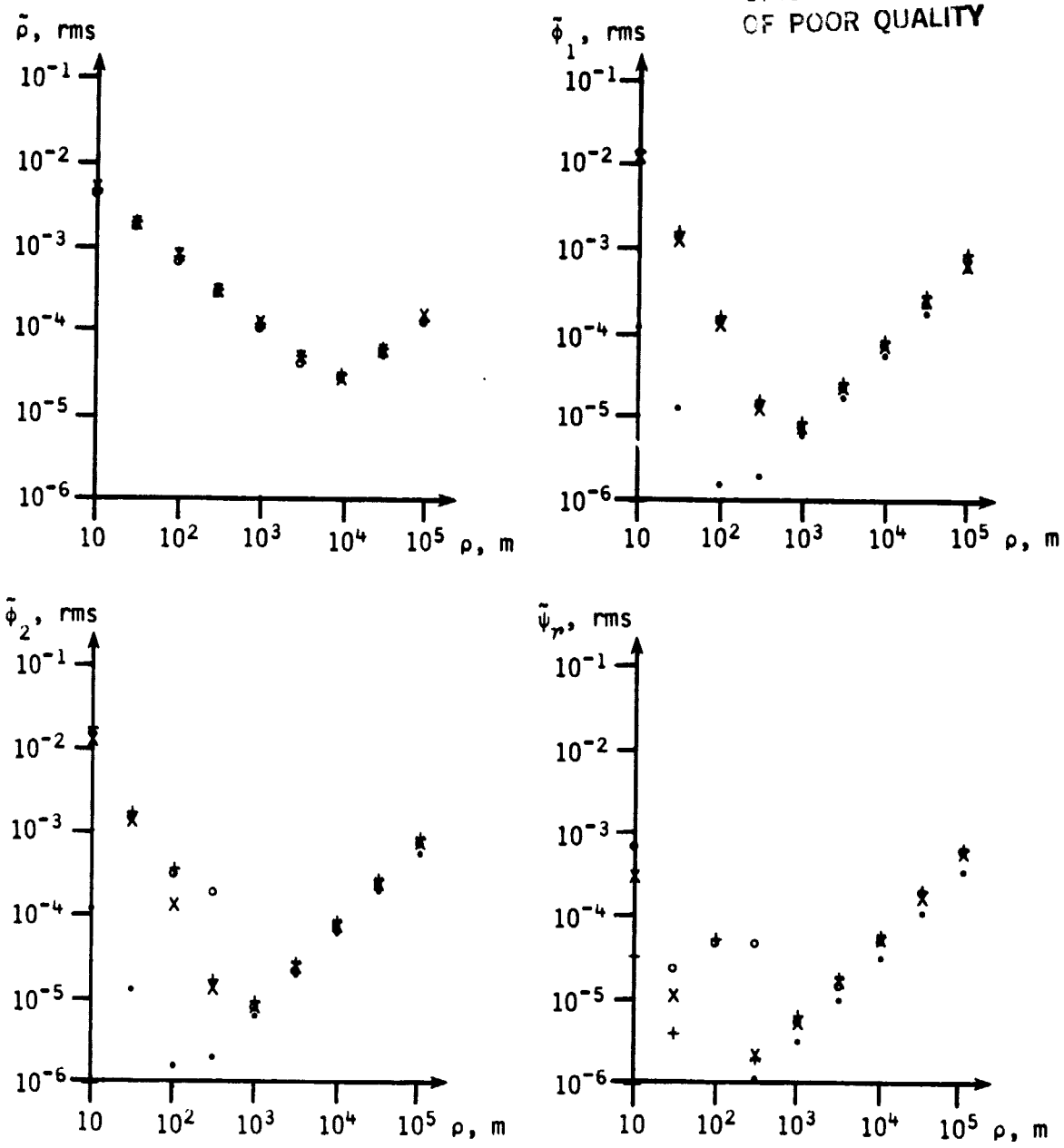

All tests: $\psi_r = \psi_x = \psi_y = \psi_z = 0°$

Symbols	.	o	+	x
α_1	0°	45°	0°	26.6°
β_1	0°	0°	45°	26.6°

Figure 8-3. Simulation error vs. range.

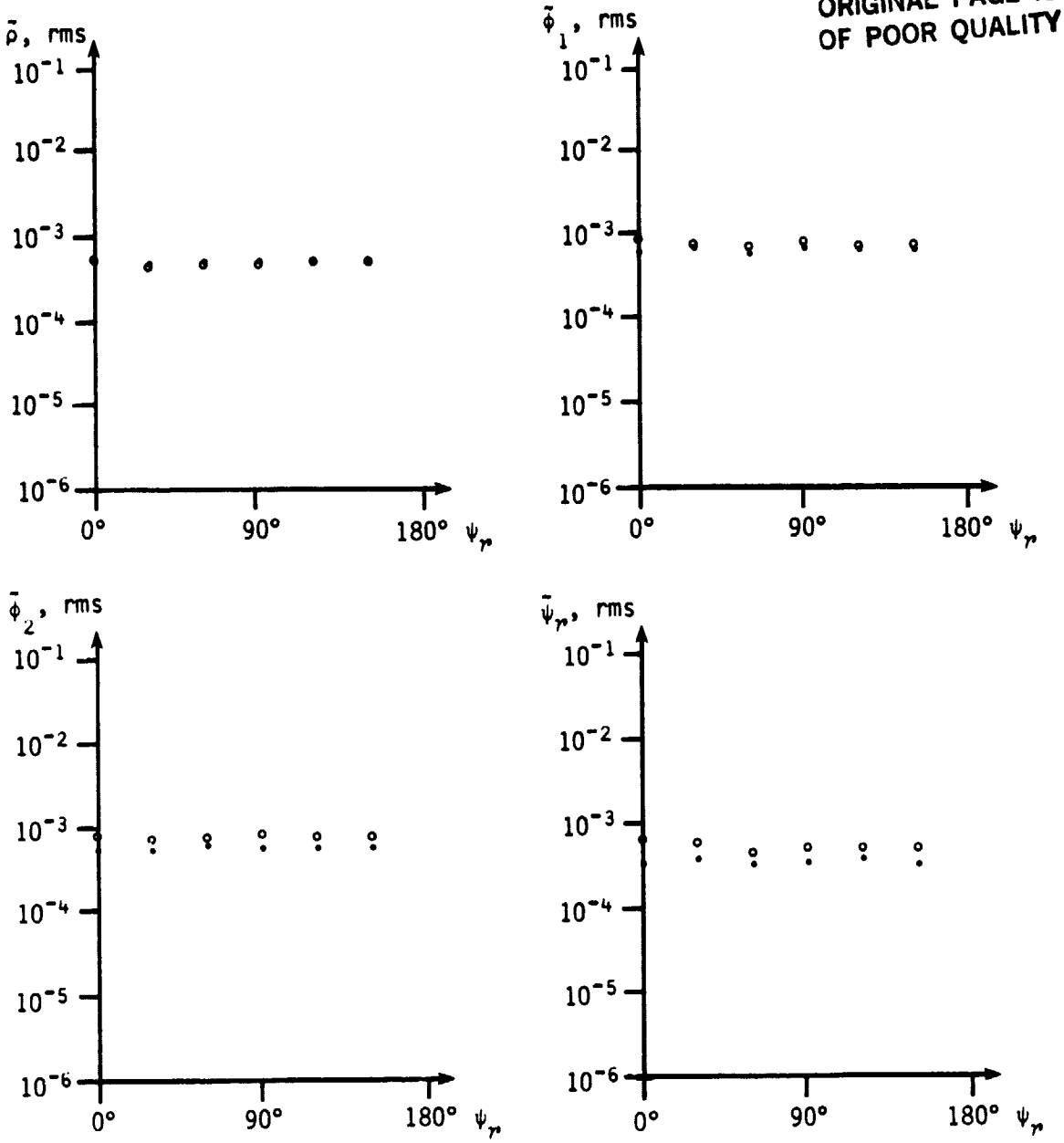

All tests: ρ = 100 km, $\psi_x = \psi_y$ = 0°

- α_1 = 0°, β_1 = 0°
- α_1 = 45°, β_1 = 0°

Figure 8-4. Simulation error vs. roll.

($\hat{\psi}_n$). Each test series comprises 100 individual trials.

The variations of rms errors with range are shown in Figure 8-3. At the maximum design range of 100 km, DF and errors do not exceed 1 mrad rms, which is well below the design goal of 3.3 mrad rms. All angular errors decrease to insignificant values as distance decreases. Range error does not exceed 1 mm rms at the maximum 100-km range. The increases in range error at short distances are due to a simplification used in the range-estimation algorithm, but are nonetheless below the desired one-percent-of-range specification. The increase in DF error at very short distances is due to the increase in the error in the range estimate.

The variations of rms errors with relative roll are shown in Figure 8-4. It is apparent that satisfactorily low values are obtained, and that roll does not significantly alter the error sensitivity.

Conclusions

The simulation results validate the system design and prove that the polarized-interferometer concept is indeed feasible. Since the rms error is in all cases smaller than the design requirement, the candidate design includes a margin for protection against additional system errors.

The algorithm developed to date requires that phase measurements be converted to two-way range measurements, which are then used to determine range, direction angles, and relative-roll angle. Because different frequencies are used in the forward and return links (and the receiving and retransmitting antennas are at different locations), two-way range cannot be determined exactly by carrier-frequency tracking. Consequently, difference-frequency tracking and the associated higher power levels are used in the simulation.

Modification of the direction-finding algorithm to use range differences instead of two-way ranges will allow the use of carrier-frequency tracking. If such an algorithm is implemented, the required radiated power drops from 2.2 W (forward) and 1.1 W (return) to 42 mW (forward) and 21 mW (return). The lower power requirement should be most useful in simplifying the passive-spacecraft transponder. The increase in rms range error at short distances can be eliminated by using a true minimum-variance range estimator, rather than the approximation used in the simulation program.

CHAPTER 9

CONCLUSIONS AND RECOMMENDATIONS

The polarized interferometer is a radio-frequency system for real-time measurement of relative position and attitude. This report presents the results of a study of the feasibility of a rendezvous-and-docking sensor based upon the polarized-interferometer concept. In the anticipated application, one spacecraft is active (maneuverable) while the other spacecraft is passive.

The major accomplishments of this study include:

- Development of an algorithm for obtaining initial position and attitude estimates without any *a priori* information,
- Development of a tracking algorithm based upon minimum-variance linear estimators,
- Determination of the sensitivity of estimates to measurement errors,
- Evaluation of concepts for the passive-spacecraft transponder,
- Establishment of a configuration for the passive-spacecraft transponder, and
- Implementation of a static simulation program.

The performance requirements used in this study are:

- Operation at distances up to 100 km,
- Operation up to 45° off boresight of either spacecraft,
- Rms range accuracy (3σ) of one percent of range,
- Direction accuracy of 10 mrad (3σ), and
- Roll accuracy of 30 mrad (3σ) at distances up to 10 km.

The preferred system configuration uses multiple-carrier CW signals for precise and unambiguous range measurement. Frequencies in the 2 - 3 GHz band are used, and the required radiated power is only 20 to 40 mW. Each antenna arrays consists of four sets of two crossed dipoles or crossed slots.

The polarized interferometer is one of several possible techniques that can be used in a rendezvous and docking sensor. However, it has several potential advantages, including:

- Measurement of position and attitude,
- Operation at both long and short ranges,
- Real-time operation,
- Stand-alone operation, and
- Simple, low-power transponder for the passive spacecraft.

The three principal conclusions of this study are:

- The analysis and design equations are correct;
- The polarized-interferometer is feasible; and
- The requirements for a rendezvous-and-docking sensor are reasonable.

A number of details should be resolved before hardware implementation and testing is initiated. Further evaluation is recommended in the following three areas:

- Tracking algorithm,
- Antenna characteristics, and
- Dynamic simulation.

The recommended work and anticipated benefits are discussed below.

The tracking algorithm developed in Chapter 4 operates upon a set of nine two-way range measurements (in addition to four amplitude measurements). Since exact two-way range can be determined only from difference-frequency measurements, the simulation (Chapter 8) must use difference-frequency tracking and its associated higher power levels (1 - 2 W). The tracking algorithm can be redesigned to use range differences rather than two-way ranges. This will allow the use of carrier-frequency tracking and its associated power levels (20 - 40 mW). It will also eliminate the need for a number of double-precision computations, which will reduce the required computation time.

The tracking algorithm must employ some form of gradient computation to operate accurately at both long and short ranges. However, many redundant gradient computations in the developmental algorithm of Chapter 4 can be eliminated. The developmental algorithm uses numerical techniques to compute all gradients. Additional reductions in computation time may be possible by computing some or all of the gradients analytically. Redesign of the tracking algorithm is therefore highly recommended.

The accuracy of the roll estimate depends directly upon the accuracy with which signal amplitude can be measured. Antenna characteristics that affect pattern ripple and variability should therefore be investigated further. If the cone of operation in which precise roll measurements are necessary can be limited to less than 45° from boresight, the antenna problem will become much less difficult. The actual requirements for roll accuracy should therefore be reviewed carefully.

The simple simulation done as part of this study involved only static spacecraft. In contrast, a real rendezvous-and-docking operation involves various combinations of spacecraft dynamics. It also may include signal outages, antenna-pattern ripple at particular relative attitudes, and other effects. The final step in the evaluation of the feasibility of the polarized-interfereometer system is therefore dynamic simulation from acquisition to docking.

REFERENCES

Bacinski, R. R. and R. J. Helgeson, "Orbiter S-band communications subsystem," *IEEE Transactions on Communications*, vol. COM-26, no. 11, pp. 1521 - 1531, November 1978.

Blanchard, E. P., R. C. Hutchinson, and L. B. Johnson, "Space shuttle vehicle automatic docking study," Final Report NASA-CR-115248 (N72 12589), MIT, Cambridge, MA, October 1971.

Brown, R. G., *An Introduction to Random Signal Analysis and Kalman Filtering*, New York: John Wiley and Sons, Inc., 1983.

Cager, R. H., Jr., D. T. LaFlame, and L. C. Parode, "Orbiter Ku-band integrated radar and communications subsystem," *IEEE Transactions on Communications*, vol. COM-26, no. 11, pp. 1604 - 1619, November 1978.

Carrier, L. M. and W. S. Pope, "An overview of the space shuttle orbiter communication and tracking system," *IEEE Transactions on Communications*, vol. COM-26, no. 11, pp. 1494 - 1505, November 1978.

Clarke, K. K. and D. T. Hess, *Communication Circuits: Analysis and Design*, Reading, Massachusetts: Addison-Wesley Publishing Company, 1971.

Dabney, R., "A digital vision system and autonomous rendezvous and docking simulation," NASA, George C. Marshall Space Flight Center, AL, November 6, 1981.

Dixon, R. C., *Spread Spectrum Systems*, New York: John Wiley and Sons, 1976.

Ellis, J. F. and G. A. Creswell, "Interferometric attitude determination with the Global Positioning System," AIAA Paper # 78-1250, 1978.

Farrel, J. L., *Integrated Aircraft Navigation*, New York: Academic Press, 1976.

Flom, T. and D. Coombies, " Multiple target tracking and target attitude determination with a scanning laser radar," *Navgiation*, vol. 21, no. 4, pp. 298 - 309, Winter 1974-1975.

Gold, R., "Optimal binary sequences for spread spectrum multiplexing," *IEEE Trans. Information Theory*, vol. IT-13, no. 4, pp. 619 - 621, October 1967.

Krauss, H. L., C. W. Bostian, and F. H. Raab, *Solid State Radio Engineering*, New York: John Wiley and Sons, 1980.

Laurie, R. J., "Advanced multipurpose rendezvous tracking system study," Report No. RCA-PRRL-82-CR-1 (NAS9-16252), RCA laboratories, Princeton, NJ, June 1, 1982.

Legostaev, V. P. and B. V. Raushenbakh, "Automatic rendezvous in space," Report AD-686,990, Foreign Technology Division, WPAFB, OH, December 1968.

Lowry, J H., "Electromagnetic guidance study," NASA CR-865, McDonnell Aircraft Corporation, St. Louis, MO, September 1967.

Michael, J. D., "A study of autonomous rendezvous and docking systems," Large Space Systems Technology Conference - 1981, Third Annual Technical Review, November 16-19, 1981.

Milliken, R. J. and C. J. Zoller, "Principle of operation of NAVSTAR and system characteristics," *Global Positioning System Monograph*, pp. 3 - 14, Washington, DC: Institute of Navigation, 1980. Also *AGARDograph No. 245, Principles and Operational Aspects of Precision Position Determination Systems* (AD-A075 208), pp. 4-1 - 4-12, July 1979.

Monzingo, R. A. and T. W. Miller, *Introduction to Adaptive Arrays*, New York: John Wiley and Sons, Inc., 1980.

Nahi, N. E., *Estimation Theory and Applications*, New York: John Wiley and Sons, Inc., 1969.

Parkinson, B. W., "Overview," *Global Positioning System Monograph*, pp. 1 - 2, Washington, DC: Institute of Navigation, 1980.

Raab, F. H., "Communication and navigation systems for aircraft-to-aircraft operation of helmet-mounted sight and display systems," GMRR-TR82-4, Green Mountain Radio Research Company, Burlington, VT, October 1982.

Raab, F. H., "Quasi-static magnetic-field technique for determining position and orientation," *IEEE Transactions on Geoscience and Remote Sensing*, vol. GE-19, no. 4, pp. 235 - 243, October 1981.

Raab, F. H., E. B. Blood, T. O. Steiner, and H. R. Jones, "Magnetic position and orientation tracking system," *IEEE Transactions on Aerospace and Electronic Systems*, vol. AES-15, no. 5, pp. 709 - 718, September 1979.

Thelander, J. A., "Aircraft motion analysis," Technical Report FDL-TDR-64-70 (AD 617,354), Air Force Flight Dynamics Laboratory, Wright-Patterson Air Force Base, OH, March 1965.

Tietz, J. C. and J. H. Kelly, "Development of an autonomous video rendezvous and docking system," Final Report No. MCR-82-569 (NAS8-34679), Martin Marietta Aerospace, Denver, CO, June 1982.

Weber, C. L. and W. K. Atem, "Space shuttle proximity operation sensor study," Final Report No. R7802-2 (NAS9-15502), Axiomatix, Marina del Rey, CA, February 15, 1978.

Wylie, C. R., Jr., *Advanced Engineering Mathematics*, Second Edition, New York: McGraw-Hill Book Company, Inc., 1960.

REFERENCES WITHOUT AUTHORS

"NBS improves accuracy of VHF-UHF antenna tests," *Microwaves*, vol. 21, no. 11, pp. 37 - 40, 1982.

APPENDIX

PROGRAM LISTINGS

Initialization Algorithm

```
C  Program # FHR-289-, 12/10/82
C  Initialization algorithm for polarized interferometer
C
C  Declarations and constants
C
      IMPLICIT LOGICAL (L)
      DIMENSION A1(3), A2(3), A3(3), P1(3), P2(3), P3(3),
     >  A(3,3), AT(3,3), VEC1(3), VEC2(3), R(3,3), AHAT(3,3),
     >  C(3,3)
      WRITE(3,10)
   10 FORMAT(' Initialization algorithm for polarized inter',
     >  'ferometer, Program # FHR-289-',/)
      DR=0.017453293
C
C  Get true parameters
C
  100 WRITE(3,110)
  110 FORMAT(' True position (rho,alpha1,beta1) = ')
      CALL ATR(RHO,IERR)
      IF(IERR.EQ.27) GO TO 100
      CALL ATR(ALPHA1,IERR)
      IF(IERR.EQ.27) GO TO 100
      IF((ALPHA1.GT.90.0).OR.(ALPHA1.LT.-90.0)) GO TO 100
      CALL ATR(BETA1,IERR)
      IF(IERR.EQ.27) GO TO 100
      ALPHA1=ALPHA1*DR
      BETA1=BETA1*DR
      WRITE(3,120)
  120 FORMAT(' True attitude (psiz, psiy, psix) = ')
      CALL ATR(PSIZ,IERR)
      IF(IERR.EQ.27) GO TO 100
      CALL ATR(PSIY,IERR)
      IF(IERR.EQ.27) GO TO 100
      CALL ATR(PSIX,IERR)
      IF(IERR.EQ.27) GO TO 100
      PSIZ=PSIZ*DR
      PSIY=PSIY*DR
      PSIX=PSIX*DR
C
C  Calculate position in rectangular coordinates and attitude matrix
C
      CALL PRC(RHO,ALPHA1,BETA1,VEC1)
      CALL ACOMP(PSIZ,PSIY,PSIX,A)
      CALL TRANS(3,3,A,AT)
C*      WRITE(3,200)
C*  200 FORMAT(/,' Position vector = ')
C*      CALL MWRITE(3,1,3,VEC1)
C*      WRITE(3,210)
C*  210 FORMAT(' Attitude matrix = ')
C*      CALL MWRITE(3,3,3,A)
C
C  Calculate locations of antenna elements
C
      CALL PATHES(VEC1,AT,R)
C
C  Calculate coupling between linearly polarized elements
      CALL COUPLE(ALPHA1,BETA1,AT,C)
C*      WRITE(3,220)
C*  220 FORMAT(/,' C = ')
C*      CALL MWRITE(3,3,3,C)
C
C  Estimate range
```

```
C
      CALL ERANGE(R,RHOHAT)
      WRITE(3,400) RHOHAT
  400 FORMAT(/,' Rhohat = ',G15.8)
C
C  DF at active array
C
      CALL DFACT(RHOHAT,R,ALPH1H,BETA1H)
      ALPH1D=ALPH1H/DR
      BETA1D=BETA1H/DR
      WRITE(3,500) ALPH1D, BETA1D
  500 FORMAT(/,' Alpha1hat = ',G15.8,' Beta1hat = ',G15.8)
C
C  DF at passive array
C
      CALL DFPAS(RHOHAT,R,ALPH2H,BETA2H)
      ALPH2D=ALPH2H/DR
      BETA2D=BETA2H/DR
      WRITE(3,600) ALPH2D, BETA2D
  600 FORMAT(/,' Alpha2hat = ',G15.8,' Beta2hat = ',G15.8)
C
C  Roll angle
C
      CALL ESTROL(C,ALPH1H,BETA1H,PSIRH)
      PSIRD=PSIRH/DR
      WRITE(3,700) PSIRD
  700 FORMAT(/,' Psirhat = ',G15.8)
C  Assemble attitude matrix
      CALL A2COMP(ALPH1H,BETA1H,PSIRH,BETA2H,ALPH2H,AHAT)
C*      WRITE(3,900)
C*  900 FORMAT(/,' Ahat = ')
C*      CALL MWRITE(3,3,3,AHAT)
C
C  Determine one-way Euler angles
      CALL EULER(AHAT,PSIZH,PSIYH,PSIXH)
      PSIZD=PSIZH/DR
      PSIYD=PSIYH/DR
      PSIXD=PSIXH/DR
      WRITE(3,1000) PSIZD, PSIYD, PSIXD
 1000 FORMAT(/,' Estimated one-way Euler angles:',/,' Psizh = ',
     >  F10.3,/,' Psiyh = ',F10.3,/,' Psixh = ',F10.3)
C
      WRITE(3,9000)
 9000 FORMAT(/,' Continue ? ')
      READ(3,9010) LCHR
 9010 FORMAT(A1)
      LCHR=LCHR.AND.95
      IF(LCHR.EQ.89) GO TO 100
      STOP
      END


      SUBROUTINE ACOMP(PSIZ,PSIY,PSIX,A)
C  Attitude matrix from Euler angles.
C  This matrix rotates coordinate frames, not vectors.
C  To rotate vectors within a coordinate frame, multiply by A-transpose.
      DIMENSION A(3,3)
      COSZ = COS(PSIZ)
      COSY = COS(PSIY)
      COSX = COS(PSIX)
      SINZ = SIN(PSIZ)
      SINY = SIN(PSIY)
      SINX = SIN(PSIX)
      A(1,1) =  COSY * COSZ
      A(1,2) =  COSY * SINZ
      A(1,3) = -SINY
      A(2,1) = -COSX * SINZ  +  SINX * SINY * COSZ
      A(2,2) =  COSX * COSZ  +  SINX * SINY * SINZ
      A(2,3) =  SINX * COSY
      A(3,1) =  SINX * SINZ  +  COSX * SINY * COSZ
      A(3,2) = -SINX * COSZ  +  COSX * SINY * SINZ
```

```
      A(3,3) =  COSX * COSY
      RETURN
      END


      SUBROUTINE PRC(RHO,ALPHA,BETA,VEC)
C  Polar-to-rectangular coordinate converter
C  Produces unit vector with RHO=1.Ø
      DIMENSION VEC(3)
      COSB=COS(BETA) * RHO
      VEC(1)=COSB * COS(ALPHA)
      VEC(2)=COSB * SIN(ALPHA)
      VEC(3)=-SIN(BETA) * RHO
      RETURN
      END


      FUNCTION RANGE(U,V)
C  Distance between points
      DIMENSION U(3), V(3)
      RANGE=Ø.Ø
      DO 1Ø J=1,3
      RANGE=RANGE + (V(J) - U(J))**2
   1Ø CONTINUE
      RANGE=SQRT(RANGE)
      RETURN
      END


      SUBROUTINE PATHES(VEC1,AT,R)
C  Compute 9 path lengths
      DIMENSION VEC1(3), VEC2(3), AT(3,3), A1(3), A2(3), A3(3),
     >  P1(3), P2(3), P3(3), R(3,3), AØ(3)
C  Active array in active-array coordinates
      AØ(1)=Ø.Ø
      AØ(2)=Ø.Ø
      AØ(3)=Ø.Ø
      A1(1)=Ø.Ø
      A1(2)=Ø.Ø
      A1(3)=-1.Ø
      A2(1)=Ø.Ø
      A2(2)=-Ø.866Ø254
      A2(3)=Ø.5
      A3(1)=Ø.Ø
      A3(2)=Ø.866Ø254
      A3(3)=Ø.5
C  Passive array in passive-array coordinates
      P1(1)=Ø.Ø
      P1(2)=Ø.Ø
      P1(3)=-1.Ø
      P2(1)=Ø.Ø
      P2(2)=-Ø.866Ø254
      P2(3)=Ø.5
      P3(1)=Ø.Ø
      P3(2)=Ø.866Ø254
      P3(3)=Ø.5
C  Rotate passive array by true attitude
      CALL SMULT(1,3,P1,1.Ø,VEC2)
      CALL MVMLT(3,3,1,AT,VEC2,P1)
      CALL SMULT(1,3,P2,1.Ø,VEC2)
      CALL MVMLT(3,3,1,AT,VEC2,P2)
      CALL SMULT(1,3,P3,1.Ø,VEC2)
      CALL MVMLT(3,3,1,AT,VEC2,P3)
C*      WRITE(3,225)
C*  225 FORMAT(/,' Rotated p vectors: ')
C*      CALL MWRITE(3,1,3,P1)
C*      CALL MWRITE(3,1,3,P2)
C*      CALL MWRITE(3,1,3,P3)
C  Translate passive array by true position (convert to act-array coord)
      CALL MADD(3,1,P1,VEC1,P1)
      CALL MADD(3,1,P2,VEC1,P2)
```

```
      CALL MADD(3,1,P3,VEC1,P3)
C*      WRITE(3,226)
C*  226 FORMAT(/,' Translated p vectors: ')
C*      CALL MWRITE(3,1,3,P1)
C*      CALL MWRITE(3,1,3,P2)
C*      CALL MWRITE(3,1,3,P3)
C  Calculate path lenghts - assume zero delay in passive transponder
      RHOØØ=RANGE(AØ,VEC1)
      R(1,1)=RANGE(A1,P1) + RHOØØ
      R(1,2)=RANGE(A1,P2) + RHOØØ
      R(1,3)=RANGE(A1,P3) + RHOØØ
      R(2,1)=RANGE(A2,P1) + RHOØØ
      R(2,2)=RANGE(A2,P2) + RHOØØ
      R(2,3)=RANGE(A2,P3) + RHOØØ
      R(3,1)=RANGE(A3,P1) + RHOØØ
      R(3,2)=RANGE(A3,P2) + RHOØØ
      R(3,3)=RANGE(A3,P3) + RHOØØ
C*      WRITE(3,23Ø)
C*  23Ø FORMAT(/,' R = ')
C*      CALL MWRITE(3,3,3,R)
      RETURN
      END


      SUBROUTINE ERANGE(R,RHOHAT)
C  Estimates AØ-PØ range (rhoØØ)
      DIMENSION R(3,3)
      RHOHAT=Ø.Ø
      DO 2Ø I=1,3
      DO 1Ø J=1,3
      RHOHAT=RHOHAT + R(I,J)
   1Ø CONTINUE
   2Ø CONTINUE
      RHOHAT=RHOHAT/18.Ø
      RETURN
      END


      SUBROUTINE DFACT(RHOHAT,R,ALPH1H,BETA1H)
C  Estimates alpha1 and beta1
C  -1.57 <= alpha1hat <= +1.57
C  -1.57 <= beta1hat <= +1.57
      DIMENSION R(3,3), SA(3), RHOØ(3)
      RA=1.Ø
      C1=1.732Ø5Ø8 * RA
      C2=3.Ø * RA
C  Compute rho1,Ø, rho2,Ø, and rho3,Ø
      DO 2Ø J=1,3
      RHOØ(J)=Ø.Ø
      DO 1Ø I=1,3
      RHOØ(J)=RHOØ(J) + R(J,I)
   1Ø CONTINUE
      RHOØ(J)=(RHOØ(J)/3.Ø) - RHOHAT
   2Ø CONTINUE
C  Determine elements of unit vector pointing to passive array
      SA(2)=(RHOØ(2) - RHOØ(3))/C1
      SA(3)=(2.Ø*RHOØ(1) - RHOØ(2) - RHOØ(3))/C2
      SA(1)=1.Ø - (SA(2))**2 - (SA(3))**2
      IF(SA(1).LT.Ø.Ø) SA(1)=Ø.Ø
      SA(1)=SQRT(SA(1))
C*      WRITE(3,3Ø)
C*   3Ø FORMAT(/,' SA = ')
C*      CALL MWRITE(3,1,3,SA)
C  Determine direction angles
      BETA1H=-ASIN(SA(3))
      ALPH1H=ATAN2(SA(2),SA(1))
      RETURN
      END


      SUBROUTINE DFPAS(RHOHAT,R,ALPH2H,BETA2H)
```

```
C  Estimates alpha2 and beta2
C  alpha2hat >= +1.57 or <= -1.57
C  -1.57 <= beta2hat <= +1.57
      DIMENSION R(3,3), SP(3), RHOØ(3)
      PI=3.1415927
      TWOPI=6.2831853
      RP=1.Ø
      C1=1.732Ø5Ø8 * RP
      C2=3.Ø * RP
C  Compute r' 1,Ø, rho2,Ø, and rho3,Ø
      DO 2Ø J=1,3
      RHOØ(J)=Ø.Ø
      DO 1Ø I=1,3
      RHOØ(J)=RHOØ(J) + R(I,J)
   1Ø CONTINUE
      RHOØ(J)=(RHOØ(J)/3.Ø) - RHOHAT
   2Ø CONTINUE
C  Determine elements of unit vector pointing to passive array
      SP(2)=(RHOØ(2) - RHOØ(3))/C1
      SP(3)=(2.Ø*RHOØ(1) - RHOØ(2) - RHOØ(3))/C2
      SP(1)=1.Ø - (SP(2))**2 - (SP(3))**2
      IF(SP(1).LT.Ø.Ø) SP(1)=Ø.Ø
      SP(1)=SQRT(SP(1))
C*      WRITE(3,3Ø)
C*   3Ø FORMAT(/,' SP = ')
C*      CALL MWRITE(3,1,3,SP)
C  Determine direction angles
      BETA2H=ASIN(SP(3))
      ALPH2H=ATAN2(SP(2),-SP(1))
      ALPH2H=PI-ALPH2H
      IF(ALPH2H.GT.PI) ALPH2H=ALPH2H-TWOPI
      RETURN
      END


      SUBROUTINE EULER(A,PSIZ,PSIY,PSIX)
C  Determines Euler attitude angles for given attitude matrix A
C  Common gain errors are eliminated by using ratios
C  As formulated, will not work with Psiy = +-9Ø°
      DIMENSION A(3,3)
      PSIZ=ATAN2(A(1,2),A(1,1))
      PSIX=ATAN2(A(2,3),A(3,3))
      COSY=(A(1,1)*COS(PSIZ) + A(1,2)*SIN(PSIZ)
     >  + A(2,3)*SIN(PSIX) + A(3,3)*COS(PSIX))/2.Ø
      PSIY=ATAN(-A(1,3)/COSY)
      RETURN
      END


      SUBROUTINE A2COMP(ALPHA1,BETA1,PSIR,BETA2,ALPHA2,A)
C  Computation of attitude matr'x from two-way parameters
      DIMENSION A(3,3), B(3,3), C(3,3), D(3,3)
      PI=3.1415926
      CALL ACOMP(ALPHA2-PI,-BETA2,Ø.Ø,A)
      CALL TRANS(3,3,A,B)
      CALL ACOMP(ALPHA1,BETA1,PSIR,C)
      CALL MVMLT(3,3,3,B,C,A)
      RETURN
      END


      SUBROUTINE COUPLE(ALPHA,BETA,AT,C)
C  Coupling between linearly polarized elements
C  Unity gain assumed
C  Columns of C correspond to received vectors for x, y, z dipole xmtr
      DIMENSION AT(3,3), C(3,3), D(3,3), F(3,3)
      DO 2Ø J=1,3
      DO 1Ø I=1,3
      F(I,J)=Ø.Ø
   1Ø CONTINUE
   2Ø CONTINUE
```

```
      F(2,2)=1.Ø
      F(3,3)=1.Ø
      CALL ACOMP(ALPHA,BETA,Ø.Ø,D)
      CALL MVMLT(3,3,3,D,AT,C)
      CALL MVMLT(3,3,3,F,C,D)
C*      WRITE(3,5Ø)
C*   5Ø FORMAT(/,' Coupling in tracking-frame = ')
C*      CALL MWRITE(3,3,3,D)
      CALL ACOMP(ALPHA,BETA,Ø.Ø,C)
      CALL TRANS(3,3,C,F)
      CALL MVMLT(3,3,3,F,D,C)
      RETURN
      END


      SUBROUTINE ESTROL(C,ALPHA1,BETA1,PSIR)
C  Estimate relative-roll angle
      DIMENSION C(3,3)
      VZØ=C(3,3)/COS(BETA1)
      VYØ=(C(2,3) - VZØ * SIN(BETA1) * SIN(ALPHA1))/COS(ALPHA1)
C*      WRITE(3,2Ø) VYØ,VZØ
C*   2Ø FORMAT(/,' VYØ, VZØ = ',2G12.4)
      PSIR=ATAN2(-VYØ,VZØ)
      RETURN
      END
```

Simulation Program

```
C  Program # FHR-321C, Ø6/27/83
C  Simulation of polarized interferometer
C
C  Declarations and constants
C
      IMPLICIT LOGICAL (L)
      DOUBLE PRECISION RR(3,3), RHO, RHOHAT, RHOHT, DRANGE,
     >  XI(3), XIHAT(3), ETA(3), ETAHAT(3), AA(3,3), DPC, DP1,
     >  RTHAT(3,3), RHOØØ
      DIMENSION A(3,3), AT(3,3), VEC1(3), VEC2(3), R(3,3), AHAT(3,3),
     >  C(3,3), CHAT(3,3), ATHAT(3,3), YC(4), VEC3(3)
      WRITE(3,1Ø)
   1Ø FORMAT(' Simulation of polarized interferometer,',
     >  ' Program # FHR-321C',/)
      DR=Ø.Ø17453293
      DP1=1.ØD+ØØ
C
C  Get true parameters
C
  1ØØ WRITE(3,11Ø)
  11Ø FORMAT(' True parameters:')
      CALL GETPA(RHO,ALPHA1,BETA1,PSIZ,PSIY,PSIX)
      PSIZD=PSIZ/DR
      PSIYD=PSIY/DR
      PSIXD=PSIX/DR
      ALPH1D=ALPHA1/DR
      BETA1D=BETA1/DR
C
C  RF parameters
C
      WRITE(3,13Ø)
  13Ø FORMAT(/,' PF, PR = ')
      CALL ATR(PF,IERR)
      CALL ATR(PR,IERR)
C
C  Test parameters
C
      WRITE(3,14Ø)
  14Ø FORMAT(' Number of tests, iterations = ')
      CALL ATI(NTEST,IERR)
      CALL ATI(NITMAX,IERR)
```

```
      WRITE(3,15Ø)
  15Ø FORMAT(' Seeds = ')
      CALL ATI(IR1,IERR)
      CALL ATI(IR2,IERR)
      CALL FOPENO(6,IERR)
C
C  Calculate true position vector and attitude matrix
C
      CALL INITPA(RHO,ALPHA1,BETA1,PSIZ,PSIY,PSIX,
     >  A,XI,ETA,PSIR)
      CALL TRANS(3,3,A,AT)
      CALL DSMC(3,1,XI,VEC1)
C
C  Calculate true locations of antenna elements
C
      CALL PATH2(RHO,XI,AT,RHOØØ,RR)
C
C  Calculate true amplitude coupling between linearly polarized elements
      CALL COUPLE(ALPHA1,BETA1,AT,C)
      CALL CYXFER(C,YC)
C
C  Calculate position of active array w.r.t. passive array
C
      CALL SDMC(3,3,A,AA)
      CALL DMVMLT(3,3,1,AA,XI,ETA)
      DPC=-1.ØD+ØØ
      CALL DSMULT(3,1,ETA,DPC,ETA)
      CALL DSMC(3,1,ETA,VEC2)
      CALL RPC(VEC2,RHOS,ALPHA2,BETA2)
      CALL ESTROL(C,ALPHA1,BETA1,PSIR)
      ALPH2D=ALPHA2/DR
      BETA2D=BETA2/DR
      PSIRD=PSIR/DR
C
C  Initialize frequency set
C
      CALL FCOMP
C
C  Headings for output file
C
      WRITE(6,1Ø)
      WRITE(6,2ØØ) RHO, ALPH1D, BETA1D
  2ØØ FORMAT(/,' Rho =    ',F1Ø.3,'   Alpha1 = ',F1Ø.3,
     >  '   Beta1 = ',F1Ø.3)
      WRITE(6,21Ø) PSIZD, PSIYD, PSIXD
  21Ø FORMAT(' Psiz =   ', F1Ø.3,'   Psiy =   ',F1Ø.3,
     >  '   Psix =  ',F1Ø.3)
      WRITE(6,22Ø) ALPH2D, BETA2D, PSIRD
  22Ø FORMAT(' Alpha2 = ',F1Ø.3,'   Beta2 =  ',F1Ø.3,
     >  '   Psir =  ',F1Ø.3)
      WRITE(6,23Ø) PF, PR
  23Ø FORMAT(/,' PF = ',F1Ø.4,'  PR = ',F1Ø.4)
      WRITE(6,24Ø) NITMAX
  24Ø FORMAT(' Number of iterations = ',I5)
      WRITE(6,25Ø) IR1, IR2
  25Ø FORMAT(' Seeds = ',2I8)
      WRITE(6,26Ø)
  26Ø FORMAT(/'  TEST',9X,'e1',13X,'e2',13X,'e3',13X,'e4',
     >  9X,'Nar',/)
C
C  Zero averages
C
      E1AVG=Ø.Ø
      E2AVG=Ø.Ø
      E3AVG=Ø.Ø
      E4AVG=Ø.Ø
      NART=Ø
      NSAMP=Ø
C
C  Begin test
C
```

```
      DO 5000 NT=1, NTEST
      CALL INTRPT(LINT)
      IF(LINT.EQ.27) GO TO 4000
C
C  Initialize estimates to true values
C
      RHOHAT=RHO
      CALL DSMULT(3,1,XI,DP1,XIHAT)
      CALL DSMULT(3,1,ETA,DP1,ETAHAT)
      PSIRH=PSIR
      CALL SMULT(3,3,A,1.0,AHAT)
      E1=0.0
      E2=0.0
      E3=0.0
      E4=0.0
C
C  RF SIMULATION
C
      CALL RF(RHO00,RR,PF,PR,RTHAT,C,CHAT,IR1,IR2)
      CALL CYXFER(CHAT,YC)
      WRITE(3,7001)
 7001 FORMAT(/,' RTHAT = ')
      DO 7003 I=1,3
      WRITE(3,7002) (RTHAT(I,J), J=1,3)
 7002 FORMAT(' ',3G15.8)
 7003 CONTINUE
      WRITE(3,7220)
 7220 FORMAT(/,' C = ')
      CALL MWRITE(3,3,3,C)
      WRITE(3,7221)
 7221 FORMAT(/,' CHAT = ')
      CALL MWRITE(3,3,3,CHAT)
C
C  Check for ambiguity-resolution errors
C
      NAR=0.0
C  Select ambiguity wavelength
      EMAX=0.12
      IF(RHO00.LT.0.999D+06) EMAX=0.72
      WRITE(3,1240) EMAX
 1240 FORMAT(' Emax = ',G12.4)
      DO 1280 I=1,3
      DO 1270 J=1,3
      ERR = ABS( SNGL( RR(I,J) + RHO00 - RTHAT(I,J)) )
      WRITE(3,1250) I,J, RR(I,J),  RTHAT(I,J), ERR
 1250 FORMAT(2I5,3G15.8)
      IF(ERR.GT.EMAX) NAR=NAR+1
 1270 CONTINUE
 1280 CONTINUE
      IF(NAR.NE.0) GO TO 4000
C
C  POSITION AND ATTITUDE ESTIMATION
C
 2000 NSAMP=NSAMP+1
      DO 3000 NIT=1, NITMAX
      WRITE(3,2400) NT, NIT
 2400 FORMAT(/,' Test ',I5,'  Iteration ',I3)
      CALL ITER(RTHAT,YC,RHOHAT,XIHAT,ETAHAT,PSIRH,AHAT,
     >  D1,D2,D3,D4,V1,V2,V3,V4,ALP1HD,BET1HD,ALP2HD,BET2HD)
C
C  Write out true values and results of iteration
C
      WRITE(3,2910) NIT
 2910 FORMAT(//,' RESULTS OF ITERATION #',I3,':')
      WRITE(3,2930) RHOHAT, ALP1HD, BET1HD
 2930 FORMAT(' Rhohat = ', G15.8,' Alphalhat = ',F10.3,
     >  ' Betalhat = ',F10.3)
      WRITE(3,2940) (XIHAT(J), J=1,3)
 2940 FORMAT(' Xihat = ',3G15.8)
      WRITE(3,2960) (ETAHAT(J), J=1,3)
 2960 FORMAT(' Etahat = ',3G15.8)
```

```
      PSIRHD=PSIRH/DR
      WRITE(3,2980) PSIRHD
 2980 FORMAT(' Psirhat = ', F10.3)
C
C  End of iteration
C
 3000 CONTINUE
C
C  End of test - evaluate error
C
C  Range error
      E1 = ABS(SNGL(RHOHAT - RHO))
      E1AVG = E1AVG + E1**2
C  Direction
      E2=SNGL( DRANGE(XI,XIHAT) )
      E2AVG = E2AVG + E2**2
C  Reverse direction
      E3=SNGL( DRANGE(ETA,ETAHAT) )
      E3AVG = E3AVG + E3**2
C  Roll
      E4 = ABS( AMOD((PSIRH - PSIR),6.2831853) )
      E4AVG = E4AVG + E4**2
C
C  Output results
C
C  Ambiguity-resolution errors
 4000 NART=NART + NAR
      WRITE(3,4900) NT, E1, E2, E3, E4, NAR
      WRITE(6,4900) NT, E1, E2, E3, E4, NAR
 4900 FORMAT(' ',I5,4(3X,G12.4),3X,I5)
 5000 CONTINUE
C
C  Compute average errors
      IF(NSAMP.EQ.0) GO TO 5010
      E1AVG=SQRT(E1AVG/NSAMP)
      E2AVG=SQRT(E2AVG/NSAMP)
      E3AVG=SQRT(E3AVG/NSAMP)
      E4AVG=SQRT(E4AVG/NSAMP)
 5010 WRITE(3,5020) E1AVG, E2AVG, E3AVG, E4AVG, NART
      WRITE(6,5020) E1AVG, E2AVG, E3AVG, E4AVG, NART
 5020 FORMAT(/,'  Rms ',4(3X,G12.4),3X,I5)
      E2AVG=E2AVG / DR
      E3AVG=E3AVG / DR
      E4AVG=E4AVG / DR
      WRITE(3,5030) E2AVG,E3AVG,E4AVG
      WRITE(6,5030) E2AVG,E3AVG,E4AVG
 5030 FORMAT('  Rms°',15X,3(3X,G12.4))
      WRITE(3,5040) NSAMP
      WRITE(6,5040) NSAMP
 5040 FORMAT(/,' Nsamp = ',I5)
      ENDFILE 6
C
C
      WRITE(3,9000)
 9000 FORMAT(/,' Continue program? ')
      READ(3,9010) LCHR
 9010 FORMAT(A1)
      LCHR=LCHR.AND.95
      IF(LCHR.EQ.89) GO TO 100
      STOP
      END


      SUBROUTINE INITPA(RHOHAT,ALPH1H,BETA1H,PSIZH,PSIYH,PSIXH,
     >  AHAT,XIHAT,ETAHAT,PSIRH)
      DOUBLE PRECISION XIHAT(3), ETAHAT(3), RHOHAT, DPC
      DIMENSION AHAT(3,3), CHAT(3,3), ATHAT(3,3), DUM1(3), DUM2(3)
      RHOS=SNGL(RHOHAT)
      CALL PRC(RHOS,ALPH1H,BETA1H,DUM1)
      CALL SDMC(3,1,DUM1,XIHAT)
      CALL ACOMP(PSIZH,PSIYH,PSIXH,AHAT)
```

```
      CALL TRANS(3,3,AHAT,ATHAT)
      CALL MVMLT(3,3,1,AHAT,DUM1,DUM2)
      CALL SDMC(3,1,DUM2,ETAHAT)
      DPC=-1.ØD+ØØ
      CALL DSMULT(3,1,ETAHAT,DPC,ETAHAT)
      CALL DNORM(3,XIHAT)
      CALL DNORM(3,ETAHAT)
      CALL COUPLE(ALPH1H,BETA1H,ATHAT,CHAT)
      CALL ESTROL(CHAT,ALPH1H,BETA1H,PSIRH1)
      RETURN
      END


      SUBROUTINE ITER(RR,YC,RHOHAT,XIHAT1,ETAH1,PSIRH1,AHAT,
     >  D1,D2,D3,D4,V1,V2,V3,V4,ALPH1D,BETA1D,ALPH2D,BETA2D)
      DOUBLE PRECISION RR(3,3), RHOHAT,
     >  XIHAT1(3), XIHAT2(3), ETAH1(3), ETAH2(3), DPC
      DIMENSION A(3,3),
     >  AT(3,3), AHAT(3,3), ATHAT(3,3), CXI(2,2), CETA(2,2),
     >  YC(4), DUM1(3)
      DR=Ø.Ø17453293
C
C  Initial calculations
C
      CALL TRANS(3,3,AHAT,ATHAT)
C
C  Range
C
      CALL MVLE1(RR,RHOHAT)
      D1=Ø.Ø
      V1=Ø.Ø
      WRITE(3,1ØØ) RHOHAT
  1ØØ FORMAT(/,' MVLE #1: Rhohat = ',G15.8)
C
C  Adjust xihat and etahat
C
C  Direction of target vehicle
C
      WRITE(3,4Ø1)
  4Ø1 FORMAT(/,' MVLE #2')
      CALL MVLE2(1,RHOHAT,RR,XIHAT1,ATHAT,XIHAT2,CXI,D2)
      WRITE(3,4Ø2) (XIHAT1(J), J=1,3), (XIHAT2(J), J=1,3)
  4Ø2 FORMAT(/,' XIHAT1/XIHAT2 =',/,3E2Ø.1Ø,/,3E2Ø.1Ø)
C*      WRITE(3,42Ø)
C*  42Ø FORMAT(/,' CXI = ')
C*      CALL MWRITE(3,2,2,CXI)
      V2=(CXI(1,1) + CXI(2,2)) * 3.Ø
      WRITE(3,43Ø) D2
  43Ø FORMAT(/,' D2 = ',G12.4)
C
C  Update estimate of xi
      DPC=1.ØD+ØØ
      CALL DSMULT(3,1,XIHAT2,DPC,XIHAT1)
C
C  Direction of active vehicle
C
      WRITE(3,4Ø1)
C  Calculate attitude and position of active w.r.t. passive
      CALL MVLE2(2,RHOHAT,RR,ETAH1,ATHAT,ETAH2,CETA,D3)
      WRITE(3,51Ø) (ETAH1(J), J=1,3), (ETAH2(J), J=1,3)
  51Ø FORMAT(/,' ETAHAT1/ETAHAT2 =',/,3E2Ø.1Ø,/,3E2Ø.1Ø)
C*      WRITE(3,52Ø)
C*  52Ø FORMAT(/,' CETA = ')
C*      CALL MWRITE(3,2,2,CETA)
      V3=(CETA(1,1) + CETA(2,2)) * 3.Ø
      WRITE(3,53Ø) D3
  53Ø FORMAT(/,' D3 = ',G12.4)
C
C  Update estimate of eta
      DPC=1.ØD+ØØ
      CALL DSMULT(3,1,ETAH2,DPC,ETAH1)
```

```
C
C  Estimate relative roll angle
C
      WRITE(3,600)
  600 FORMAT(/,' MVLE #3')
      CALL DSMC(3,1,XIHAT1,DUM1)
      RHOS=SNGL(RHOHAT)
      CALL RPC(DUM1,RHOS,ALPH1H,BETA1H)
      CALL DSMC(3,1,ETAH1,DUM1)
      CALL RPC2(DUM1,RHOS,ALPH2H,BETA2H)
      ALPH1D=ALPH1H/DR
      BETA1D=BETA1H/DR
      ALPH2D=ALPH2H/DR
      BETA2D=BETA2H/DR
      CALL MVLE3(YC,ALPH1H,BETA1H,ALPH2H,BETA2H,PSIRH1,
     >  PSIRH2,V4,D4)
      PSIRD1=PSIRH1/DR
      PSIRD2=PSIRH2/DR
      WRITE(3,620) PSIRD1, PSIRD2
  620 FORMAT(/,' Psirh1 = ',G12.4,' Psirh2 = ', G12.4)
      WRITE(3,630) V4, D4
  630 FORMAT(' V4 = ',G12.4,' D4 = ',G12.4)
C
C  Update attitude matrix and roll angle
C
      CALL A2COMP(ALPH1H,BETA1H,PSIRH2,BETA2H,ALPH2H,AHAT)
      PSIRH1=PSIRH2
C
      RETURN
      END


      SUBROUTINE MVLE1(RR,RHOHAT)
C  Range
      DOUBLE PRECISION RR(3,3), RHOHAT
      RHOHAT=0.0
      DO 20 I=1, 3
      DO 10 J=1, 3
      RHOHAT=RHOHAT + RR(I,J)
   10 CONTINUE
   20 CONTINUE
      RHOHAT=RHOHAT / 18.0
      RETURN
      END


      SUBROUTINE MVLE2(L,RHO,RIN,XIHAT1,AT,XIHAT2,CXI,RSSDIF)
C  MVLE for direction angles
C  Inputs
C     RIN:    range measurements
C     CN:     noise covariance
C     XIHAT1: old estimate
C     AT:     transpose of estimated attitude matrix
C     RHO:    range
C  Outputs
C     XIHAT2: new estimate
C     CXI:    estimate covariance
C     RSSDIF: rss difference in estimates
      IMPLICIT LOGICAL (L)
      DOUBLE PRECISION RIN(3,3), R(3,3), RHAT(3,3), RHO, DPC,
     >  Y(3), YHAT(3), DELTYY(3), XIHAT1(3), XIHAT2(3), AI(3,3)
      DIMENSION CNI(3,3), CXI(2,2),
     >  AT(3,3), DELTAY(3), G(3,2), T(3,2), GT(2,3),
     >  DUM1(2,2), DUM2(2,2), B(2,3), DUM3(3,3), DUM4(2,3), X(2)
C
C  Invert measurement covariance matrix
      CALL MIDENT(3,CNI)
C
C  Forward or reverse mode?
      IF(L.EQ.2) GO TO 10
      DPC=1.0D+00
```

```
      CALL DSMULT(3,3,RIN,DPC,R)
      GO TO 2Ø
   1Ø CALL DTRANS(3,3,RIN,R)
C
C  Form set of three differences
   2Ø CALL RYXFER(RHO,R,Y)
C
C  Predict measurements and find difference vector
      CALL PATHES(RHO,XIHAT1,AT,RHAT)
      CALL RYXFER(RHO,RHAT,YHAT)
      DPC=-1.ØD+ØØ
      CALL DSMULT(1,3,YHAT,DPC,YHAT)
      CALL DMADD(1,3,Y,YHAT,DELTYY)
      CALL DSMC(1,3,DELTYY,DELTAY)
C
C  Gradient matrix
      CALL GRAD2(RHO,XIHAT1,AT,G)
C
C  Error-covariance matrix
      CALL MVMLT(3,3,2,CNI,G,T)
      CALL TRANS(3,2,G,GT)
      CALL MVMLT(2,3,2,GT,T,CXI)
      CALL INVERT(CXI,2,DET,DUM1,DUM2)
      WRITE(3,38) DET
   38 FORMAT(/,' DET = ',G12.4)
C
C  Blending matrix
      CALL MVMLT(2,3,3,GT,CNI,DUM4)
      CALL MVMLT(2,2,3,CXI,DUM4,B)
C
C  Estimated error
      CALL MVMLT(2,3,1,B,DELTAY,X)
C
C  Rss error
      CALL MVMLT(1,2,1,X,X,RSSDIF)
      RSSDIF=SQRT(RSSDIF)
C
C  Update estimate
      CALL IACOMP(-X(1),-X(2),Ø.Ø,DUM3)
      CALL SDMC(3,3,DUM3,AI)
      CALL DMVMLT(3,3,1,AI,XIHAT1,XIHAT2)
      CALL DNORM(3,XIHAT2)
      RETURN
      END


      SUBROUTINE GRAD2(RHO,XI1,AT,G)
C  Gradient of range measurements with respect to direction
      DOUBLE PRECISION RHO, R1(3,3), R2(3,3), Y1(3), Y2(3),
     >  XI1(3), XI2(3), AAI(3,3), DPC
      DIMENSION AT(3,3), G(3,2), AI(3,3)
      DELTAA=Ø.Ø1
C  Measurements at nominal location
      CALL PATHES(RHO,XI1,AT,R1)
      CALL RYXFER(RHO,R1,Y1)
      DPC=-1.ØD+ØØ
      CALL DSMULT(3,1,Y1,DPC,Y1)
C
C  Gradient in alpha direction
C
      CALL IACOMP(-DELTAA,Ø.Ø,Ø.Ø,AI)
      CALL SDMC(3,3,AI,AAI)
      CALL DMVMLT(3,3,1,AAI,XI1,XI2)
      CALL DNORM(3,XI2)
      CALL PATHES(RHO,XI2,AT,R2)
      CALL RYXFER(RHO,R2,Y2)
      CALL DMADD(9,1,Y1,Y2,Y2)
      DO 2Ø J=1, 3
      G(J,1)=Y2(J) / DELTAA
   2Ø CONTINUE
C
```

```
C  Gradient in beta direction
C
      CALL IACOMP(0.0,-DELTAA,0.0,A1)
      CALL SDMC(3,3,A1,AA1)
      CALL DMVMLT(3,3,1,AA1,X11,X12)
      CALL DNORM(3,X12)
      CALL PATHES(RHO,X12,AT,R2)
      CALL RYXFER(RHO,R2,Y2)
      CALL DMADD(9,1,Y1,Y2,Y2)
      DO 30 J=1, 3
      G(J,2)=Y2(J) / DELTAA
   30 CONTINUE
C
      RETURN
      END


      SUBROUTINE MVLE3(Y,ALPHA1,BETA1,ALPHA2,BETA2,PSIRH1,
     >  PSIRH2,VARP,ERP)
C  MVLE for relative roll angle
C  Inputs
C     Y:       coupling measurement
C     CN:      noise covariance
C     ALPHA1, BETA1,ALPHA2,BETA2:  DOA angles
C     PSIRH1: previous estimate of roll angle
C  Outputs
C     PSIRH2: updated estimate of roll angle
C     VARP:    estimate variance
C     ERP:    magnitude of difference in estimates
      DIMENSION Y(4), CNI(4,4), YHAT(4), A(3,3), AT(3,3),
     >  DELTAY(4), G(4), T(4), B(4), DUM3(4,4), C(3,3)
      DATA PI, TWOPI /3.1415926, 6.2831852/
C
C  Invert measurement covariance matrix
      CALL MIDENT(4,CNI)
C
C  Predict measurements and find difference vector
      CALL A2COMP(ALPHA1,BETA1,PSIRH1,BETA2,ALPHA2,A)
      CALL TRANS(3,3,A,AT)
      CALL COUPLE(ALPHA1,BETA1,AT,C)
      CALL CYXFER(C,YHAT)
      CALL SMULT(4,1,YHAT,-1.0,YHAT)
      CALL MADD(4,1,Y,YHAT,DELTAY)
C
C  Gradient matrix
      CALL GRAD3(ALPHA1,BETA1,PSIRH1,BETA2,ALPHA2,G)
C
C  Error-covariance matrix
      CALL MVMLT(4,4,1,CNI,G,T)
      CALL MVMLT(1,4,1,G,T,VARP)
      VARP=1.0/VARP
C
C  Blending matrix
      CALL MVMLT(1,4,4,G,CNI,B)
      CALL SMULT(1,4,B,VARP,B)
C
C  Estimated error
      CALL MVMLT(1,4,1,B,DELTAY,X)
C
C  Rss error
      ERP=ABS(X)
C  Update estimate
      PSIRH2=PSIRH1 + X
      IF(PSIRH2.GT.PI) PSIRH2=PSIRH2-TWOPI
      IF(PSIRH2.LT.-PI) PSIRH2=PSIRH2+TWOPI
      RETURN
      END


      SUBROUTINE GRAD3(ALPHA1,BETA1,PSIR1,BETA2,ALPHA2,G)
C  Gradient of coupling vector w.r.t. relative roll angle
```

```
      DIMENSION G(4), Y1(4), A(3,3), AT(3,3), C(3,3)
      DELTAA=0.01
      F=1.0/DELTAA
C  Coupling at nominal attitude
      CALL A2COMP(ALPHA1,BETA1,PSIR1,BETA2,ALPHA2,A)
      CALL TRANS(3,3,A,AT)
      CALL COUPLE(ALPHA1,BETA1,AT,C)
      CALL CYXFER(C,Y1)
      CALL SMULT(4,1,Y1,-1.0,Y1)
C  Coupling at incremented attitude
      PSIR2=PSIR1 + DELTAA
      CALL A2COMP(ALPHA1,BETA1,PSIR2,BETA2,ALPHA2,A)
      CALL TRANS(3,3,A,AT)
      CALL COUPLE(ALPHA',BETA1,AT,C)
      CALL CYXFER(C,G)
C  Gradient
      CALL MADD(4,1,Y1,G,G)
      CALL SMULT(4,1,G,F,G)
      RETURN
      END


      SUBROUTINE GETPA(RHO,ALPHA1,BETA1,PSIZ,PSIY,PSIX)
C  Get position and attitude
      DOUBLE PRECISION RHO
      DR=0.017453293
  100 WRITE(3,110)
  110 FORMAT(' Position (rho,alpha1,beta1) = ')
      CALL ATR(RHOS,IERR)
      RHO=DBLE(RHOS)
      IF(IERR.EQ.27) GO TO 100
      CALL ATR(ALPHA1,IERR)
      IF(IERR.EQ.27) GO TO 100
      IF((ALPHA1.GT.90.0).OR.(ALPHA1.LT.-90.0)) GO TO 100
      CALL ATR(BETA1,IERR)
      IF(IERR.EQ.27) GO TO 100
      ALPHA1=ALPHA1*DR
      BETA1=BETA1*DR
      WRITE(3,120)
  120 FORMAT(' Attitude (psiz, psiy, psix) = ')
      CALL ATR(PSIZ,IERR)
      IF(IERR.EQ.27) GO TO 100
      CALL ATR(PSIY,IERR)
      IF(IERR.EQ.27) GO TO 100
      CALL ATR(PSIX,IERR)
      IF(IERR.EQ.27) GO TO 100
      PSIZ=PSIZ*DR
      PSIY=PSIY*DR
      PSIX=PSIX*DR
      RETURN
      END


      SUBROUTINE ACOMP(PSIZ,PSIY,PSIX,A)
C  Attitude matrix from Euler angles.
C  This matrix rotates coordinate frames, not vectors.
C  To rotate vectors within a coordinate frame, multiply by A-transpose.
      DIMENSION A(3,3)
      COSZ = COS(PSIZ)
      COSY = COS(PSIY)
      COSX = COS(PSIX)
      SINZ = SIN(PSIZ)
      SINY = SIN(PSIY)
      SINX = SIN(PSIX)
      A(1,1) =  COSY * COSZ
      A(1,2) =  COSY * SINZ
      A(1,3) = -SINY
      A(2,1) = -COSX * SINZ  +  SINX * SINY * COSZ
      A(2,2) =  COSX * COSZ  +  SINX * SINY * SINZ
      A(2,3) =  SINX * COSY
      A(3,1) =  SINX * SINZ  +  COSX * SINY * COSZ
```

```
      A(3,2) = -SINX * COSZ  +  COSX * SINY * SINZ
      A(3,3) =  COSX * COSY
      RETURN
      END


      FUNCTION RANGE(U,V)
C  Distance between points
      DOUBLE PRECISION RANGE, DSQRT, V
      DIMENSION U(3), V(3)
      RANGE=Ø.ØD+ØØ
      DO 1Ø J=1,3
      RANGE=RANGE + (V(J) - U(J))**2
   1Ø CONTINUE
      RANGE=DSQRT(RANGE)
      RETURN
      END


      FUNCTION DRANGE(U,V)
C  Distance between points
      IMPLICIT DOUBLE PRECISION (A-H,O-Z)
      DIMENSION U(3) ,V(3)
      DRANGE=Ø.ØD+ØØ
      DO 1Ø J=1,3
      DRANGE=DRANGE + (V(J) - U(J))**2
   1Ø CONTINUE
      DRANGE=DSQRT(DRANGE)
      RETURN
      END


      SUBROUTINE PATHES(RHO,VEC1,AT,R)
C  Compute 9 path lengths
      DOUBLE PRECISION RHOØØ, R(3,3), VEC1(3), RHO
      DIMENSION AT(3,3)
C
C  Compute one-way lengths
C
      CALL PATH2(RHO,VEC1,AT,RHOØØ,R)
C
C  Add pathes
C
      DO 2Ø I=1,3
      DO 1Ø J=1,3
      R(I,J) = R(I,J) + RHOØØ
   1Ø CONTINUE
   2Ø CONTINUE
      RETURN
      END


      SUBROUTINE PATH2(RHO,VEC3,AT,RHOØØ,R)
C  Compute 9 path lengths
      DOUBLE PRECISION RHOØØ, R(3,3), VEC1(3), VEC3(3),
     >  DP1(3), DP2(3), DP3(3), RANGE, RHO
      DIMENSION VEC2(3), AT(3,3), A1(3), A2(3), A3(3),
     >  P1(3), P2(3), P3(3), AØ(3)
C
C  Convert direction vector to position vector
C
      CALL DSMULT(3,1,VEC3,RHO,VEC1)
C
C  Active array in active-array coordinates
      AØ(1)=Ø.Ø
      AØ(2)=Ø.Ø
      AØ(3)=Ø.Ø
      A1(1)=Ø.Ø
      A1(2)=Ø.Ø
      A1(3)=-1.Ø
      A2(1)=Ø.Ø
```

```
      A2(2)=-Ø.866Ø254
      A2(3)=Ø.5
      A3(1)=Ø.Ø
      A3(2)=Ø.866Ø254
      A3(3)=Ø.5
C  Passive array in passive-array coordinates
      P1(1)=Ø.Ø
      P1(2)=Ø.Ø
      P1(3)=-1.Ø
      P2(1)=Ø.Ø
      P2(2)=-Ø.866Ø254
      P2(3)=Ø.5
      P3(1)=Ø.Ø
      P3(2)=Ø.866Ø254
      P3(3)=Ø.5
C  Rotate passive array by true attitude
      CALL SMULT(1,3,P1,1.Ø,VEC2)
      CALL MVMLT(3,3,1,AT,VEC2,P1)
      CALL SMULT(1,3,P2,1.Ø,VEC2)
      CALL MVMLT(3,3,1,AT,VEC2,P2)
      CALL SMULT(1,3,P3,1.Ø,VEC2)
      CALL MVMLT(3,3,1,AT,VEC2,P3)
C  Translate passive array by true position (convert to act-array coord)
      CALL SDMC(3,1,P1,DP1)
      CALL SDMC(3,1,P2,DP2)
      CALL SDMC(3,1,P3,DP3)
      CALL DMADD(3,1,DP1,VEC1,DP1)
      CALL DMADD(3,1,DP2,VEC1,DP2)
      CALL DMADD(3,1,DP3,VEC1,DP3)
C  Length of forward path
      RHOØØ=RANGE(AØ,VEC1)
C  Lengthes of return pathes
      R(1,1)=RANGE(A1,DP1)
      R(1,2)=RANGE(A1,DP2)
      R(1,3)=RANGE(A1,DP3)
      R(2,1)=RANGE(A2,DP1)
      R(2,2)=RANGE(A2,DP2)
      R(2,3)=RANGE(A2,DP3)
      R(3,1)=RANGE(A3,DP1)
      R(3,2)=RANGE(A3,DP2)
      R(3,3)=RANGE(A3,DP3)
      RETURN
      END


      SUBROUTINE EULER(A,PSIZ,PSIY,PSIX)
C  Determines Euler attitude angles for given attitude matrix A
C  Common gain errors are eliminated by using ratios
C  As formulated, will not work with Psiy = +-9Ø°
      DIMENSION A(3,3)
      PSIZ=ATAN2(A(1,2),A(1,1))
      PSIX=ATAN2(A(2,3),A(3,3))
      COSY=(A(1,1)*COS(PSIZ) + A(1,2)*SIN(PSIZ)
     >  + A(2,3)*SIN(PSIX) + A(3,3)*COS(PSIX))/2.Ø
      PSIY=ATAN(-A(1,3)/COSY)
      RETURN
      END


      SUBROUTINE A2COMP(ALPHA1,BETA1,PSIR,BETA2,ALPHA2,A)
C  Computation of attitude matrix from two-way parameters
      DIMENSION A(3,3), B(3,3), C(3,3), D(3,3)
      PI=3.1415926
      CALL ACOMP(ALPHA2-PI,-BETA2,Ø.Ø,A)
      CALL TRANS(3,3,A,B)
      CALL ACOMP(ALPHA1,BETA1,PSIR,C)
      CALL MVMLT(3,3,3,B,C,A)
      RETURN
      END
```

```
      SUBROUTINE COUPLE(ALPHA,BETA,AT,C)
C  Coupling between linearly polarized elements
C  Unity gain assumed
C  Columns of C correspond to received vectors for x, y, z dipole xmtr
      DIMENSION AT(3,3), C(3,3), D(3,3), F(3,3)
      DO 2Ø J=1,3
      DO 1Ø I=1,3
      F(I,J)=Ø.Ø
   1Ø CONTINUE
   2Ø CONTINUE
      F(2,2)=1.Ø
      F(3,3)=1.Ø
      CALL ACOMP(ALPHA,BETA,Ø.Ø,D)
      CALL MVMLT(3,3,3,D,AT,C)
      CALL MVMLT(3,3,3,F,C,D)
      CALL ACOMP(ALPHA,BETA,Ø.Ø,C)
      CALL TRANS(3,3,C,F)
      CALL MVMLT(3,3,3,F,D,C)
      RETURN
      END


      SUBROUTINE IACOMP(PSIZ,PSIY,PSIX,A)
C  Attitude matrix for incremental rotations
      DIMENSION A(3,3)
      CALL MIDENT(3,A)
      A(1,2)=PSIZ
      A(2,1)=-PSIZ
      A(1,3)=-PSIY
      A(3,1)=PSIY
      A(2,3)=PSIX
      A(3,2)=-PSIX
      RETURN
      END


      SUBROUTINE SHUFL(RIN,R)
      DIMENSION RIN(9), R(9)
      R(1)=RIN(1)
      R(2)=RIN(4)
      R(3)=RIN(7)
      R(4)=RIN(2)
      R(5)=RIN(5)
      R(6)=RIN(8)
      R(7)=RIN(3)
      R(8)=RIN(6)
      R(9)=RIN(9)
      RETURN
      END


      SUBROUTINE ESTROL(C,ALPHA1,BETA1,PSIR)
C  Estimate relative-roll angle
      DIMENSION C(3,3)
      VZØ=C(3,3)/COS(BETA1)
      VYØ=(C(2,3) - VZØ * SIN(BETA1) * SIN(ALPHA1))/COS(ALPHA1)
      PSIR=ATAN2(-VYØ,VZØ)
      RETURN
      END


      SUBROUTINE CYXFER(C,Y)
      DIMENSION C(3,3),Y(4)
      Y(1)=C(2,2)
      Y(2)=C(2,3)
      Y(3)=C(3,2)
      Y(4)=C(3,3)
      RETURN
      END
```

```
      SUBROUTINE RYXFER(RHO,R,Y)
      DOUBLE PRECISION RHO, R(3,3), Y(3)
      Y(1)=R(1,1) + R(1,2) + R(1,3) - 6.Ø * RHO
      Y(2)=R(2,1) + R(2,2) + R(2,3) - 6.Ø * RHO
      Y(3)=R(3,1) + R(3,2) + R(3,3) - 6.Ø * RHO
      RETURN
      END


      SUBROUTINE RPC2(V,RHO,ALPHA,BETA)
C  Converts vector to polar coordinates
C  Smooth transition across alpha=18Ø°
      DIMENSION V(3)
      DATA PI, TWOPI /3.1415926, 6.2831852/
      RHO=Ø.Ø
      DO 1Ø I=1, 3
      RHO=RHO + V(I)**2
   1Ø CONTINUE
      RHO=SQRT(RHO)
      ALPHA=ATAN2(V(2),-V(1))
      ALPHA=PI-ALPHA
      IF(ALPHA.GT.PI) ALPHA=ALPHA-TWOPI
      BETA=-ASIN(V(3)/RHO)
      RETURN
      END


      SUBROUTINE FCOMP
C  Compute set of forward and reverse frequencies
      DOUBLE PRECISION FØ, FFØ, FRØ, FF(9), FR(9), FD,
     >   ANU, ANUK
      COMMON /FSET/ FFØ, FRØ, FØ, FF, FR
C
C  Basic frequency plan
C
      FFØ = 3.ØD+Ø9
      FRØ = 2.ØD+Ø9
      FØ  = 1.25ØD+Ø3
      ANU = 6.1324D+ØØ
C
C  Forward and reverse frequencies
C
      FF(1) = FFØ
      FR(1) = FRØ
      ANUK = 1.ØD+ØØ
C
      DO 1ØØ KK=2,9
      FD = FØ * ANUK
      FF(KK) = FFØ + FD
      FR(KK) = FRØ + FD
      ANUK = ANUK * ANU
  1ØØ CONTINUE
      RETURN
      END


      SUBROUTINE RF(RHOØØ,RR,PF,PR,RTHAT,AC,ACHAT,IR1,IR2)
C
C  Simulation of RF subsystems
C
      DOUBLE PRECISION RR(3,3), RTHAT(3,3), PHI(3,3,9), TWOPI,
     >  FFØ, FRØ, FØ, FF(9), FR(9), RHOØØ, RHOCFT, PHIF,
     >  DMOD, RHO1, RHO2, RHO3, RHOA, RHOHAT, C, DP1, DP2
      DIMENSION AC(3,3), ACHAT(3,3)
      COMMON /FSET/ FFØ, FRØ, FØ, FF, FR
      COMMON /AR/ PHI, TWOPI, C, DP1, DP2
      DATA TWOPI, C / 6.283185308D+ØØ, 3.ØD+Ø8 /
      DATA DP1, DP2 / 1.ØD+ØØ, 2.ØD+ØØ /
      DATA RHOCFT / 1.ØD+Ø6 /
      DATA GT, GR, FN, BK, T, B
     >  /2.Ø, 2.Ø, 1Ø.Ø, 1.38E-23, 3ØØ.Ø, 1ØØ.Ø/
```

```
C
C  Receiver noise
C
      PN = BK * T * B * FN
C
C  Phase shifts for each of nine carriers
C
      DO 100 N=1,9
C
C  Forward-link
C
      PHIF = TWOPI / C * RHO00 * FF(N)
      PS = PF * GT * GR / PLOSS(RHO00,FF(N))
      SIGMA = SQRT(0.5 * PN / PS)
      CALL GAUSS(IR1,IR2,0.0,SIGMA,DELPHI)
      PHIF = PHIF + DELPHI
C
C  Reverse links
C
      DO 90 I=1,3
      DO 80 J=1,3
      PHI(I,J,N) = TWOPI / C * RR(I,J) * FR(N)
      PS = PR * GT * GR / PLOSS(RR(I,J),FR(N))
      SIGMA = SQRT(0.5 * PN / PS)
      CALL GAUSS(IR1,IR2,0.0,SIGMA,DELPHI)
      PHI(I,J,N) = TWOPI / C * RR(I,J) * FR(N) + PHIF + DELPHI
C  Map phase into (0,twopi) interval
      PHI(I,J,N)=DMOD(PHI(I,J,N),TWOPI)
   80 CONTINUE
   90 CONTINUE
C
  100 CONTINUE
C
C  Noise-induced errors in normalized amplitude measurements
C
      DO 150 N=1,9
C  SNR
      PS = PF * GT * GR / PLOSS(RHO00,FR(N))
      SIGMA = SQRT(0.5 * PN / PS)
C  Average measurements at all nine frequencies
      CALL MZERO(3,3,ACHAT)
      DO 130 I=2,3
      DO 120 J=2,3
      CALL GAUSS(IR1,IR2,0.0,SIGMA,DELPHI)
      ACHAT(I,J)=ACHAT(I,J) + DELPHI
  120 CONTINUE
  130 CONTINUE
  150 CONTINUE
      CONST=0.1111111
      CALL SMULT(3,3,ACHAT,CONST,ACHAT)
C  Corrupt measurements
      CALL MADD(3,3,AC,ACHAT,ACHAT)

C  Estimate nine round-trip ranges
C
      DO 700 I=1,3
      DO 690 J=1,3
      WRITE(3,290) I,J
  290 FORMAT(/,' I, J = ',2I5)
C
C  Estimate range from lowest difference frequency
C
      CALL ERD(I,J,2,RHOHAT,RHOA)
      WRITE(3,300) RHOHAT
  300 FORMAT(/,' Dif #  2 Rhohat = ',G20.12)
C
C  Estimate range from next-higher difference frequency
C
      DO 400 N = 3, 9
      CALL ERD(I,J,N,RHO2,RHOA)
      CALL AMBRES(RHOA,RHOHAT,RHO2)
```

```
      RHO = RHOA * PHI(I,J,N2) / TWOPI
      RETURN
      END


      SUBROUTINE AMBRES(RHOA,RHO1,RHO2)
C  Resolve cycle ambiguity
      DOUBLE PRECISION DMOD, RHO1, RHO2, RHOA,
     >  DP1, DP2, DL, DLHAT
C  Estimate lane number
      DL = RHO1 / RHOA
      DL = DL - DMOD(DL,1.ØD+ØØ)
      DL=DL - 4.ØD+ØØ
      EHAT = 1.ØE+2Ø
      DO 33Ø NL=1, 7
      DL = DL + 1.ØD+ØØ
      IF(DL.LT.-Ø.5D+ØØ) GO TO 315
      E = ABS( SNGL(RHO2 + DL*RHOA - RHO1) )
      IF(E.GE.EHAT) GO TO 32Ø
      DLHAT = DL
      EHAT=E
  32Ø CONTINUE
  315 CONTINUE
  33Ø CONTINUE
      RHO1 = RHO2 + DLHAT*RHOA
      RETURN
      END
```